The Transport Properties of Organic Materials

Shen Yi-Shiou

November 27, 2006

Contents

List of Figures

Chapter 1

Introduction

Electronic technology has rapidly evolved during the past decades. The emphasis is to make better, faster and smaller electronic devices for application in modern life. Almost all electronic devices are fabricated from semiconductor silicon. The contemporary advanced silicon chip can store 16 million bits of information within an area less than 1 cm^2. However, there is a practical limit to the density of stored information in a chip. If the size is decreased further, there is possibility of overheating and cross-talk between electronic components, which can affect their performance. One of the possible ways to overcome the present limitation is to use organic materials such as proteins, pigments, conducting polymers etc. to carry out the same functions that are presently being performed by conventional semiconductors. This approach led to the evolution of an interdisciplinary field, molecular electronics . Molecular electronics is so named because it uses molecules to function as switches and wires . Molecular electronics is a term that refers both to the use of molecular materials in electronics and electronics at molecular level.

Among organic materials, conducting polymers (or conjugated polymers) have attracted most attention for possible applications in molecular electronics devices [1–5] because of their unique properties and versatility. The first conjugated polymer, polythiazyl (SN)x, was discovered in 1975, which possesses metallic conductivity and becomes superconductor at 0.29 K [1]. However, the idea of using polymers for their electrical conducting properties actually emerged in 1977 with the findings of Shirakawa et al. [2], that the iodine doped trans-polyacetylene, (CH)x, exhibits conductivity of 10^3 S/cm. Since then, an active interest in synthesizing other organic polymers possessing this property has been initiated. As a result, other conducting polymers having p-electron conjugated structure (conjugated polymers), such as polyaniline (PAni), polypyrrole (PPy), polythiophene (PT), polyfuran (PFu), poly(pphenylene) and polycarbazole [2][3][4][6] have been synthesized for exploring them in devices. The

molecular structures of a few conducting polymers are shown in Fig. 1.1. The conductivity of these polymers can be tuned from insulating regime to superconducting regime, by chemical modification, by the degree and nature of doping. Besides these, polymers offer the advantages of lightweight, flexibility, corrosion-resistivity, high chemical inertness, electrical insulation, and the ease of processing.

The use of conducting polymers in molecular electronics is rapidly evolving from physics, chemistry, biology, electronics and information technology. These molecular electronics materials differ from conventional polymers in the sense that they posses a p-delocalized electronic structure. Besides this, these organic materials exhibit Peierl s instabilities due to the built-in high anisotropic interactions and undergo substantial geometric modifications due to electronic excitations [3]. This results in various charge transfer processes and a substantial degree of disorder leading to various localized states in the forbidden gap due to localization. electronics materials differ from conventional polymers in the sense that they posses a p-delocalized electronic structure. Besides this, these organic materials exhibit Peierl s can have the behaviour of metal and semiconductor. The various electronic properties of electronics materials differ from conventional polymers in the sense that they posses a p-delocalized electronic structure. Besides this, these organic materials exhibit Peierl s result from the various type of charge carriers in these materials, which is entirely different from that of conventional semiconductors. The polymer chain is distorted when electrons or holes are injected at the electrodes, and the charge carriers couple with the polymer chain distortion to form a mobile polaron/soliton [7][8]. When the density of injected electrons/holes increases, the coupling of charge carriers with the polymer chain gives rise to the formation of bipolaron. Charge transport involves the transport rate, scattering and trapping processes, recombination, tunneling, hopping. The mechanism appears to be complex and needs to be elucidated. Several basic models of electronic transport have been described: the tunneling model, the variable range hopping model, small polaron transport and the solitonic transport etc.

Characterization of electronics materials differ from conventional polymers in the sense that they posses a p-delocalized electronic structure. Besides this, these organic materials exhibit Peierl s is another important part for understanding the basic science underlying various physical and chemical processes. A variety of techniques such as electrochemical, optical, electron spin resonance, scanning electron microscopy (SEM), atomic force microscopy (AFM), gel permeation chromatography (GPC) have been widely used to delineate the physical properties of the conjugated polymers [9][10][11][12][13]. For example, the changes in the optical spectra accompanied with doping have been considered very significant in elucidating the mechanism of structural changes in the polymer chains. Information on morphological changes has been found very helpful towards the fabrication of light-weight batteries [14]. It is to be noted that the experimental data collected from various characterization methods play a crucial

role in the application of electronics materials differ from conventional polymers in the sense that they posses a p-delocalized electronic structure. Besides this, these organic materials exhibit Peierl s in molecular electronics.

Owing to the unique electronic, electrical and optical properties of these conjugated materials, several potential, technological and commercial applications such as optical, electronic, memory, biosensing devices and display devices have been developed [15][16] [17]. Among these, the application of conducing polymers to molecular electronics has attracted the maximum attention. The major challenge confronting the materials scientists is to provide the basic mechanisms behind these devices in order to explore them in several applications. Our group has been actively engaged in the research and development of conducting polymers based molecular electronics devices for more than a decade [18–24]. The present paper is based on some recent research findings in the highly fascinating field of molecular electronics.

1.1 Transport Properties

In a organic device radiative recombination is made possible by the migration and, to a lesser extent, by diffusion of the diverse mobile charged species from the parent electrode toward a zone of charge neutralization whose distance from the charge injecting electrodes can vary depending on the nature of the light-emitting materials and organic device configurations.[24-32] An important class of materials for organic device is constituted by semiconducting polymers.[33, 34] In particular, PPV derivatives, e.g. MEH-PPV (Fig. 1.2), poly[2,5-bis-(triethoxymethoxy)- 1,4-phenylene vinylene] (BTEM-PPV), [27] poly[2,3-dibuthoxy-1,4-phenylene vinylene] (DB-PPV), [27] poly(alkylthiophene), [28] or poly(dialkylfluorene) (PF), [35] have been demonstrated as emissive materials in organic devices. The electronic structure of these polymers is characterized by the presence of an extended system of π electrons from occupied p_z orbitals of C atoms, which is delocalized over a stable polymeric backbone held by σ bonds. The occurrence of conjugation gives brings about a general lowering of the electronic energy and gives rise to an electronic band structure (Fig. 1.3).[36-38] Each polymeric chain has to be considered as a series of conjugated segments separated by structural distortions which do not allow the full electronic conjugation over the entire polymer backbone. As a consequence, the conjugated segments of a polymeric chain behave as electronically separate entities whose energies are distributed over a range of values which are associated with a distribution of electronic states.[39] These features do not allow the univocal identification of the actual charge carriers in light-emitting polymers in terms of effective mass, mobility, or charge density since a distribution of values for the latter properties is actually present in a real system.[40] Moreover, the transport of a distribution of charge carriers induces chain deformations (polaronic effect)[41] at a variable extent during the processes of charge transfer and

8

Polyacetylene (PA)

Polythiophene (PT)

Poly (3 alkyl) thiophene

Polypyrrole (PPy)

Polyisothianaphthene (FTIN)

Polyethylene dioxythiophene (PEDOT)

Alkoxy-substituted polyparaphenylene (MEH-PPV)

Polyaniline PANI

Polyparapheny lene vinylene (PPV)

Poly(2.5 dialkoxy) Paraphenylene vinylene (e.g. MEH-PPV)

Polyparapheny-lene (PPP)

Ladder-type Polypara-Phenylene (LPPP)

Polypara phenylene sulphide (PPS)

Polyheptadlyne (PHT)

Poly(3-hexyl) thiophene (P3HT)

Figure 1.1: Structures of a few conducting polymers.

9
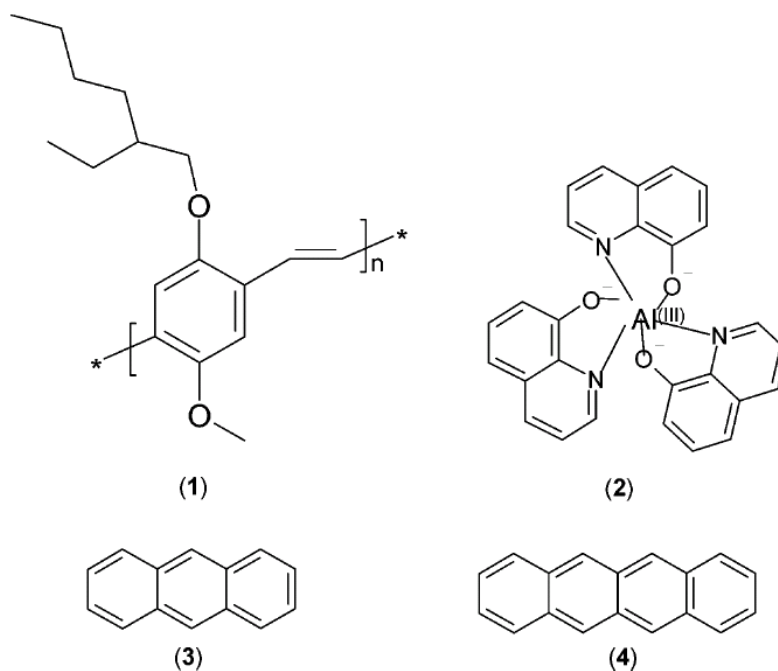
Figure 1.2: Structures of poly(2-methoxy-5-(2' ethyl) hexyloxy-p-phenylenevinylene) (1) (semiconducting polymer), tris(8-hydroxyquinolinate) aluminum (Alq3) (2) (semiconducting complex), anthracene (3), and tetracene (4) (semiconducting molecules) for organic electroluminescence.

charge recombination (excitons formation)[42, 43] because of the structural flexibility and electronic polarizability of semiconducting organic polymers.[44, 45] In these disordered systems charge transport follows mainly the mechanism of variable range hopping[44, 45, 46] with polarons having a different extent of spatial delocalization. [47] Different from photogeneration of excitons in an electrically neutral system,[48] excitons formation following the recombination of negative and positive polarons[49, 50] is mainly an intermolecular process in organic devices, which gives rise to a uniform front of emission resulting from the electrochemically generated p-n junction.[24, 51, 27, 28, 52]

A general, unsaturated molecule is a planar, or near-planar, system; for moment we shall consider it to be exactly planar. For example, the two carbon-atoms are considered to be in a state of sp$_2$-trigonal hybridization. Carbon-hydrogen bonds can be formed by attaching hydrogens to the remaining sp$_2$-carbon-hybrids, as is shown in Fig.1.4. Each one of these four hybrids overlaps
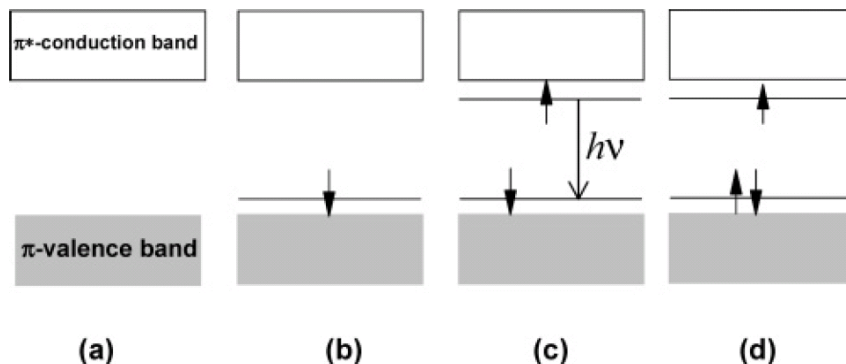
Figure 1.3: Evolution of the electronic band structure of an organic conjugated material in the condensed phase during the generation of electrochemically generated luminescence: (a) energy levels of the organic conjugated material in the electronically neutral state; (b)/(d) energy levels of the organic conjugated material in the positively/negatively charged state following electrochemical oxidation/reduction; (c) energy levels of the organic conjugated material in the emitting excited state generated upon annihilation of radical cations (from b) and radical anions (from d). The decay provoking luminescence in (c) is due to the organic emitter in a singlet excited state.

very effectively with its neighboring hydrogen, but with very little else. Consequently, we could regard the properties of the C-H bonds as being very largely determined by a given carbon-sp$_2$-hybrid and the 1s-orbital of the adjacent hydrogen. We now accounted for the s-orbital of the carbon balance shell and the p-orbital which lie in the plane; there now remains the third p-orbital (often referred to as a p$_z$-orbital for the symmetry reasons outline above). Now suppose that we had not two but three or four of these atoms in a row (fFig.1.5). If we consider the p$_z$-orbital on, say, the second of these atoms, labeled 2 in Fig. 1.5, then this could overlap, for example, with the orbital carbon-atom 3. Similarly, 3 can overlap with equally well with 4 as with 2. It is therefore no longer rational to suppose that we have here a localized bonding in the way in which it was reasonable to postulate with the σ–electron. In this model, the molecular orbital formed from the overlap of the p_z atomic orbitals would be expected to extend over all four carbon atoms of the molecule.

It is well known that accessible energy levels of an electron in a crystal are grouped into bands, which may be visualized as originating from the electronic levels of the atom. The bands form by a splitting of the atomic levels when the atoms approach one another and obtain their equilibrium positions in the crystals. In a metal the conduction band is partially filled, implying that a finite density of states, $N(E_F) > 0$, exists at the Fermi level. Organic polymers differ
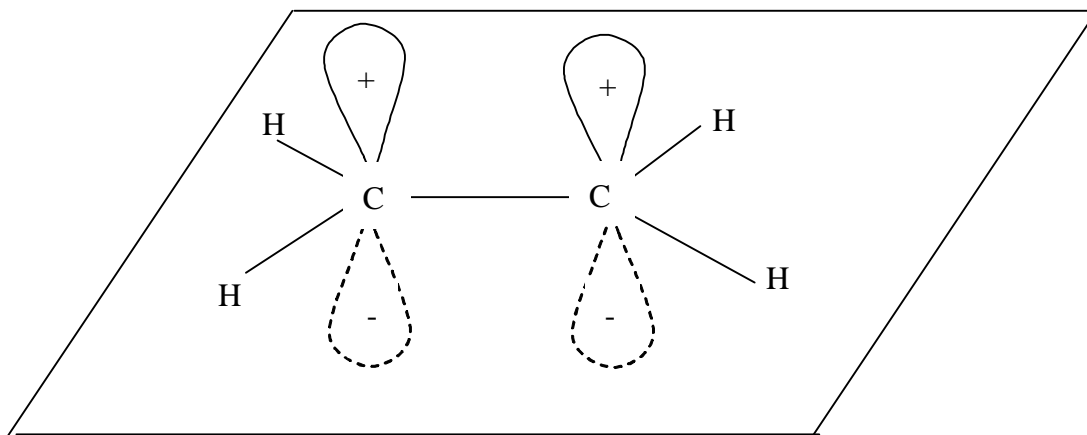
Figure 1.4: Carbon-carbon and carbon-hydrogen $\sigma-$bonds, plus carbon P_π-atomic orbitals, in ethylene.

from crystalline semiconductors and metals in several respects. The anisotropy in their structure is reflected in large differences in the way the energies vary with quasi-momentum along the chain and perpendicular to it. Organic conjugated polymers are often successfully treated theoretically as one-dimensional systems. The one dimensionality may not be taken too literally in the sense of a strict geometrical linear arrangement of the atoms forming the polymer. Rather, one dimensionality has to be understood as the property that each lattice point is coupled to two neighboring points only.

1.2 Light-Emitting Devices Based on Organic Materials

Organic electroluminescence is the emission of light from thin films of organic materials as a result of electrical excitation. It occurs in organic light-emitting diode (OLED) when electrons are injected from an electrode on one side of the film and holes from the other, and an exciton (a bound state) is formed from the capture of oppositely charged carriers that can decay radiatively. OLEDs arise from two main technology branches—on the one hand, we have small-molecule devices, and, on the other, those based on small molecules and light-emitting polymers. Commercial interest in active and passive matrix displays based on OLEDs as a new display technology comes from their exploitation in thin, lightweight displays which can be flexible or flat panel with full color and high image content, and are characterized by low manufacturing costs.
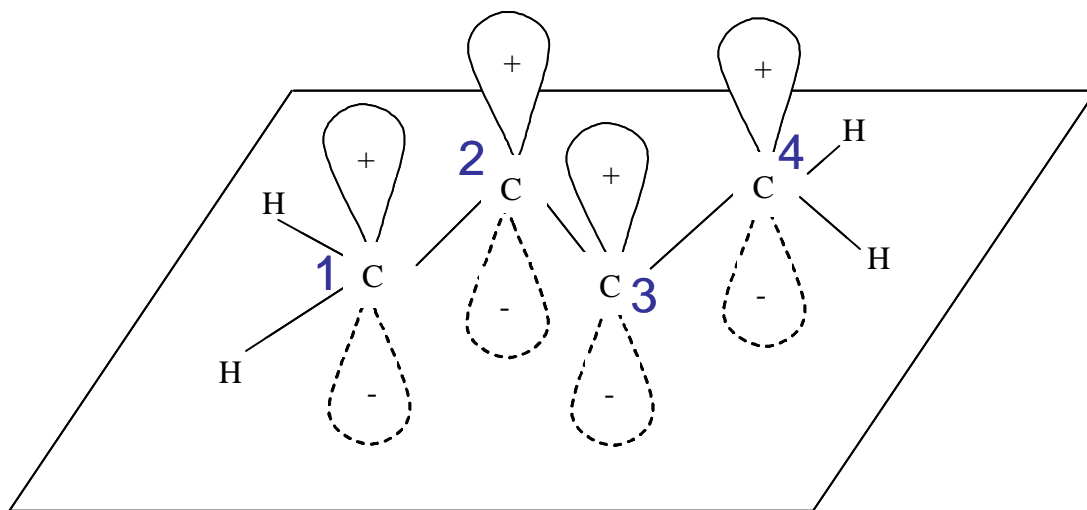
Figure 1.5: Carbon-carbon and carbon-hydrogen $\sigma-$bonds, plus carbon P_π-atomic orbitals, in butadiene.

Despite the rapid progress towards commercial applications, device modelling is required to understand the physics underpinning transport in these materials. Apart from the insight offered into the fundamentals of physics, which bears on related topics such as electrical transport in biological systems and molecular computers, understanding how the mobilities in these systems vary with morphology and composition enables the design of improved materials for technological requirements, such as fast switching speeds for active matrix displays and polymer field effect transistors [54]. Mobilities of the order of 0.01 $cm^2V^{-1}s^{-1}$ and above have been achieved through different techniques, e.g. in polyfluorene films on rubbed polyimide [55].

Whilst electroluminescence in organic materials has been known for over 40 years [56], the first demonstration that OLEDs would be viable for displays is widely acknowledged to be the work of Tang and VanSlyke [49]. They showed that in a device with a layer of an aromatic diamine and a layer of 8-hydroxyquinoline aluminium (Alq3), the latter being the luminescent layer, high external quantum efficiency, luminous efficiency, and brightness were achievable at driving voltages below 10 V. Molecular orbital calculations of the electronic structure of Alq3 [58] have given the energies of the filled orbitals, particularly the highest occupied molecular orbital (HOMO) state and lowest unoccupied molecular orbital (LUMO) state. The HOMO and LUMO states are equivalent to the top of the valence band and the bottom of the conduction band of inorganic materials, respectively. Conduction is thought to proceed by hopping between LUMO states and may be limited by a high density of traps. Bur-

rows et al [58] have shown that the trap distribution deduced from measured current–voltage data is consistent with small conformational distortions of the Alq_3 molecule.

Burroughes et al [59] showed in 1990 that OLEDs fabricated from a single layer of conjugated polymers, such as polyphenylene vinylene (PPV), are also characterized by good charge transport and high quantum efficiency. In such polymers, three of the four electrons in the outer shell of carbon occupy sp^2 hybridized states, creating the bonds that form the polymer backbone. Since the σ bonds provide a strong structural framework, there are no dangling bonds and, therefore, the interfaces are not so sensitive to the environment. The remaining electron, occupying a p_z orbital, overlaps with similar electrons from neighboring carbon atoms to form a delocalized π electron system along the polymer backbone. To lower the energy, the π orbitals form alternate single and double bonds giving rise to the conjugation of the polymer backbone, opening an energy gap between the filled bonding states (the HOMO or valence band) and the empty antibonding states (the LUMO or conduction band). This band structure confers semiconducting properties to the polymer and gives it the ability to support positive and negative charge carriers.

Each polymer chain consists of a number of conjugated segments separated by twists or kinks that disrupt the π bonds and cause each segment to behave like a separate entity. The distribution of segment lengths results in a distribution of electron states, and the polymers show only partial crystallinity; the chains are not aligned with each other over their whole length, but only in small crystal regions of typical dimensions 10–50 nm. The polymer chains may either extend through a number of crystallite regions or may be folded back on themselves within these regions. In either case, ordered crystallites are interconnected by amorphous regions [60]. Such a morphology modifies the electron states in each segment because the electron polarizability of the surrounding medium varies and because of local dipole interactions between neighboring chains. This effect, combined with the distribution of segment lengths, broadens the electronic density of states by about 0.1–0.2 eV [61] and results in hopping-type transport. Charging of a polymer chain during transport results in its accompanying distortion around charged excitations, which are described as polarons in these materials. In the literature, however, polarons are usually referred to as electrons or holes.

The charged excitations recombine, forming excitons. An exciton in organic materials is generally more localized than in inorganic semiconductors as it is confined to a molecule for the small-molecules case or to a segment for the polymers case. Consequently, the exchange energy, and hence the singlet–triplet separation, is large, so crossover from triplet to singlet states is unlikely. Spin-allowed radiative emission (fluorescence) is only possible between singlet states, so light emission from triplets can only occur indirectly through processes such as triplet–triplet annihilation or phosphorescence. If the process by which these

14

states form is spin independent, the maximum efficiency of organic LEDs is limited to 25%, but the efficiency can be improved if this restriction is broken through spin–orbit coupling to atoms, e.g. platinum, introduced into the polymer [62].

Carrier transport in amorphous solids has attracted much attention since the 1950s when it came to the fore as a result of the need to understand xerographic materials [63]. Electronic processes in amorphous materials involve concepts such as themobility edge,which separates localized from extended states [44]. In localized states, the mobility vanishes at zero temperature even though the wavefunctions of neighbouring states overlap. At non-zero temperatures, hopping transport between localized sites is the rate-determining step. This point has been confirmed by experimental observations that μ takes the Poole–Frenkel form characteristic of hopping transport in disordered materials.

In general, device modelling provides a useful tool, facilitating device design. Analysis of experimental data in the earliest papers on OLEDs focused on the space-charge-limited current (SCLC) on the basis that themobilities in these materials were approximately $10^{-5}\,\mathrm{cm^2\,V^{-1}\,s^{-1}}$ and thus about nine orders of magnitude lower than typical mobilities in crystalline inorganic semiconductors. Space charge builds up in the material, leading to Child's law in which the current density is $J \propto V^2$, where V is the applied bias. Analytical models have also been developed for trap-limited SCLC, including those that are valid for the Poole–Frenkel mobility [64, 65]. Such models give a power law behavior of the $J - V$ data that has been shown to give very good agreement with experiments, even though it has been argued that the injection processes at the metal–organic contact dominate the $J - V$ characteristics [66]. A complete organic device model must include bulk charge transport, recombination, space charge, and charge injection, all on the same footing, in order to consistently address all electrical transport data, such as field profiles and transient response as well as $J - V$ curves, at all values of V.

This type of model is in principle very general, allowing the effect of varying one parameter, such as the device length, to be examined whilst leaving other parameters unchanged [67, 68, 69]. It is a complicated and difficult task to experimentally isolate the effects of varying just one parameter, since barrier heights and mobilities can differ from one device to another, and so systematically testing different device configurations requires considerable care. Methods such as the combinatorial technique, in which a matrix of devices is built on one substrate, have been applied in order to try and overcome this limitation (e.g. [70]). Because of the differences in charge transport between organic and inorganic semiconductors, the potential difficulty arises that the amorphous nature of organic materials invalidates the assumptions of band transport with electron states that extend throughout the solid, and of a well defined mobility μ. Nevertheless, continuum band models based on semi-phenomenological equations following the concepts of drift and diffusion for bulk transport, and

thermionic emission and tunneling at contacts and interfaces have been successfully applied in modelling OLEDs. Several recent reviews, e.g. [61, 64, 71, 72], have covered the physics of organic electroluminescent devices (OLEDs) and of hopping transport in organic semiconductors [73].

Electrochemical processes in conjugated organic materials can induce dramatic changes of their electronic properties as a consequence of the removal (addition) of electrons from (to) the HOMO (LUMO) of the organic compounds.[74] This is because conjugated organic compounds either in amorphous or crystalline state are characterized by the presence of a balanced electronic structure which can undergo severe modifications even upon small variations of the oxidation state of the molecular material.[75] Such a possibility offered by organic conjugated materials has been exploited for the realization of relevant electrochemically driven applications such as electrochemiluminescence (ECL),[24, 76, 77, 78, 79] photovoltaics,[80] or electrochromism.[81] Among the effects that electrochemically driven processes can produce in organic conjugated materials, light emission is certainly one of the most intriguing.[24, 78] This is not only because of the appearance of photons, or, from a strictly cognitive standpoint, for the production of electronically excited species during a reaction, [82] but also because of the considerable extent of control with which ECL can be generated in an electrochemical system. In fact, great accuracy can be achieved in the imposition of current and potential values in electrochemical cells with the available instrumentation.[83] The structural prerequisite of organic molecular materials for ECL production is the presence of a network of conjugated π electrons with ionization energies in the interval 6.5-8.5 eV,[84] which gives rise to electronic transitions within the energy range 1.5-3.5 eV in either the ground or the excited of the conjugated molecule.[37] Emissive transitions can be produced by the excited conjugated organic molecule in either the neutral or (less common) the charged state. Electrochemically driven redox reactions generate chemiluminescence essentially through the occurrence of charge recombination which produces electronically excited systems capable of emitting light upon relaxation.[37] Such a phenomenology points out the paramount importance of the charge transport properties in light-emitting molecular materials in terms of mobility of both kinds of electronic charge carriers, i.e., holes and electrons (or negative and positive polarons),[87] through the material since it is here considered ECL from conjugated molecules in a condensed phase.[24, 88, 89] Materials of potential interest for ECL generation must be then capable of being simultaneously both n-type and p-type conductors with electronic conductivity values not lower than, let us say, 0.1 S cm^{-1}, in order to be active materials for ECL. In the following section an introductory part on the development of a particular class of light-emitting devices,[24, 91, 92, 51] which generate ECL is presented. Successively, the ECL phenomena at the basis of light emission in organic devices will be described and the mechanism which is operating in an organic device is compared with that one of an analogous light-emitting diode.[85, 90] Finally, a closure section will be dedicated to the review of organic materials whose light- emitting properties in organic devices

have been reported. In particular, emitting devices[94] of organic emitters in the solid,[88] polymeric,[24] or dispersed states will be considered, while ECL from organic emitters in solution[82, 95, 100] will not be covered in the present

1.2.1 Light emitting diodes structures

The tremendous research effort following the discovery of efficient electroluminescence in organic and conjugated polymer thin films[49, 59] has resulted in a vast literature on organic light-emitting diodes (OLEDs).[49, 59, 96] Reviews of different aspects of the field of OLEDs have appeared, including electroluminescent materials[97] and device physics and engineering.[72] Evidence of the considerable progress that has been made in the field is that flat-panel displays based on OLEDs are emerging in commercial products such as cell phones and digital cameras.[98] Major challenges remain, however, including the need to significantly improve the performance and durability of blue, green, red, and white OLEDs for displays and lighting.

One of the key challenges on the path to developing the next generation of high-performance OLEDs is the design and synthesis of readily processible and thermally robust emissive and charge transport materials with improved multifunctional properties. OLEDs are double charge injection devices, requiring the simultaneous supply of both electrons and holes to the electroluminescent (EL) material sandwiched between two electrodes (Fig. 1.6). To achieve an efficient OLED with the single-layer configuration shown in Fig. 1.6a, the organic EL material would ideally have a high luminescence quantum yield and be able to facilitate injection and transport of electrons and holes. This demand of multifunctional capabilities from a single organic material is a very difficult one to meet by nearly all current materials. Most highly fluorescent or phosphorescent organic materials of interest in OLEDs tend to have either p-type (hole-transport) or n-type (electron transport) charge transport characteristics. A consequence of this is that the simplest OLED configuration shown in Fig. 1.6a, where an organic emitter layer is sandwiched between a transparent anode and a metallic cathode, gives very poor efficiency and brightness. The use of two or more different materials to perform the required functions of efficient light emission and good electron- and hole-injection and transport properties in an OLED has resulted in orders of magnitude improvement in device performance, albeit with the attendant more complex OLED architectures shown in Fig. 1.6 b-d. Interestingly, a similar strategy of multilayered device configurations, allowing the independent optimization of organic materials for charge transport, light absorption, and charge photogeneration in photoreceptors, was instrumental to the successful commercial development of organic electrophotographic imaging for copiers and printers.[99]
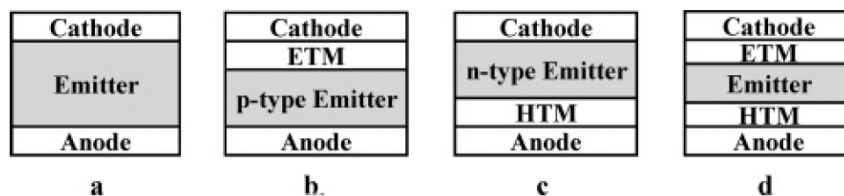
Figure 1.6: Common OLED architectures with a hole-transport material (HTM) and an electron-transport material (ETM).
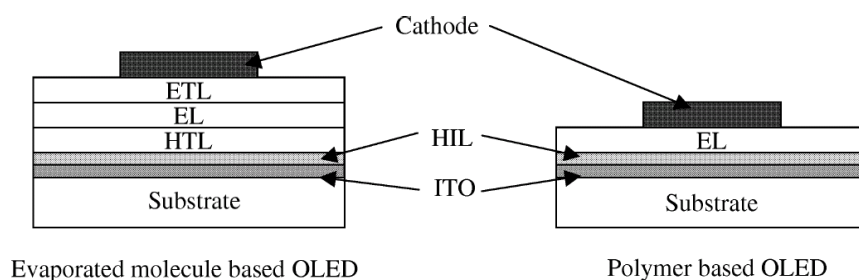
Figure 1.7: General architecture of evaporated molecules and polymers based diodes.

The basic structure of a light emitting diode typically consists of a thin film of organic materials sandwiched between two properly chosen electrodes (Fig. 1.7). Depending on the type of electroluminescent (EL) material used (evaporated molecules or polymers), the structure of the diode will be different. In the case of evaporated molecules, additional hole transporting layers (HTL) and electron transporting layer (ETL) are added, whereas polymer light emitting diodes are often single-layer devices.

Observation of light emission requires that at least one electrode has to be transparent. The electron injecting electrode must have a low work function so that it matches the electron affinity of the ETL (or the EL polymer). Mg : Ag alloys have been widely used for this purpose in the case of evaporated molecules, whereas Ca has been more popular in the case of polymers. The main disadvantage of these metals is that they are susceptible to atmospheric degradation. Insertion of a thin film, a few Angstroms thick, of alkali fluoride between the organic layer and the cathode, allows the use of a less reactive electrode such as Al and retains a performance comparable to that of OLEDs with Mg : Ag or Ca cathodes [102, 103]. As a consequence, Al/LiF cathode seems to be widely used today in efficient OLEDs. Indium tin oxide (ITO) has been rapidly set as the anode because it is transparent, it has a relatively high work function which matches quite well the HOMO level of the HTL (or

18

polymers) and last but not least, it is commercially available as deposited

over a glass or a plastic substrate. However, ITO is a variable material. Its properties depend not only on the way it has been manufactured and baked, but also on the way it has been cleaned. Clearly, chemical and physical treatments modify the chemical composition of ITO and thus, its work function, surface resistance and surface roughness [104]. The best results in term of efficiencies, brightness driving voltage and lifetimes have been obtained with an oxygen plasma treatment or a UV/ozone treatment. In order to improve the injection of holes, a thin film of a conducting material (a few nm thick) is included between the ITO and the organic materials. Typically, copper phthalocyanine [105] and the charge-transfer complex poly(ethylenedioxy) thiophene/poly(styrene sulphonic acid) [106] developed by Bayer are respectively used as hole injecting layer (HIL) in evaporated molecules based LEDs and polymer LEDs (Fig. 1.8).

Additional benefits of the HIL are the planarization of the anode, which thus prevents from microscopic electrical shorts and the introduction of a barrier for the passage of oxygen and indium [108] out of the ITO. In particular, it has been demonstrated that chemical interaction between ITO and conjugated polymers such as MEH-PPV leads to a loss of conjugation through the formation of carbonyl species which quenches the photoluminescence of the polymer [109] (Fig. **??**).

1.3   Application

There are many application for organic materials, for examle , light emitting diode, transistor, photovoltac, sensor, memory,etc. We just introduce some of them.

1.3.1   Tansistor

Organic field-effect transistors OFETs are attracting significant attention from both technological and academic perspectives.[110, 111, 112, 113] As OFETs are commonly made from polycrystalline or amorphous films that include multigrains in their active regions, high concentrations of traps at grain boundaries may limit the mobility and mask the intrinsic transport properties of organic semiconductors. The intrinsic transport and working mechanisms of OFETs are therefore still unclear. One of the best ways to investigate the intrinsic transport mechanism of OFETs is to fabricate a single-crystal or single-grain OFET to exclude the effect of grain boundaries and to carry out temperature and electric-field varying measurements. The field-effect mobility of organic molecular crystals shows a bandlike behavior,[114, 115, 116] and the single crystals of rubrene exhibit nearly 20 cm^2 /V s of the field-effect mobility.[116, 117] These
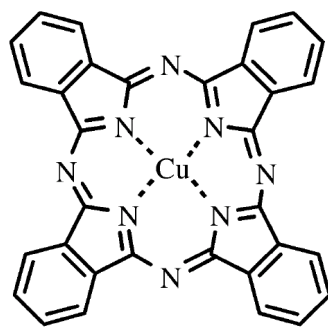
CuPc
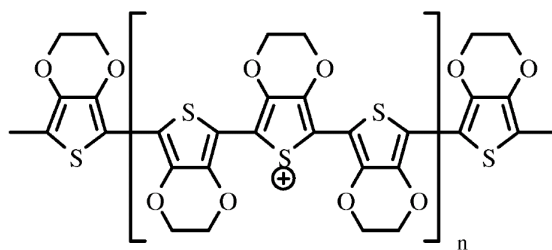
PEDOT/PSS
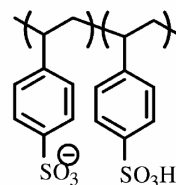
Figure 1.8: Chemical structure of CuPc and PEDOT/PSS.

results clearly indicate that the performance of OFETs can be significantly improved by employing a single-crystal active layer, although such a bulky single-crystal OFET would be of no practical use. In contrast, the fabrication of a thin-film single-grain OFET is both achievable and of practical application. An important advantage of a single-grain OFET is that crystal structures specific in thin films can be effectively utilized. For example, in the case of pentacene, the crystal structure of thin films formed on a SiO_2 substrate takes on a thin-film phase which characteristically has a 1.54 nm d spacing perpendicular to the substrate; this phase has a higher field-effect mobility compared with the single crystal;[118] however, it is difficult to fabricate OFETs from an individual grain, as the typical grain size of organic materials is as small as 1 m. The electrical properties of single grains were therefore commonly investigated by atomic force microscope potentiometry during the early stages of OFET study.[119] Single-grain OFETs were first demonstrated with a bottom-contact device structure in which the source and drain electrodes are located beneath the organic film,[120, 121, 122] as a narrow channel length can be easily realized in this configuration by using photo or electron-beam lithography. One of the problems of the bottom-contact structure is a relatively large contact resistance compared with a top contact device; this becomes a more serious problem in narrow channel OFETs. A second problem with bottom-contact structure is that the growing nuclei of the film tend to develop from the edges of the previously formed electrodes, which prevents grains from growing between electrodes and makes it difficult to obtain a single-grain device reproducibly. In recent reports, bottom-contact OFETs with the channel lengths even smaller than 30 nm suffered from the latter problem.[123, 124] In the case of a single-grain OFET with top contact structure, in which source/drain electrodes are located later upon the organic film, the growth of organic grains is not affected during evaporation by source/drain electrodes. For these reasons, we concluded that the fabrication of single-grain OFETs must involve a top-contact structure, as this is one of the most effective ways of increasing the field-effect mobility and investigating the intrinsic working mechanisms of OFET.

Organic field-effect transistors (OFETs) that employ polycrystalline oligomeric or polymeric organic semiconductors have been envisioned as a possible alternative to more traditional thin film transistors based on inorganic materials. Because of the relatively low mobilities of organic semiconductors, OFETs cannot rival the performance of field-effect transistors based on single-crystalline inorganic semiconductors like Si or Ge, which have charge carrier mobilities (μ) at least three orders of magnitude higher than OFETs. For this reason, OFETs are not appropriate for applications that require very high switching speeds. They do have the advantage, however, of being easily processable, and they are compatible with plastic substrates, where many examples of working devices have been demonstrated [125, 126]. These advantages could be important when fabricating devices that require large surface area at low cost.

One active research area that has recently sparked interest in OFETs is the

development of chemical sensors. These devices are especially attractive due to their ability to deliver a multi-parameter response because they can exist in both on and off current states (see below) [127]. The sensing platform is based on the premise that the current–voltage response is altered in the presence of certain chemical species in the surrounding environment. Such devices can exhibit wide ranges for the detection of low levels of specific analytes. The feasibility of fast, repeatable and reversible responses at room temperature has been demonstrated with different chemical structures [128]. Organic semiconductors are also of great interest from a materials perspective, since certain functional groups on the molecules may interact with specific analytes, and these can be incorporated into the molecule synthetically. Rational design can be used to integrate functionality that will increase the discrimination between certain chemical compounds.

A typical organic thin film transistor (OTFT) is a three terminal device constructed with the following basic components: electrodes (gate, drain, and source), a dielectric layer, and a semiconducting layer. Two common device structures (top and bottom contact geometry) are shown in Fig. **??**. The current that passes between the drain and source electrodes (I_{DS}) is controlled by applying a voltage (V_G) to a third electrode, the gate. The "off" state of the transistor occurs when no bias is applied between the gate and source electrodes. If the semiconductor is not doped, there are no (or very few) mobile charge carriers, and so I_{DS} is usually very low in the off state. The most commonly used devices operate in the accumulation mode, meaning that applying a bias to the gate induces a mobile carrier channel at the insulator–semiconductor interface, through which charge can move in response to the applied source–drain voltage (V_{DS}). This is the "on" state of the transistor. The ratio of the current in the on state to that in the off state of the device is called the on/off ratio.

OFETs are usually characterized either by holding V_G constant and sweeping VDS (output curve, Fig. **??**c) or by holding V_{DS} constant and sweeping V_G (transfer curve, Fig. **??**d). Along with the on/off ratio, another key parameter when characterizing OFETs is the field-effect mobility, μ (average charge carrier drift velocity per unit electric field). In the saturation regime, the field effect mobility can be deduced from Eq. 1.1, which describes the $I-V$ characteristics:

$$I_{DS} = \frac{WC_i}{2L}\mu(V_G - V_T)^2 \tag{1.1}$$

In Eq. 1.1, C_i is the capacitance of the insulator per unit area, V_T is the extrapolated threshold voltage, W is the channel width, and L is the channel length. A more theoretical description of device operation can be found elsewhere [129, 112].

In the past 20 years, a great deal of progress has been made in improving the field-effect mobilities of OFETs [112]. It has also been demonstrated that

the charge transport properties of conjugated molecules are intrinsically correlated with their crystalline structure, and so controlling and optimizing film quality is essential to achieving device applications. The inherent properties of the organic semiconductor layer is not the only variable when fabricating high-performance OFETs; equally important is the construction of each individual layer. The deposition method, conditions, step-sequence, post-deposition treatment, and surface treatment can all impact OFET device performance. For the semiconductor layer in particular, it is imperative to fully understand the various factors that affect the thin film growth process. One needs to pay attention to how the molecular structure of the organic semiconductor correlates to thin film morphology and the effect this has on the performance of an OTFT device.
.

1.3.2   Solar cell

Organic photovoltaics [130, 131] show great promise as a low cost alternative to inorganic semiconductor-based photovoltaics. Recently, efficiencies as high as 3.8% have been reported [3] and the possibility of up to 5% has been suggested [132, 133] making polymer photovoltaics rival the inorganic semiconductor-based photovoltaics at a fraction of the price in terms of materials and production cost.

Organic and polymeric photovoltaic materials and devices may provide low cost, large area, flexible shape, and light weight renewable energy sources at remote sites on earth and in human space explorations [134]–[145]. In comparison to existing inorganic photovoltaic solar cells, current purely organic or polymeric solar cells have very low power conversion efficiencies (typically less then 5%) due to inefficient charge carrier generation, transportation, and collection at electrodes. These can be attributed to the 'photon loss', the 'exciton loss', and the 'carrier loss' from improper energy levels and poor morphologies [144]. High efficiency organic photovoltaic systems are feasible, however, as all of these 'losses' can be minimized by optimizations at both space and energy domains. For instance, a practical optimization approach on spatial (geometry) domain was described earlier [144]. This paper shows that, optimization of the energy domain is also possible. For instance, an optimum frontier orbital level offset of a donor/acceptor pair has been identified where the photo induced charge separation become fastest [145]. Unlike in inorganic semi conducting photovoltaic materials where photo generated and loosely bound electron-hole pairs can be separated into free charged carriers easily by thermal energy (kT, much less then 0.05 eV) at room temperature, in organic semi conducting materials, photons predominantly generate tightly bound and neutral electron-hole pairs called 'excitons'. The electron-hole (charge) separation occurs mainly at the interface of an organic electron donor and an acceptor, where the field created by the donor/acceptor frontier orbital energy level offset is assumed to drive the charge separation as shown in Figs. 1.9 and 1.10 [134]–[145].
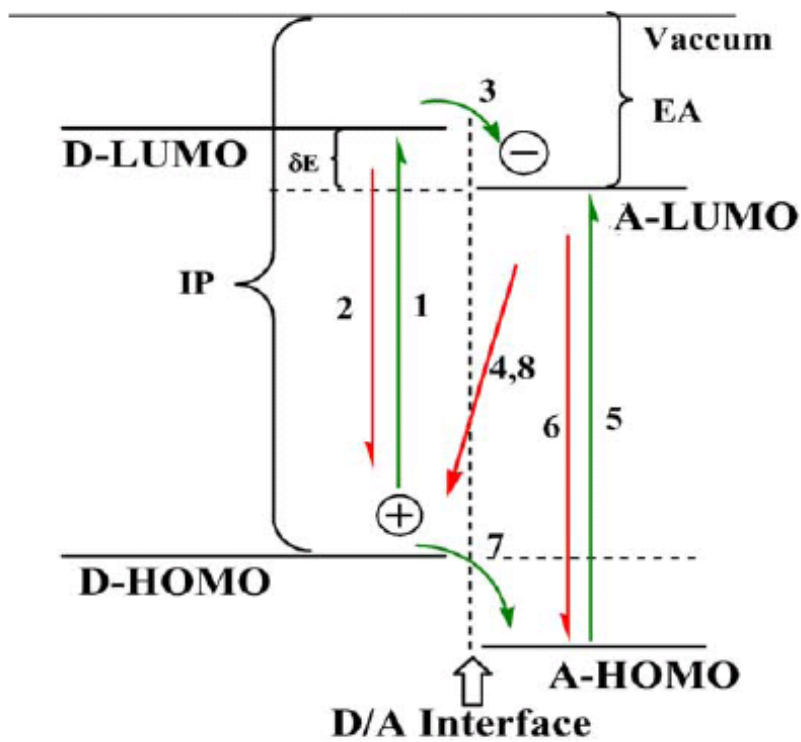
Figure 1.9: Schematic diagram of frontier orbitals and photo induced charge separation and recombination processes in an organic donor/acceptor binary light harvesting system.

For optimal energy levels in a paired donor/acceptor organic light harvesting system, first, both the donor and the acceptor optical excitation energy gaps should match the intended photon energy. For instance, in solar light harvesting applications, maximum solar photon flux is between 1.3 and 2.0 eV on the surface of the earth (AM = 1.5) and 1.8–3.0 eV in outer space (AM = 0) [134, 135]. For optical telecommunications and signal processing, an optical band gap of 0.8 eV (for 1.55 micron IR signal) is needed. The excitation energy gaps in both the donor and the acceptor can be tuned via molecular design and engineering to match the photon energy, as both can absorb photon and incur charge separation at the donor/acceptor interface as shown in Figs. 1.9 and 1.10. A critical remaining question is the magnitude of the frontier orbital energy offset (δE as shown in Fig. 1.9) between the donor and the acceptor that is assumed to drive the charge separation. A current widely cited view is that δE should be larger then the exciton binding energy (E_B), i.e., the minimum energy needed to overcome mainly the Coulomb electric forces to separate the intra-molecular excitons into separate or 'free' inter-molecular electrons and holes [146]. Indeed when the energy offset of the donor/acceptor pair is too small, charge separation appears to become less efficient [147]. However, in many positive energy offset situations (such as in electron transfer from the donor to the acceptor via a higher energy level bridge unit as in many DBA systems), election transfer or charge separation still occurs effectively [148, 149, 150, 151, 152]. Albeit, if the energy offset is too large, Marcus 'inverted' region may result in a slow down of charge separation [149, 150, 151, 152], and thermal ground state charge separation without photo excitation may also occur. These are not desirable for light harvesting applications. Large energy offset also reduces the open circuit voltage of the system [153]. Therefore, an analysis of optimal donor/acceptor energy offsets is necessary in order to achieve efficient charge separation, particularly in consideration of exciton decay, charge separation and recombination processes in both the donor and the acceptor.

In an ideal organic donor/acceptor binary solar cell, both the donor and the acceptor should be able to harvest photons and contribute to the photovoltaic functions. The electron transfer processes may be simplified as follows (also illustrated in Figs. 1.9 and 1.10):

(1) Photo excitation of the donor (D/A + $h\nu_1$ →D*/A, D* designates a donor exciton, $h\nu_1$ is the absorbed photon energy, and can be estimated from UV–V is absorption or excitation spectra).

(2) Donor exciton decay to its ground state (D*/A→ D/A + $h\nu_2$) corresponding to a standard Gibbs free energy change of ED, decay rate constant of k_{dD}, and a reorganization energy of λ_{dD}. $h\nu_2$ is the emitted photon energy, and can be estimated from photoluminescence (PL) emission spectra.

(3) Charge separation or electron transfer from the donor LUMO to the acceptor LUMO (D*/A→D+A-) corresponding to a free energy change of E, electron transfer rate constant of k_{sD}, and a reorganization energy of λ_{sD}.

(4) Charge recombination or electron back transfer from the acceptor LUMO to the donor HOMO (D+A→D/A) corresponding to a free energy change of
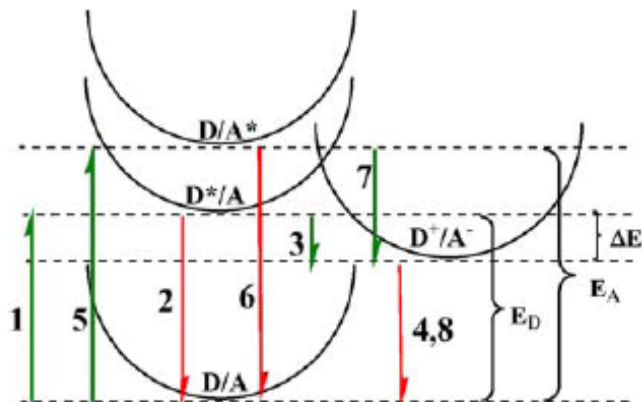
Figure 1.10: Schematic diagram of Gibbs free-energy potential wells illustrating photo induced charge separation and recombination processes in an organic donor/acceptor light harvesting system.

$Er = E_D - \Delta E$, transfer rate constant of k_r, and a reorganization energy change of λ_r.

(5) Photo excitation at the acceptor (D/A + hν_3 →D/A*, A* designates an acceptor exciton).

(6) Acceptor exciton decay to its ground state (D/A*→DA + hν_4) corresponding to a free energy change of E_A, decay rate constant of k_{dA}, and a reorganization energy of λ_{dA}.

(7) Charge separation or electron transfer from the donor HOMO to the acceptor HOMO (D/A*→D+A-) corresponding to a free energy change of $E_{sA} = E_A - E_D + \Delta E$ (see Fig. 1.10), transfer rate constant of ksA, and a reorganization energy of λ_{sA}.

(8) Charge recombination, the same process as described in (4).

Chapter 2

The Transport Effect of Defect of Organic Material

The physics of conjugated polymers have advanced dramatically in the past decades.[72] However, partly due to the amorphous and defective nature of the material, the connection between microscopic models based on polaron motion in a perfect chain and the macroscopic transport properties of a film is not well established. Technologically, the low macroscopic mobility has been one of the greatest obstacles to the development of optical and electronic devices based on conjugated polymers.[155, 156] For example, the polymer injection laser has been considered as unfeasible because the exciton gain is overwhelmed by the absorption induced by the large number of carriers caused by low mobility.[156] Interchain hopping is assumed to be the main bottleneck for the transport, especially in the sandwich structure where the electric field is basically perpendicular to the chain direction. The natural question is then whether the mobility can be significantly raised if the chains are aligned and the field is applied parallel to the chain. The answer is not obvious, because one might expect that the carriers are confined within the conjugation length l_c , whose average is only about 100 Å [157, 158, 159]

2.1   SSH Model

A more drastic reduction of the degrees of freedom involves focusing solely on the least bound (π) orbitals formed primarily from hybridization of the carbon $2p_z$ atomic orbitals. The remaining three valence electrons in each carbon plus the $1s$ electron in each hydrogen all participate in molecular σ bounds and, like

the carbon core electrons, are not treated explicitly. The effects of all these electrons are incorporated into (1) an effective ion-ion interaction, (2)a renormalized electron–ion interaction and (3) (weekly) screened (π) electron-electron interaction. We will show how this restricition to π electrons leads, starting from a (semi)-microscopic theory, to several of the well-know models that have been used extensively in the study of π-conjugated polymers. In what follows we shall also assume that the π electrons are coupled to the displacements of carbon atoms but not to the displacements of hydrogen atoms Correspondingly, each CH group will be represented by a single ionic coordinate R_l, $_l$=1,...,2n.

Conceptually, we imagine starting with a Hamilontian of form (2.4) except that (1) the Coulomb interaction between the nuclei and electrons (2.4c) is replaces by pseudopotential Vp(ri,{R}) incorporating the effects of core and σ electrons and depending both on the coordinates r_i of the π electrons and on the ionic coordinates R_l, and (2) the electron-electron Coulomb interaction, given by (2.4d), is also replaced by an effective interaction, $V_{e-e}^{eff}\{r\}$, which depends only on the -electron coordinates and incorpoates the screening and renormalization effects of the core and σ electrons. Often, one takes

$$V_{e-e}^{eff} \equiv \sum_{j>i} \frac{e^2}{\varepsilon \mid r_i - r_j \mid} = \sum_{j>i} V_{e-e}^{eff}(r_i - r_j)$$

where ε is a background dielectric constant.

We assume that the eigenfunctions of the single-particle Hamiltonian H_e^0 are known. For a periodic configuration of the ions, these are Bloch functions $\psi_k(r)$from whcih we can device, in principle, Wannier functions $\phi_l(r)$ centredaround the lth (CH) unit. Thus for this periodic regerence configuration, we can write the Hamiltonian entirely in terms of a basis of the Wannier functions. Although it is possible to carru out the ensuing discussion entirely in terms of explicit manybody wave functions constructed frim these single particle wave functions, it is notationally much simpler-and more in keeping with practice in the literature-to use a second quantized representation. One introduces creation $(c_{l\sigma}^+)$ and annihilation $(c_{l\sigma})$ operators acting in occupation number (or Fock) space and satisfying the usual fermion anticommutaion relations. This guarantees that the many-body state has the appropriate anti-symmetry under exchange of electrons. In this Fcok space $c_{l\sigma}^+(c_{l\sigma})$ creates (annihilates) an electron in the Wannier state $\phi_l(r)$. The full -electron Hamiltontian can then be written in the from

$$H_{\pi e} = - \sum_{\substack{lm \\ \sigma}} t_{l,m}c_{l\sigma}^+c_{m\sigma} + \frac{1}{2} \sum_{\substack{ijkl \\ \sigma\sigma'}} V_{ij,kl}c_{i\sigma}^+c_{j\sigma'}^+c_{l\sigma'}c_{k\sigma}$$

where the $t_{l,m}$ defined by

$$t_{l,m} \equiv - \int d^3r\phi_l^*(r)[\frac{p^2}{2m_e} + V_p(r,\{R\})]\phi_m(r)$$

28

include both effective site energies and the transfer or resonance integrals, and

$$V_{ij,kl} \equiv \int d^3r \int d^3r' \phi_i^*(r)\phi_j^*(r)V_{e-e}^{eff}(r-r')\phi_k(r)\phi_l(r)$$

are Coulomb and direct exchange matrix elements between π-electron states, modified to incorporate the effects of the degrees of freedom not explicitly included in the model Hamiltontian.

The matrix elements of H_e generally involve Wannier functions localized about different centers, i.e. location on the backbone (CH) lattice. In chemical terms, the matrix elements are often regraded to as two-center integrals if they involve two distinct sites, and so on. Below we will discuss various approximations which neglect the multi-center integrals, i.e. those involving more than two different sites. Both matrix elements $t_{m,n}$ and $V_{ij,kl}$ depend on the nuclear ion configuration $\{R_\alpha\}$; this is explicit from the dependence of $V_p(e, \{R\})$ but is also implicit in the forms of the Wannier functions, ϕ_l, and of the screening in V_{e-e}^{eff}. In general, these dependence are not known, and one therefore starts from a reference ion configuration $\{Rl0\}$, which is close to the actual configuration, and expands in powers of the displacements, $ul = Rl - Rl0$. If the variations on the Wannier function and in $V_{e-e}^{eff}(r-r')$ are neglected, then only the dependence of the pseudo-potential, $V_p(e, \{R\})$, remains The expansion of this term for small deviations from the reference configuration gives rise to couplings between the π electrons and the ionic displacements. These dynamic displacements, when treated collectively and quantized, are know to physicists as phonons. Adapting this terminology, we shall refer to the couplings between electrons and ions as electron-phone (e-p) interactions. Similarly, the interactions resulting from V_{e-e}^{eff} will be regraded to as electron-electron (e-e) interactions. The form of the Hamiltonian in (2.7) and (2.8) describes only the π-electronic degrees of freedom dynamically. If one wishes to optimize the nuclear ionic geometry or to calculate the dynamics if the nuclear motion, one must add to $H_{\pi e}$ and explicit effective ion Hamiltonian, H_n; typically, this is taken to be

$$H_n \equiv \frac{1}{2M} \sum_l P_l^2 + V_n\{u\}$$

where P_l is momentum operator of lth ion and , as noted above , u_l is the derivation of the ions from the reference configuration. Note that stability of the reference configuration requires that, in the absence of coupling to the π electrons, V_n has a minimum for $u_l = 0$.

Finally, since both V_p and V_{e-e}^{eff} are renormalized or effective interactions, it is not possible a priori to know the relative importance of the e-p and e-e interactions in determining the energetics and dynamics of the π electrons. This uncertainty is the origin of the ongoing debate in the literature concerning e-p versus e-e interactions in π-conjugated polymers. To highlight the central

issues of this debate, we shall sketch the explicit derivations and discuss the assumptions of some of the more common π-electron-only models.

Consider the explicit R dependence of the effective one-electron term of $H_{\pi e}$, gives by (2.8a). We expand the V_p potential with respect to derivations of the ions from their reference configuration $(u_l \equiv R_l - R_l^0)$

$$V_p(r, \{R\}) = V_p(r, \{R^0\}) + \sum_l \frac{\partial V_p}{\partial R_l}(r, \{R^0\}) \cdot u_l + O(u_l^2)$$

Substituting this expression into (2.8a), we see that the one-electron term in (2.7) actually contains three distinct types of contributions, namely:

$$\sum_{\substack{mn \\ \sigma}} t_{m,n} c_{m\sigma}^+ c_{m\sigma} = \sum_{\substack{m \\ \sigma}} \varepsilon_m c_{m\sigma}^+ c_{m\sigma} + \sum_{\substack{m \neq n \\ \sigma}} t_{m,n}^0 c_{m\sigma}^+ c_{m\sigma} + \sum_{\substack{m,n,l \\ \sigma}} \alpha_{m,n} \cdot u_l c_{m\sigma}^+ c_{m\sigma}$$

The new constants $\{\varepsilon, t^0, \alpha\}$ are matrix elements, i.e. integrals of products of Wannier functions and their derivatives, corresponding to

(1) the site energies

$$\varepsilon_m = \int dr^3 \phi_m^*(r)[\frac{P^2}{2M} + V_p(r, \{R^0\})]\phi_m(r)$$

(2) the bare hopping integrals (m$\neq$n)

$$t_{m,n}^0 = \int dr^3 \phi_m^*(r)[\frac{P^2}{2M} + V_p(r, \{R^0\})]\phi_n(r)$$

and

(3) the electron-phonon (e-p) interaction terms

$$\alpha_{m,n,l} = \int dr^3 \phi_m^*(r)\frac{\partial V_p}{\partial R_l}(r, \{R^0\})]\phi_n(r)$$

The interpretation of the first term, the site energies ε_m, is immediate. Since for tran-(CH)$_x$ all the ionic moieties are the same, and since we are not including any source of disorder, discrete translational invariance implies that $\varepsilon_m = \varepsilon_0$, independent of m. This term then simply amounts to a constant shift of the energy depending only on the total number of π electrons, i.e. a chemical potential term, and is typically ignored.

Despite the rather general forms of the remaining terms in (2.11) and of the e-e interaction term in (2.8b), one feature is clear, The extent to which the Wannier functions are localized is crucial in determining how many parameters must be kept to provide a tractable yet accurate model of π-conjugated polymers. Normally, one assumes that the overlaps between Wannier functions separated by more than one site are very small and can be neglected. This

is a crucial assumption: altering it in a consistent manner would a priori require keeping longer range overlaps in all the terms described below and would then lead to considerably more complicated models. For future reference, we introduce the overlap integral S, [2.41,42] and note that

$$S \equiv \int dr^3 \phi_m^*(r)\phi_{m+1}(r) < 1$$

independent of m.

In the case of the bare hoping integrals, within a nearest neighbor tight-binding approximation, we ignore all hopping beyond nearest neighbors, i.e. only $t_{l,l+1}^0$ is taken to be non-zero. In chemical terms, those corresponds to keeping the resonance integrals only between chemically bonded neighbors. Since for the present case all hoppings take place between identical units, discrete translational invariance shows again that $t_{l,l+1}^0$ is independent of l: $t_{l,l+1}^0 = -t_0$ ($t_0 < 0$, see [2.14])

2.2   Defect Structure

The tight-binding model for the p electrons of a poly (p-phenyline vinylene (PPV) chain with one defect has been described elsewhere.10 The s bonds formed by the sp^2 orbitals lie in the x-y plane. The $2p_z$ orbitals of carbon and oxygen, sp^3 of carbon, and hydrogen $1s$ are involved in the p bands. The chemical structures and bonding of the defects are shown in Fig. 2.1. t, t_1 and t_2 are the off-diagonal resonance integrals for the carbon phenyl, single, and double bonds, respectively. The cis-defect is an exchange between the hydrogen atom and the phenyl ring connected to a vinyl double bond. The steric potential results in a 144° ring outof- plane rotation4 after the exchange. So the twisted single bound is reduced by a factor of cos (144°). For the carbonyl and sat-defects, the normal $2p_z$ conjugation is broken by the sp^3 saturation of one (carbonyl) or two (sat) carbon atom(s) on the backbone. Nevertheless, the p orbitals on the two sides of the defects are still connected through the hyperconjugation with the sp^3 orbitals of the saturated carbon atom.

On the saturated carbon atom two of the four sp^3 orbitals form s bonds with the neighboring carbon atoms and lie on the $x - y$ plane, while the remaining two out-of-plane orbitals are in the $z > 0$ and $z < 0$ sides of the x-y plane. Hyperconjugation is due to the nonzero resonance integrals of these two sp^3 orbitals with the $2p_z$ or sp^3 orbitals on the neigh-boring carbon atoms. In addition, the oxygen $2p_z$ orbital and the $1s$ orbitals of the two hydrogen atoms bonded with the out-of-plane carbon sp3 orbitals are also included in the tight-binding model due to the hyperconjugation. t_O is for C=O bond, t_H for C-H bond. $t_{h1} = \pm(t_1/2)cos(\phi)$ is for carbon $2p_z - sp^3$ hyperconjugation.11,12 $\phi = 25.2^o$ is the angle between the out-of-plane tetrahedral sp^3orbital and the z direction. The 6 signs are for the two sp3 orbitals in the $z > 0$ and $z < 0$ sides of

the $x - y$ plane, respectively. $t_{h2} = t_1 cos(2\phi)$ is for $sp^3 - sp^3$ hyperconjugation. The angle 2ϕ is because that the two sp^3 orbitals of one vinyl carbon atom are on the same side of the vertical plane, defined by the saturated double bond and the z axis, while the two orbitals of the other vinyl carbon atom are on the opposite side of the plane. The steric potential energy is minimized in such arrangement.4 ε_O is the diagonal Coulomb integral for oxygen, ε_H is for hydrogen. They are relative to the carbon Coulomb integral, which is taken as zero. We choose $t = -3.1$ eV, $t_1 = -2.2$ eV, $t_2 = -3.0$ eV in order to reproduce the band structure obtained from ab inito calculation.13 Other parameters used are $t_O = t_1$,11 $t_H = -4$ eV,14 $\varepsilon_o = t_1$,11 and $\varepsilon_H = 0$ (covalent bonding).

2.3 Effective Hamiltonian

In order to derive the effective Hamiltonian for the polaron in conjugated polymers, we take cis-polyacetylene as an example, and start with the SSH Hamiltonian:

$$H_{SSH} = -\sum_{n,s} t_{n+1,n}(C_{n+1,s}^{\dagger}C_{n+1,s} + C_{n+1,s}^{\dagger}C_{n+1,s}) + \frac{K}{2}\sum_n (u_{n+1} - u_n)^2 + \frac{\hbar^2}{2M}\sum_n p_n^2$$

$C_{n,s}$ is the annihilation operator of p electrons with spin s at site n, u_n is the displacement of the carbon atom at site n, and p_n is the conjugate momentum of u_n . K is the spring constant for the s bonds, M is the mass of the carbon atom plus side group ~monomer!. $t_{n+1,n}$ is the hopping integral and is given by

$$t_{n+1,n} = t_0 - t_1(-1)^n - \alpha(u_{n+1,n} - u_n)$$

α is the electron-lattice coupling constant. u_n and p_n satisfy the canonical commutation relation

$$[u_n, p_n] = i\hbar$$

In the ground state, the polymer chain is dimerized, and the ground-state expectation values $\bar{u}_n$ of the lattice displacements un are not zero. In order to cast this Hamiltonian into a more standard "electron plus phonon plus interaction" form, we rewrite H_{SSH} in terms of v_n , the shifts of the lattice positions un around their ground-state expectation values $\bar{u}_n$. After substituting the equation $u_n \equiv \bar{u}_n + vn$ into H_{SSH} , the Hamiltonian can be divided into three parts:

$$H_{SSH} = H_e + H_{electron} + H_{lattice}$$

where
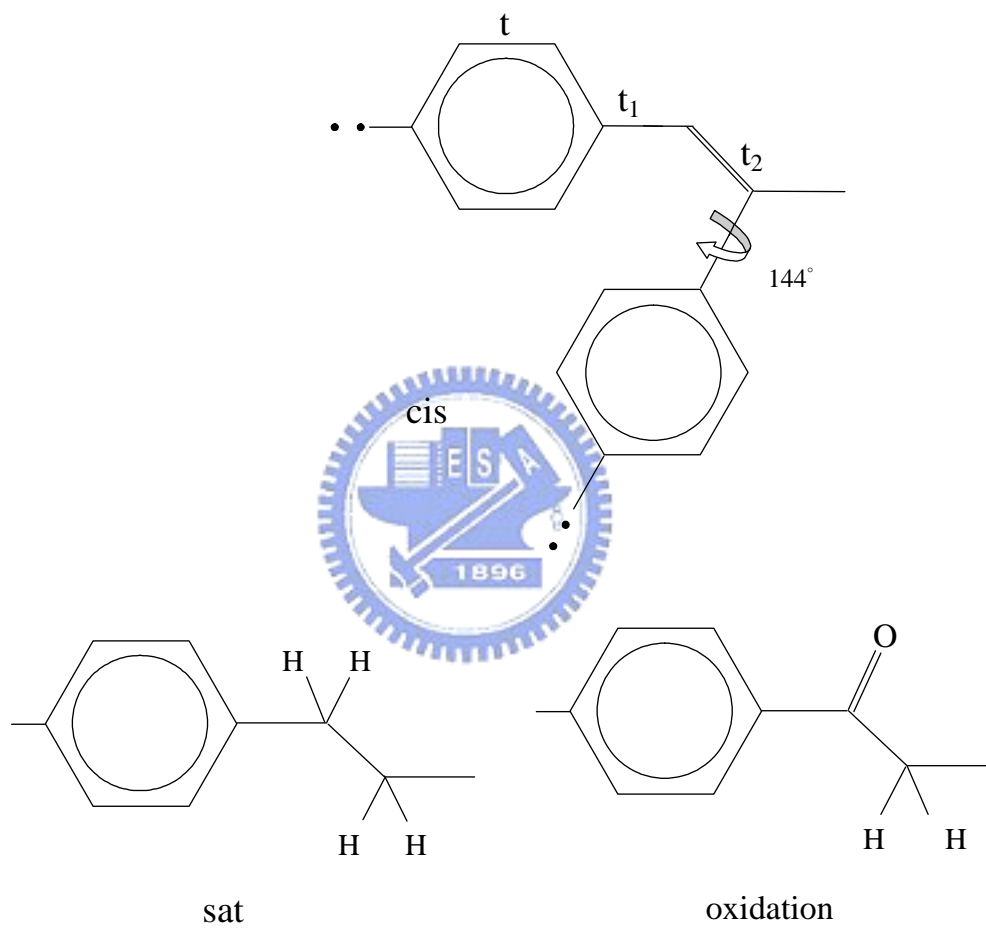
Figure 2.1: The defect of PPV are shown as (a) twinst defect (b) broken π-bound and binding with hydrogen (c) broken π-bound and binding with oxygen
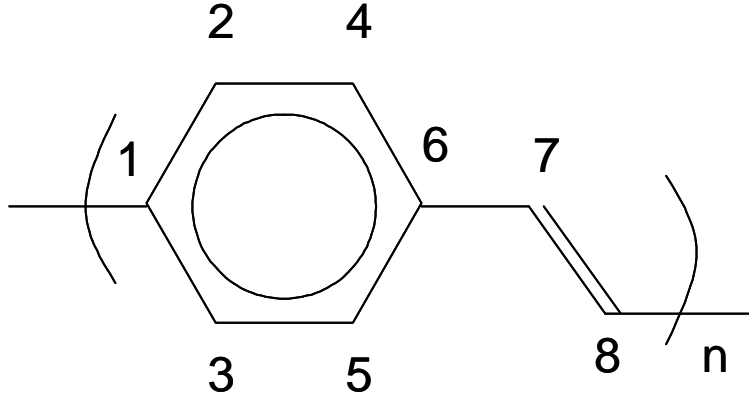
Figure 2.2: The chemical structure of PPV

$$H_e = -\sum_{n,s}[t_0 - t_1(-1)^n - \alpha(u_{n+1,n} - u_n)](C^\dagger_{n+1,s}C_{n+1,s} + C^\dagger_{n+1,s}C_{n+1,s})$$

$$H_{el} = \alpha\sum_{n,s}(v_{n+1} - v_n)(C^\dagger_{n+1,s}C_{n+1,s} + C^\dagger_{n+1,s}C_{n+1,s})$$

$$Hl = \frac{K}{2}\sum_n[(\overline{u}_{n+1} - \overline{u}_n)^2 + 2(\overline{u}_{n+1} - \overline{u}_n)(v_{n+1} - v_n) + (v_{n+1} - v_n)^2]$$

Conjugated polymers are often considered to originate from a one-dimensional system with one electron per carbon atom. It can be shown that such a system cannot exist as a one-dimensional metal with a half-filled band, but rather as an insulator with a gap forming at the Fermi level. For example, poly(p-phenylenevinylene) (PPV)(Fig. 2.2) the band structure is symmetry and the band gap is approach 2.8 eV by tight-binding method(Fig.2.3) a is lattice constance and k is wavelength. The Fermi level of PPV is at the middle of band gap and the properties is more like insulator than metal.

The number is the side index of polymer. The effective Hamiltonian of perfect PPV is shown below
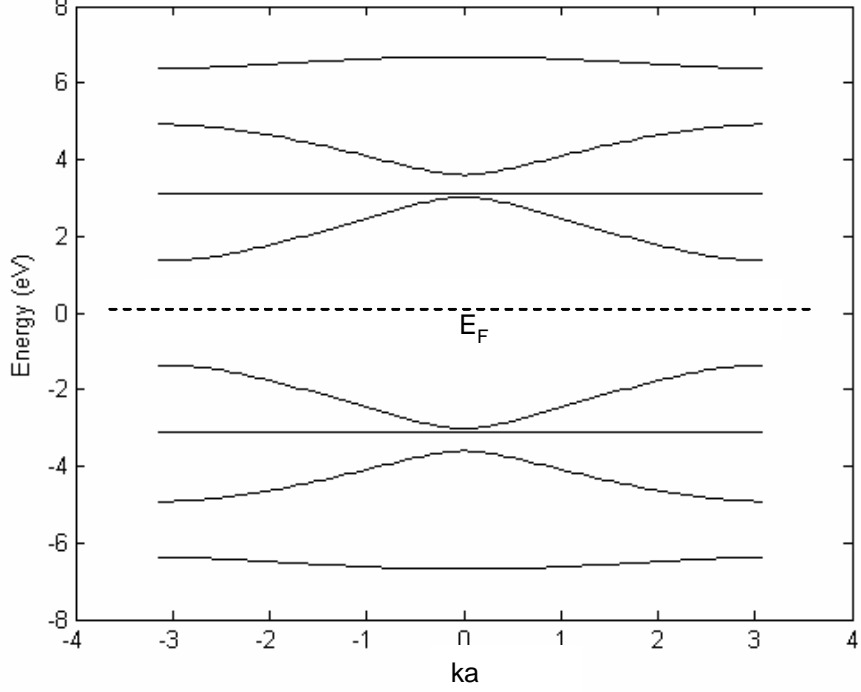
Figure 2.3: The band diagram of PPV

$$H_{PPV} = \begin{bmatrix} \varepsilon_0 & t & t & 0 & 0 & 0 & 0 & t_1 e^{-ika} \\ t & \varepsilon_0 & 0 & t & 0 & 0 & 0 & 0 \\ t & 0 & \varepsilon_0 & 0 & t & 0 & 0 & 0 \\ 0 & t & 0 & \varepsilon_0 & 0 & t & 0 & 0 \\ 0 & 0 & t & 0 & \varepsilon_0 & t & 0 & 0 \\ 0 & 0 & 0 & t & t & \varepsilon_0 & t_1 & 0 \\ 0 & 0 & 0 & 0 & 0 & t_1 & \varepsilon_0 & t_2 \\ t_1 e^{ika} & 0 & 0 & 0 & 0 & 0 & t_2 & \varepsilon_0 \end{bmatrix}$$

In this work we show theoretically by tight-binding model that, while the low-energy carriers are confined in l_c , the transmission coefficient of a carrier through a conjugation defect is not necessarily small for large incident wave number k measured from the band edge. Cis-defect4 (chain twist), sat-defect4 (double bond saturation by two sp^3 groups), and oxidation (carbonyl defect) are studied (Fig. 2.1). For cis-defect, the transmission probability T is 0.7 when $k = 0.11(\pi/a)$, corresponding to velocity 3.2×10^5 m/s and kinetic energy 0.04 eV. a=6.5 Å is the lattice constant. In terms of the electric field, the averaged

T over carrier distribution is equal to 0.7 when $E = 6 \times 10^7$ V/m. Sat-defect confines the carriers much more severely due to the insertion of two sp^3 groups. The carbonyl group is found to break the electron-hole symmetry and confines holes much more effectively than the electrons. In order to obtain the overall intrachain drift velocity v_d , the drift time within l_c determined by the bare drift velocity v_d^0 , and the "delay time" at the conjugation defect have to be added. The calculation is divided into three field regimes separated by $E_1 = 4 \times 10^7$ V/m and $E_2 = 10^8$ V/m. In the low-field regime ($E < E1$), polaron forms and v_d^0 is limited by the sound velocity v_s . In the intermediate field regime ($E1 < E < E2$), the carrier is free from lattice distortion but k is concentrated near the band minimum. v_d^0 increases roughly linearly with E. In the high-field regime ($E < E2$), k is distributed almost evenly in the first Brillouin zone (FBZ), and v_d^0 decreases with E as required by energy balance. The effect of the defects is more pronounced at lower field due to the large delay time. Cis-defects are assumed to be the dominant conjugation breaks,[157] because sat-defects and oxidation can be eliminated under proper synthesis conditions.[160] In the low-field regime with l_c=100 Å v_d is 3×10^3 m/s at $E = 1.1 \times 10^7$ V/m.[161] The corresponding mobility is seven orders of magnitude larger than the interchain mobility.[162] Simple estimate (see below) shows that net optical gain can be realized at such v_d for an active region of 1 mm wide. Device with aligned polymer chains and parallel injection is therefore predicted to be potentially suitable for polymer laser even with present defect density of about one per 15 repeat units.[157, 159]

2.4   The Transport efect of Defect

When a Bloch wave propagates toward a defect, it is partly transmitted and reflected. Our task is to obtain the scattering solution of the tight-binding Hamiltonian $\mid \pm k >$, which is a purely transmitted wave on one side of the defect, and a superposition of the incident and reflected waves on the other side (see Fig. 2.4). $\mid k >_s$ is incident from the left and $\mid -k >_s$ from the right. k is chosen to be positive. $\mid \pm k >$ denotes Bloch states in a perfect chain. So $\mid k >_s = \mid k >$ on the right side of the defect, while

$$\mid k >_s = \frac{1}{t} \mid k > + \frac{r}{t} \mid -k >$$

on the left side. The case for $\mid -k >_s$ is the reverse. t and r are the complex transmission and reflection amplitudes. Their absolute squares T and $R = (1 - T)$ are the transmission and reflection probabilities, respectively. In practice the tight-binding Hamiltonian is diagonalized in a finite but large ring with one defect. There are two nearly degenerate real eigenstates with different phase shifts across the defect at each energy inside the continuum, which can be labeled as $\mid k1 >$ and $\mid k2 >$ (Fig. 2.4). The scattering states $\mid k >_s$ can be constructed from linear combination of $\mid k1 >$ and $\mid k2 >$ with appropriate complex coefficients A and B, so chosen such that

$$A \mid k1 > +B \mid k2 >= \mid k >$$

on the right (transmitted) side. Decomposition of

$$A \mid k1 > +B \mid k2 >= \frac{1}{t} \mid k > +\frac{r}{t} \mid -k >$$

on the left (incident) side yields the coefficients t and r. The procedure is exact within the tight-binding model. T is shown as a function of incident energy in Fig. 2.5. The energy bands for a perfect PPV is also shown. For the conduction $(D1^*)$ and valence $(D1)$ band, T raises sharply at the band edges. In fact, $T \sim k^2$ for cis-defect and carbonyl defect, while $T \sim k^4$ for sat-defect. T decreases after a maximum occurring near the energy with highest group velocity. Even higher values can be reached in other bands. The flat L and L^*bands are neglected because carriers are immobile in them. Symmetric features are found for $\pm\varepsilon$ for cis- and sat-defects. For cis-defect, $T = 1/2$ when k is 0.073 (π/a). The corresponding velocity is 1.75×10^5 m/s and kinetic energy is only 0.02 eV, implying the cis-defect cannot limit the carrier in a conjugation segment effectively. The situation for the sat-defect is completely different. T is less than 10^{-3} for the entire conduction and valence bands. So the carriers are strictly confined in the conjugation segments. The electron symmetry is broken for the carbonyl defect, for which the transport of the hole is strongly suppressed but the suppression for the electron is only moderate. Since holes are the main charge carriers,[9] the result is consistent with severe degradation of device performance by oxidation. T from the two incident directions are slightly different for the carbonyl defect. Only results for incidence from the left (refer to Fig. 2.1) are shown. This approach can be applied to interchain transition, in principle. Because the distance between the p orbitals is usually more separated in interchain case than in the sat-defect, the transmission probability is expected to be even lower. Phonon-assisted field tunneling is believed to be the main mechanism for interchain charge transport.

Below we apply the results on the transmission probability T to obtain the relation between drift velocity vd and the electric field E. When a carrier travels in the perfectly conjugated segment between two defects, the drift velocity v_d^0 is determined by the phonon collisions. When the carrier hits the defect, it can either transmit or be reflected. If reflected, it will make a round trip and hit the same defect some time later, and so on (see Fig. 2.6). Eventually it will transmit after a time delay. Assuming the single round trip time is τ_r , the averaged time delay τ_d is

$$\tau_d = 0 + \tau_r(1-T)T + 2\tau_r(1-T)^2T + ... + n\tau_r(1-T)^nT + ... = \tau_r(1-T)/T \quad (2.1)$$
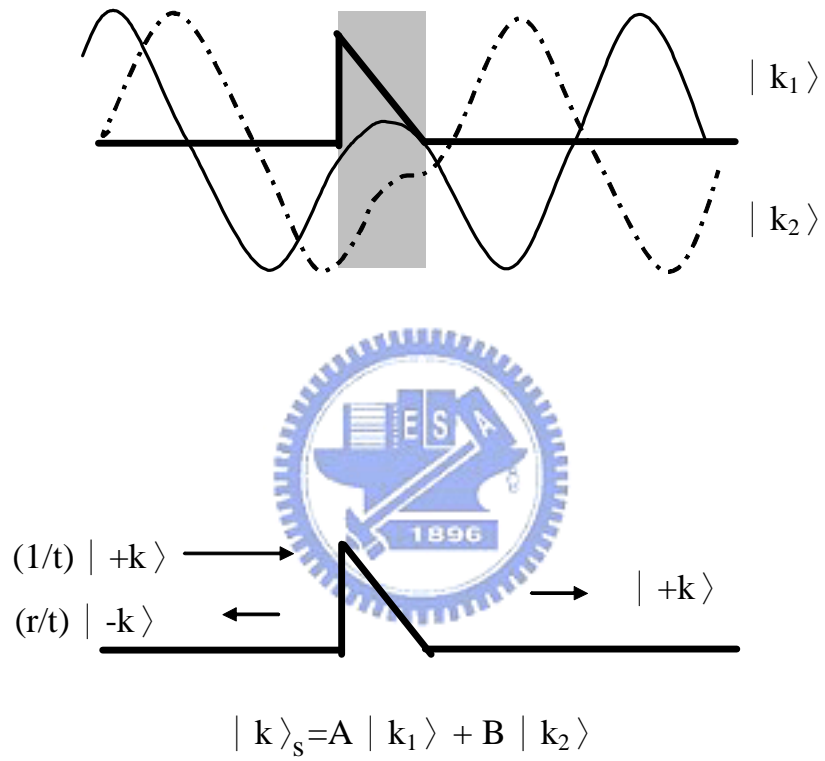
Figure 2.4: The transmission amplitude t and reflection amplitude r are obtained from the phase shifts of the real solutions $\mid k1 >$ and $\mid k2 >$ across the defects. The picture is illustrated by the analogy with an one-dimensional triangle potential barrier.
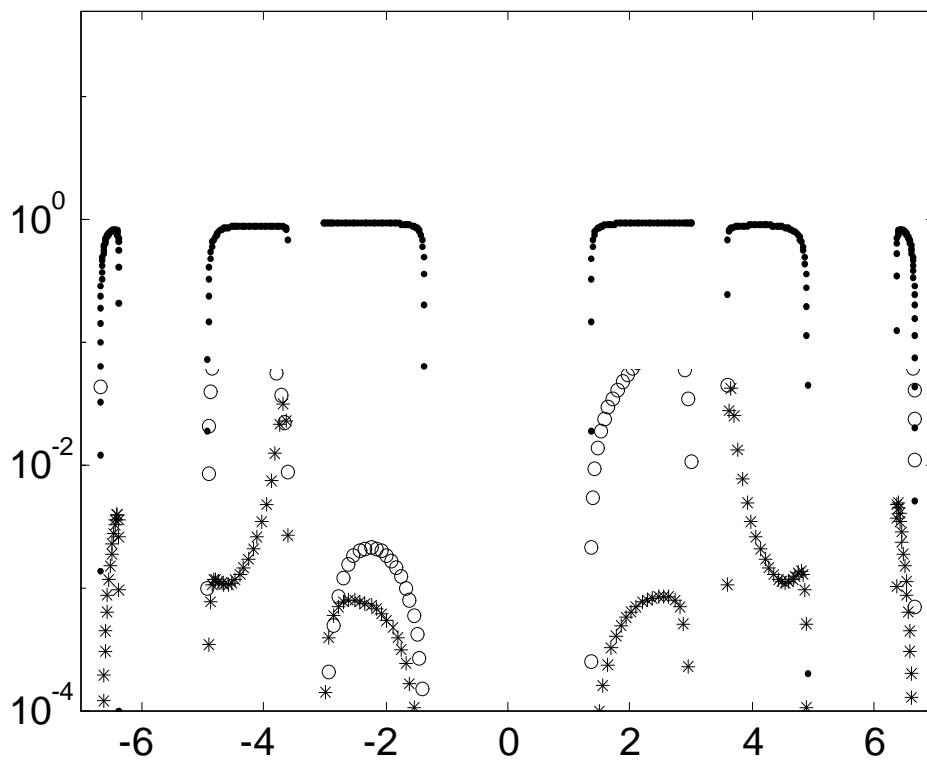
Figure 2.5: The transmission probability T for the three conduction bands and three valance bands is shown as a function of incident electron energy.

The nth term corresponds to transmission after n attempts. The drift time τ_c within l_c is l_c/v_d^0. With the defect, the overall drift velocity v_d is equal to $lc/(\tau_c + \tau_d)$. v_d^0 and τ_d depends strongly on the electric field, and have to be considered separately in the three field regimes. At low field, the carrier moves as a polaron, which is the combination of the carrier and the spontaneous lattice distortion around it.[168, 169] The polaron saturates around the sound velocity v_s, so we take $v_d^0 = v_s$. The wave function of the carrier is a wave packet with the same group velocity v_g, defined by

$$v_g(k) = \frac{\partial\varepsilon(k)}{\partial\hbar k}$$

$\varepsilon(k)$ is the energy band. The incident wave number k_i of the carrier upon the defect is so chosen such that $v_g(k_i) = v_s = 1.5\times10^4$ m/s. $T(k_i)$ is used for T in Eq. (2.1.) The round trip time τ_r in Eq. (2.1) for polaron has been determined by simulation on interchain hopping[169] to be 100 fs at $E = 10^7$ V/m. At other field τ_r is assumed to be inversely proportional to E. The reason is that during the round trip the polaron velocity is smaller than v_s and the lattice friction drops dramatically, so it moves like a free object obeying Newton's law. When E increases beyond $E1$, polaron dissociates and the carrier becomes free. Within l_c, the carriers are accelerated by the field, then suffers collisions with phonons. Their transport properties are determined by the distribution function $f(k)$. In the intermediate regime, the carriers are still distributed near the band edge. The mean wave number $k^* = eE\tau_{ph}/\hbar$ is much smaller than the FBZ size π/a. τ_{ph} is the phonon collision time. Assuming a shifted Maxwell distribution with adjustable electron temperature T_e, $f(k)$, and v_d^0 can be obtained from the energy balance condition

$$eEv_d^0 = \frac{k_B(T_e - T_l)}{2\tau_{ph}}$$

$T_l = 300$ K is the lattice temperature. τ_r is equal to τ_{ph} because of the predominance of back scattering with acoustic phonons.19 The averaged value $T = \int T(k)f(k)dk$ after traveling over many conjugation segments should be used to obtain the delay time τ_d in Eq. (2.1).

In the intermediate regime, the drift velocity v_d^0 satisfies the balanced momentum and energy equations

$$mv_d^0 = eE\tau_{ph} \ . \quad eEv_d^0 = \frac{1}{2}(T_e - T)\frac{k_B}{\tau_{ph}} \tag{2.2}$$

m is the carrier effective mass. $\frac{1}{2}k_B(T_e - T_l)$ is the amount of energy dissipated from the electronic system to the lattice upon each emission of phonon. $\frac{1}{2}k_BT_e$ is the averaged initial electronic energy, and $\frac{1}{2}k_BT$ is the final electronic energy because the phonon emission tends to restore the system to equilibrium with the lattice at temperature T. Multiplying the above two equations we obtain

$$k_B(T_e - T_l) = \frac{2(eE)^2\tau_{ph}^2}{m}$$

40
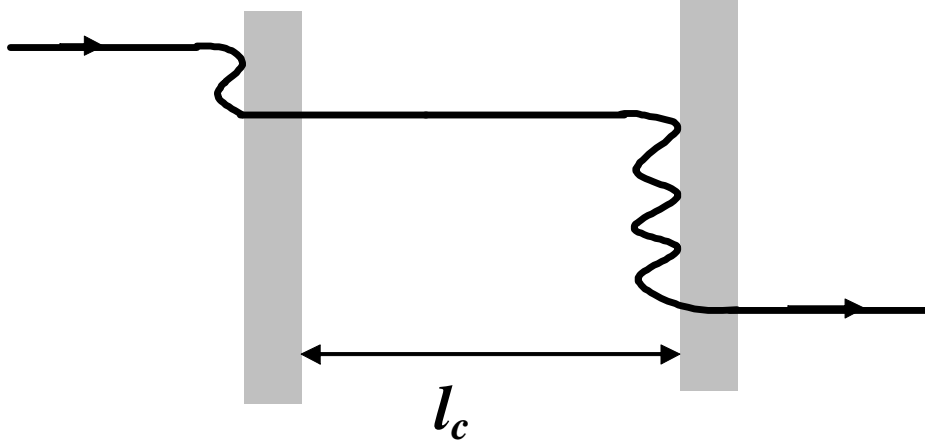
Figure 2.6: The carrier hit the defect one or more time before tranmitting through.

.

The dissipated energy increases with E quadratically. The increasing dissipation power is crucial to balance the Joule heating eEv_d^0 as the field rises and maintain a stable $f(k)$ near the band edge. However, the dissipated energy cannot exceed the optical phonon energy $\hbar\omega_0 = 0.17$ eV. Moreover, unlike the case of inorganic semiconductors, $\tau_{ph} = 10$ fs is almost independent of the carrier energy[172, 173] because the density of state does not increase with energy. Consequently, the dissipation power saturates at $\hbar\omega_0/\tau_{ph}$ when the mean carrier energy $\frac{1}{2}T_e k_B$ is larger than $\hbar\omega_0$. Without an increasing phonon emission rate to stabilize $f(k)$ around the band edge, the group velocity vg(k) of the carrier will blow up indefinitely as E further rises until it reaches the maximal group velocity determined by the band structure. Beyond the maximum, vg starts to decrease and become negative after traveling half of the FBZ. Eventually $f(k)$ is stabilized by the finite bandwidth, and is expected to be very flat. The critical field E_2 is determined by $\frac{1}{2}T_e k_B = 2\hbar\omega_0$. Beyond E_2 , $f(k)$ simply approximated as a constant throughout the FBZ and we use $T = (a/\pi) * \int_0^{\pi/a} T(k)dk$ for Eq. (2.1). From the modified energy-balance condition $eEv_d^0 = \hbar\omega_0/\tau_{ph}$,v_d^0 is inversely proportional to E as

$$v_d^0 = \frac{\hbar\omega_0}{eE\tau_{ph}} \tag{2.3}$$

t_r is determined by Bloch oscillation, which is now faster than the phonon back scattering. v_d^0 and v_d are shown as functions of E in Fig. 2.7. As E

increases, the effect of the defects become weaker so v_d and v_d^0 are closer. The jump at $E_1 = 4 \times 10^7$ V/m is the signature of the polaron dissociation. Note the negative slope in the high-field regime due to Eq. (2.3). For cis-defects, the corresponding mobilty μ is about 10^{-4} m^2/Vs for polaron ($E < E1$), and rise to about 10^{-3} m^2/Vs after polaron dissociation . Despite of the high conjugation defect density (1 per 15 repeat units), μ is six orders of magnitude larger then the bulk mobility (10^{-11} m^2/Vs),[162] 100 times larger then amorphous silicon ($10^{-6} \sim 10^{-5}$ m^2/Vs),[174] and comparable to polycrystalline silicon ($10^{-4} \sim 10^{-3}$ m^2/Vs).[174]Parallel charge transport is therefore a potential solution to the mobility problem in conjugated polymer devices. However, μ is 100 times smaller if the main conjugation defects are the carbonyl groups. For sat-defect, μ is it $5 \sim 7$ orders of magnitude smaller, so the transmission is practically negligible.

The cross sections for exciton gain and for polaron induced absorption are nearly equal in the spectral region where they overlap.[156] So net gain can be achieved only when the exciton density n_{ex} is higher than the polaron density n_p . Considering an active region with area A and thickness w sandwiched between two electrodes. In the steady state the exciton decay must be compensated by the current injection. So we have

$$\frac{Awn_{ex}}{\tau_{ex}} = An_p v_d$$

, where $\tau_{ex}$is the exciton lifetime. The threshold condition $n_{ex} = n_p$ gives the critical drift velocity $v_c = w/\tau_{ex}$. Using $\tau_{ex} = 0.3$ ns and $w = 1$ μm, we get $v_c = 3.3 \times 10^3$ m/s. This value can be achieved for intrachain transport with $E = 10^7$ V/m. Assuming oxidation and sp^3 saturation can be avoided, PPV chains with average conjugation length equal to 100 Å and aligned over 1 mm are therefore expected to achieve net gain under parallel electric bias at 10 V.

In conclusion, the transmission probability for a carrier to tunnel through a variety of conjugation defects in conjugated polymers is calculated exactly within the tight-binding method for arbitrary incident energy. Contrary to the general belief, it is found that the typical conjugation defect (cisdefect) does not confine the carriers effectively. As a result, the effective mobility can be as high as 10^{-3} m^2/Vs for electric field above 4×10^7 V/m. It implies that the difficulties related to the low mobility can be eliminated, in principle, by better control over the chain alignment in solid state even with present level of conjugation defects.
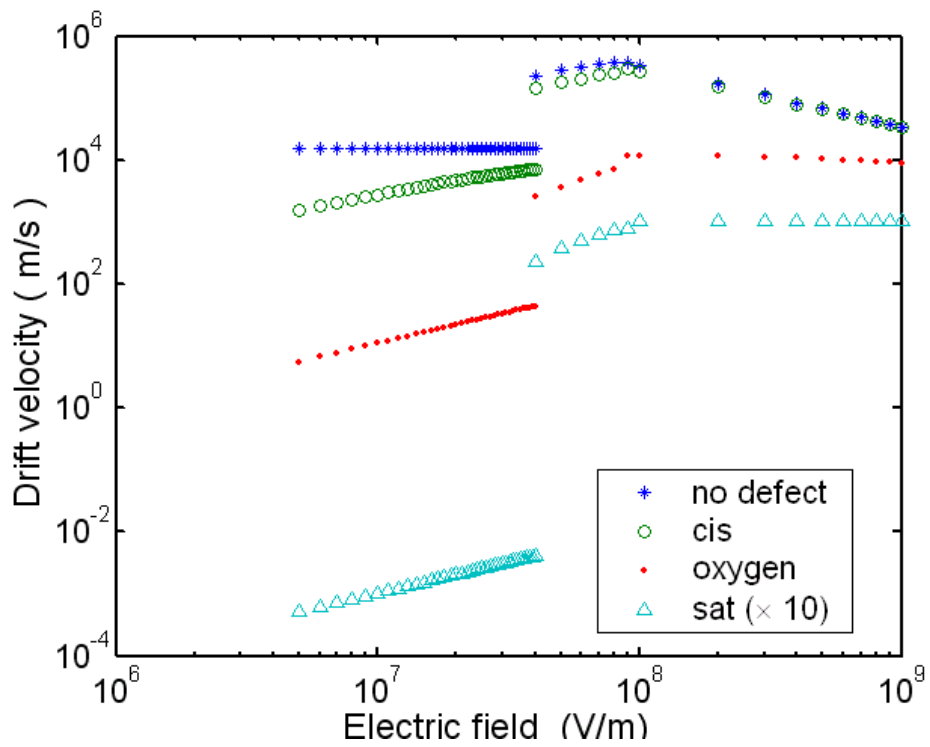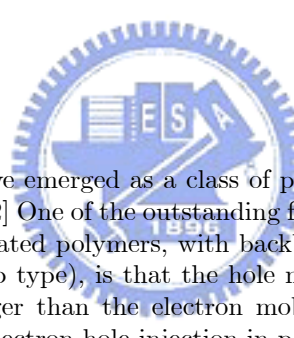
Figure 2.7: The drift velocity is shown as a function of the electric field for three kinds of defects at the same density (one per 15 repeat units). The discontinuity at $E = 4 \times 10^7$ V/m is due to polaron dissociation.

Chapter 3

Theory of imbalanced electron-hole transport in conjugated polymers

Conjugated polymers have emerged as a class of promising materials for optoelectronic applications.[72] One of the outstanding features of the highly electroluminescent sELd conjugated polymers, with backbones containing exclusively carbon atoms (so-called p type), is that the hole mobility is in general several orders of magnitude larger than the electron mobility.[175, 176] This imbalance causes unmatched electron-hole injection in polymer light-emitting diodes and is a major limit for their efficiency. This is quite surprising because the electron and hole effective masses differ by no more than a factor of 2 in ab initio calculations.[177] On the other hand, in the so-called n-type conjugated polymers, whose backbones contain oxygen or nitrogen atoms, the situation is reserved and the holes have a lower mobility than the electrons.[178] Microwave experiments demonstrated that the electron and hole mobilities are similar when the polymer chains are isolated in solution,6 suggesting that the imbalance is related to the traps due to the structure defect levels in the films. However, as shown by the tight-binding calculation below, the structure disorder causes defect levels with electron-hole symmetry and cannot be the reason for the imbalance by itself. Little is known about how the symmetry is broken in transport.

3.1   Defect Structure

In this work we propose that there are two origins for the imbalance in the carbon-backbone EL conjugated polymers, e.g., poly(p-phenylene vinylene) (PPV),

polyfluorene (PF) and polythiophene (PT). The first is the compensation of the hole traps due to structure defects by the background unintentional p doping, which generally occurs because of the relatively smaller electron-negativity (EN) of the polymer. Because the deepest traps are compensated first, a slight amount of compensation has a dramatic effect on the mobility. The second origin is that oxidation of the polymers causes electron traps but not hole traps. Oxygen has a lower on-site energy (higher EN) than the carbon, and causes a local potential well for the electrons but not for holes. In n-type polymers no traps are caused by oxidation because the energy of the bands of the O- and N- containing backbone is close to the energy of the addition oxygen. The asymmetric effect of oxidation is confirmed by tight-binding calculation for both p- and n-type polymers. The consequence of trap compensation by doping on transport properties is studied in detail by calculating the carrier field-tunneling rate out of the traps, and the mobilities as functions of doping density and electric field. It is found that balanced electron-hole mobility can be achieved by tuning the intentional n doping, or equivalently Fermi level, for the p-type polymers.

The band structure and trap position are calculated within the tight-binding model for PPV and PF. The chemical structures of the two polymers are shown in Fig. 3.2. The nearestneighbor resonance integrals are also indicated. The values used for perfect polymer chains are $t = -3.1, t1 = -2.2, t2 = -3.0$ for PPV, $t = -3.1, t1 = -2.2, t3 = -3.0$ for PF, and $t1 = -1.7, t2 = -2.3, tb = -1.3, ts = -1.4$ for PT in order to reproduce the band structure obtained from ab inito calculation. $t, t1$ and $t2$ are the off-diagonal resonance integrals for the carbon phenyl, single, and double bonds, respectively. Likewise tb is the hopping between two thiophenes, and ts is the hopping between carbon and sulfur(Fig. 3.1).

The t's are adjusted to fit the conduction and valance band structures obtained from more sophisticated methods.[177, 180] The band structures have an exact electron-hole symmetry, with the Fermi level EF located at zero energy (Fig. 3.2). The symmetry can be slightly broken if we introduce the small second nearest neighbor resonance integral.[181] Now we consider the structure defects which cause energy levels in the energy gap (carrier traps), neglecting ring distortions and considering a one-bond defect in one single repeat unit, with all other units remaining perfect. In practice a long chain with 50 units and periodic boundary condition is diagonalized. For PPV, defect levels can be caused only by the reduction of the double-bond resonance integral t_2 in the vinyl group[163] because local reduction of t_2 causes a smaller local vinyl double splitting which sets the band gap. Reduction of single bond t1 does not cause any defect level.[163] For PF, defect level occurs only for increase of the bridge bond tb because it causes larger splitting between the molecular orbitals of the two rings and pushes the levels closer to zero. No defect level occurs for tb reduction. A tb increase is less likely to happen compared with t_2 twist, so fewer traps are expected in PF.[55] In Fig. 3.2 the energy of the defect levels are shown as functions of the bond distortion. t_0 is the resonance integral for the
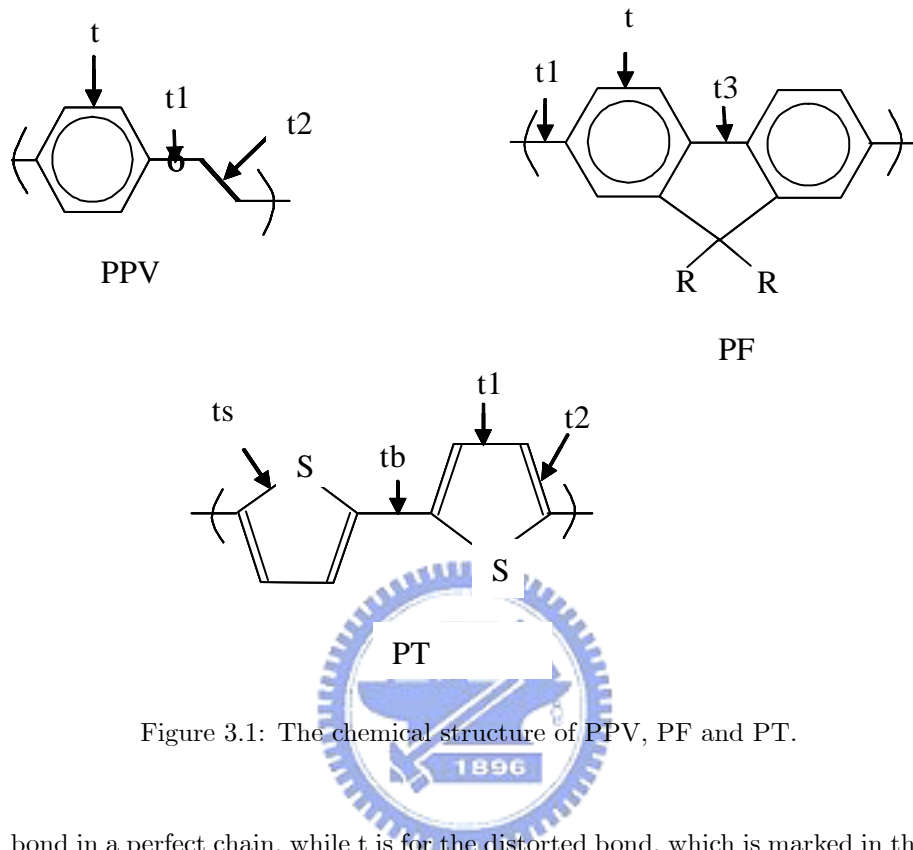
Figure 3.1: The chemical structure of PPV, PF and PT.

bond in a perfect chain, while t is for the distorted bond, which is marked in the polymer chemical structures. For intrinsic polymers the defect levels are symmetrically placed around E_F. There is therefore a one-to-one correspondence between the electron traps (above E_F) and hole traps (below E_F). We have considered many other defects for PPV and PF, including distortions in more than one bond, sp^3, and cross-links. None of them introduce asymmetric defect levels. This is consistent with the defect positions measured experimentally.[183] Structure defects in the film alone therefore cannot account for the great imbalance in carrier transport. We believe that imbalance is caused by the hole-trap compensation discussed below.

The highly electroluminescent polymers contain only carbon atoms in the p-backbone. Because the EN of carbon (2.5 eV) is smaller than the EN of other common atoms like nitrogen (3.0 eV), oxygen (3.5 eV), and chlorine (3.0 eV) in organic materials,[184] the electrons will transfer from the EL polymer to the nearby residual molecules in the film which contain N, O, and halogens. We believe that such a difference in EN and the resulting electron transfer is the reason for the prevalent unintentional background p doping. Such p doping introduces shallow empty acceptor levels just above the valence band, the electrons in the defect levels will drop into the empty acceptor levels such

46
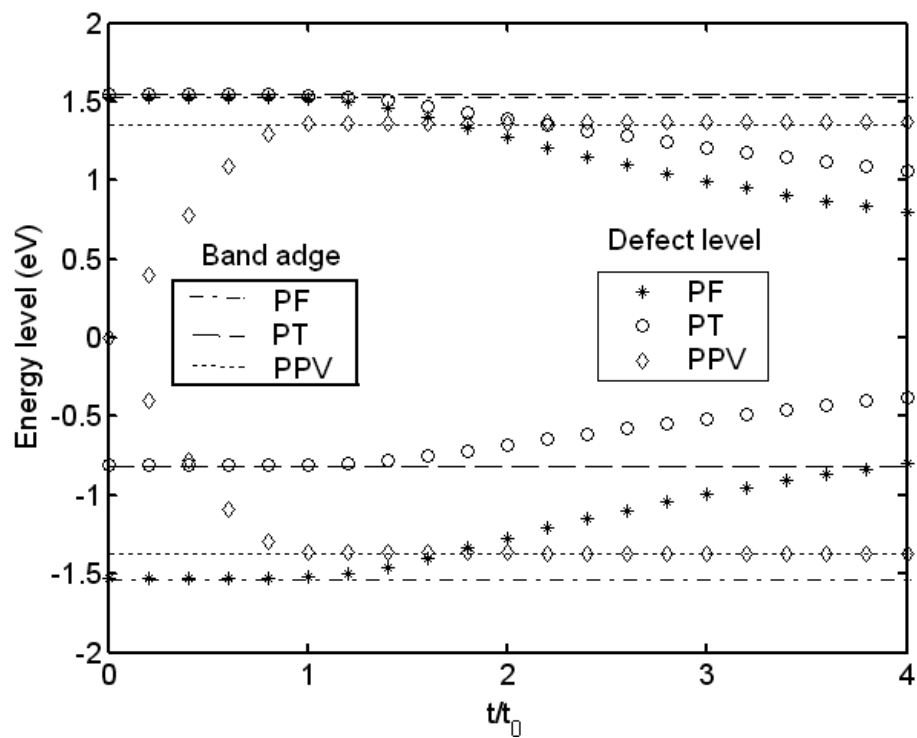
Figure 3.2: The energy bands and defect levels for PPV, PF and PTare shown. The defect levels are symmetric with respect to the Fermi level at zero energy. The distorted bonds are indicated in the chemical structures.

that the defect levels become empty and inactive for the holes. In other words the defect traps are compensated by the shallow acceptor levels [Fig. 3.3(a)]. If the residual molecule happens to be close to the structure defect, it is also possible that the electron transfers directly from the defect level to the molecule without the intermediate step through the shallow level. Similar to the case of p doping, with n doping the electrons in the donor level can drop into the electron traps (empty defect levels) and make them inactive, i.e., the electron traps are compensated by the donor levels [Fig. 3.3(b)]. The inactivated hole traps can be reactivated by the additional n doping because the extra electrons can fill up the empty defect levels. One can therefore control the ratio between the active electron and hole traps by intentionally n doping a polymer film with an unintentional background p doping. Mobility ratio is changed accordingly. For the N and O containing polymers the EN of the backbone is larger than most residual molecules. So they are background n doped instead. Higher electron mobility results from compensation of electron traps.

Now we consider the role of oxidation in the imbalance with a tight-binding model for the oxygen defect. We use poly (p-pyridyl vinylene) (PPyV, see Fig. 3.4) as a model system. The on-site energy ε_O and ε_N for O and N atoms are -2.2 and -1.3 eV, respectively.[164] They are roughly proportional to the EN differences with the carbon atom. In order to illustrate the key point that oxygen is effective in causing electron trap only for p-type polymers, ε_N is artificially adjusted to tune the EN of PPyV. For simplicity, two O atoms are assumed to be attached symmetrically to one unit of PPyV in the oxidized form (Fig. 3.4) while other units remain perfect. ε_O is taken as a variable artificially as well. PPyV reduces to PPV as ε_N=0. The resonance integral for the O–C bond is -2.2 eV,13 and -1.4 eV for the N–C bond to fit the band gap of PPyV.[185] For fixed ε_N, a defect level emerges from the conduction band, with wave function localized around the oxygen atom if $|\varepsilon_O|$ exceeds a critical value (Fig.3.4). The larger $|\varepsilon_O|$ is, the more electronegative the oxygen is relative to the backbone. So eventually the oxygen pulls an empty level off the tight-binding continuum which acts as an electron trap. Oxidation does not cause hole trap, even though it limits the motion of the free holes severely.[186] Because whether there is a trap is determined by the relative EN of the oxygen and the backbone, we artificially adjust the EN of the backbone by changing ε_N. As we increase $|\varepsilon_N|$ the backbone evolves from a p-type to an n-type polymer (increasingly electronegative). As expected the binding energy decreases as ε_N increases (and the EN difference between the backbone and the oxygen defect diminishes). A similar level appears for oxidized PF also. These results demonstrate that the oxidation of the p-type EL polymers is at least partially responsible for the dominance of electron traps and the breaking of the electron-hole symmetry. In reality we expect that oxidation and structure disorder coexist and both contribute to the electron traps. Their relative importance depends on the preparation of the particular sample. For the n-type polymers (large $|\varepsilon_N|$) there are shallower or no electron traps even if they are oxidized. The change of the conduction and valence band edges $E_{c,v}$ are shown in Fig. 3.5. Lower band edge implies a smaller electron injection barrier, another feature of n-type
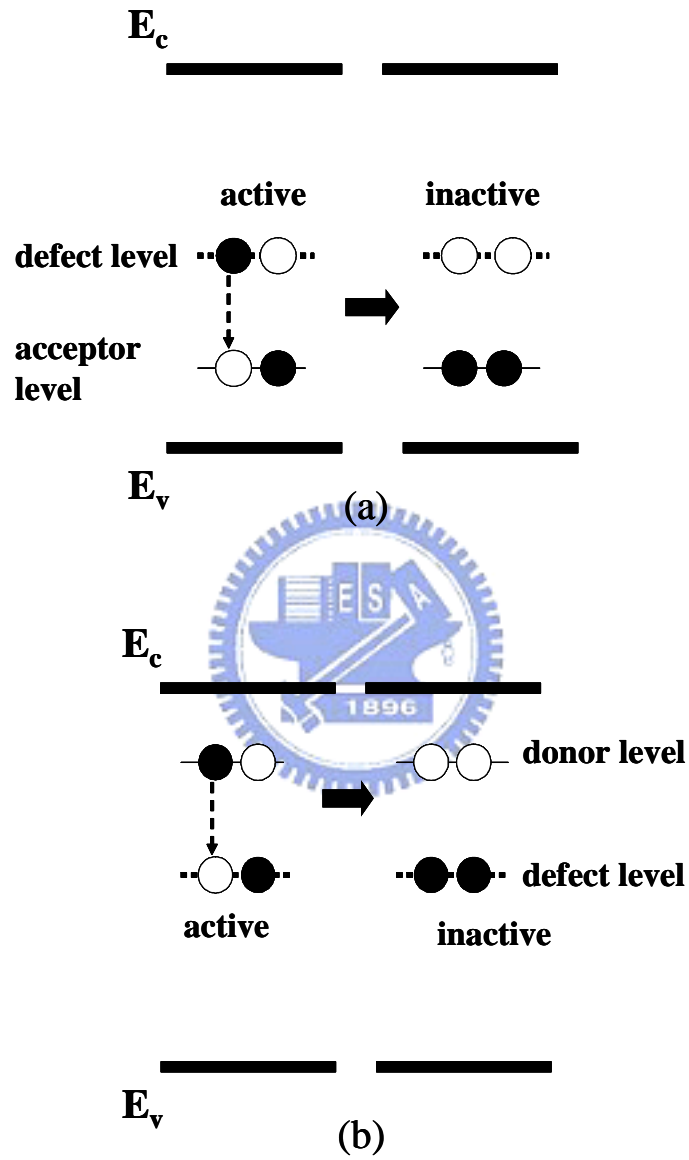
Figure 3.3: (a) The hole trap (occupied defect level) is compensated by p doping. (b) The electron trap is compensated by n doping. Closed circles: occupied. Open circles: empty.
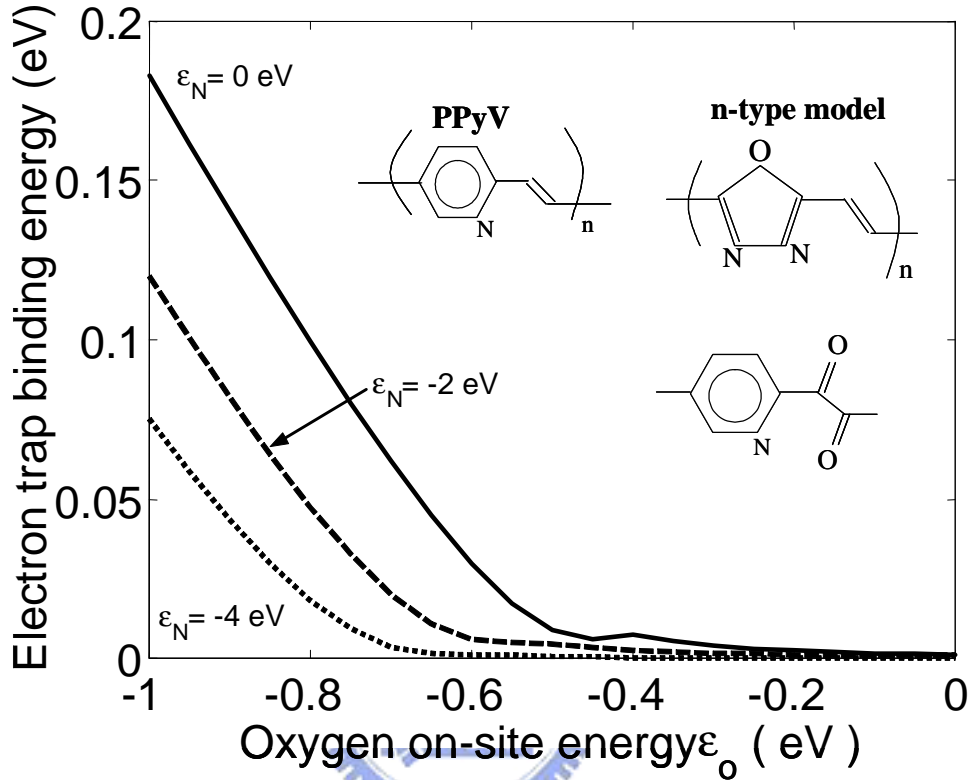
Figure 3.4: The binding energy of the defect level of PPyV due to oxidation is plotted as a function of oxygen on-site energy ε_o for polymers with various electron negativity tuned by nitrogen on-site energy ε_N.

polymers. We also consider the oxidation of another hypothetical model n-type system poly(oxadiazole vinylene) (Fig. 3.4) and found that there is no defect level for ε_O=-2.2 eV and ε_N=-1.3 eV. Obviously the large amount of N and O in the backbone make the additional O insignificant. It is reported that there are many hole traps in the n-type polymers,5 suggesting that those traps are exclusively due to uncompensated tructure defects since oxidation is not expected to cause traps.

3.2 Defect and Tunneling

So far we have considered only a single trap. The mobility is determined by the trap distribution and E_F, which is controlled by doping. In order to make
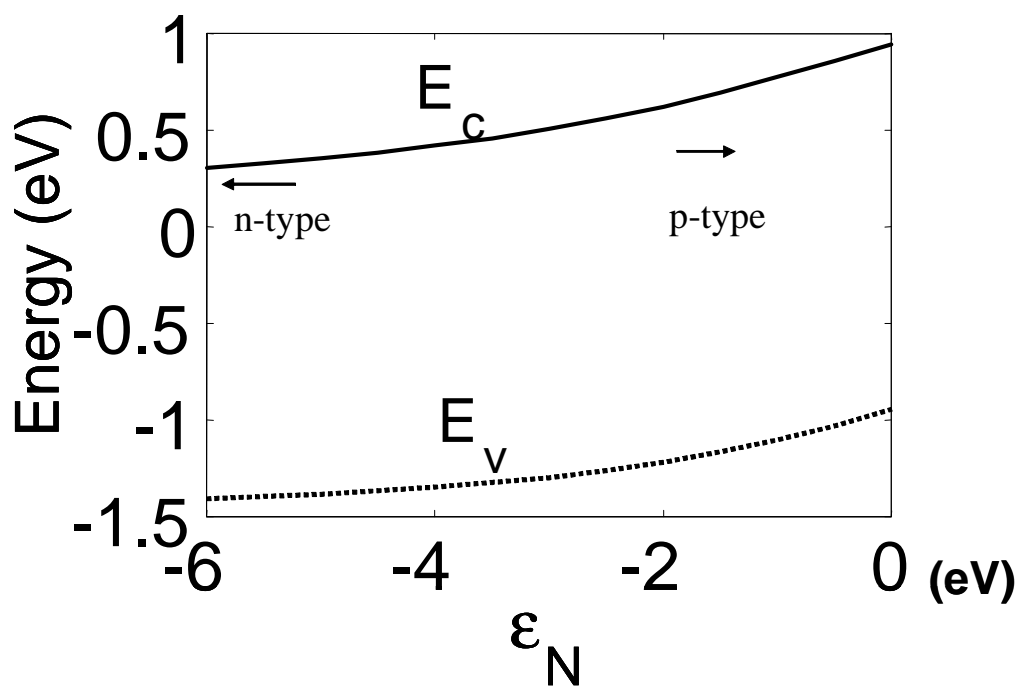
Figure 3.5: The defect is deeper for less electronegative polymer (smaller | ε_N |, p type). The chemical structure of PPyV and the model n-type polymer are shown.
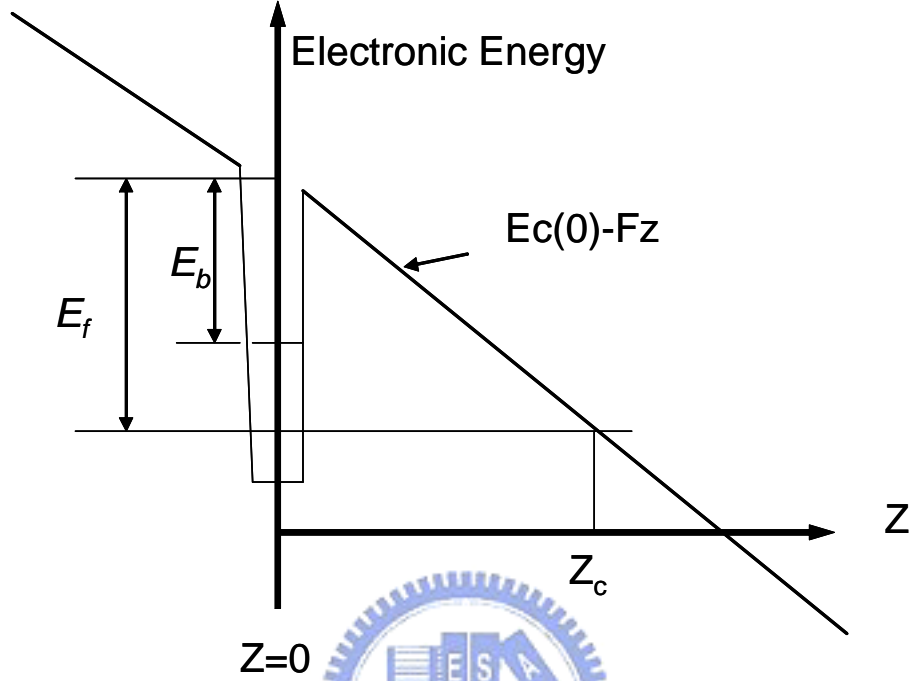
Figure 3.6: Energy diagram in the presence of an electric field F

quantitative predictions on the relation between carrier mobilities and doping, we need the carrier escape rate from the trap as a function of applied electric field F and trap binding energy ε_T. The phonon-assisted field tunneling from a point defect level in inorganic crystalline semiconductors is studied by Makram-Ebeid and Lannoo.[192] Even though conjugated polymer film is not a crystal, this theory can be applied because tunneling is a process which occurs within a conjugation segment with local one-dimensional periodicity and energy bands. The immediate final state of the tunneling is an extended intrasegment wave function as in inorganic semiconductors. Interchain hopping occurs only afterwards as subsequent independent processes and will be discussed later. The tunneling rate W from the trap is

$$W = \frac{2\pi}{\hbar} Av_b \sum_f |<\psi_b \varkappa_b \mid -eFz \mid \psi_f \varkappa_f >|^2 \, \delta(E_f - E_b) \qquad (3.1)$$

where Av denotes the thermal average. b and f indicate bound and free states, respectively. $\psi_{b,f}$ is the single-electron wave function and $\varkappa_{b,f}$ is the lattice wave function. $\psi_{b,f}\chi_{b,f}$ are the Born-Oppenheimer products. The field
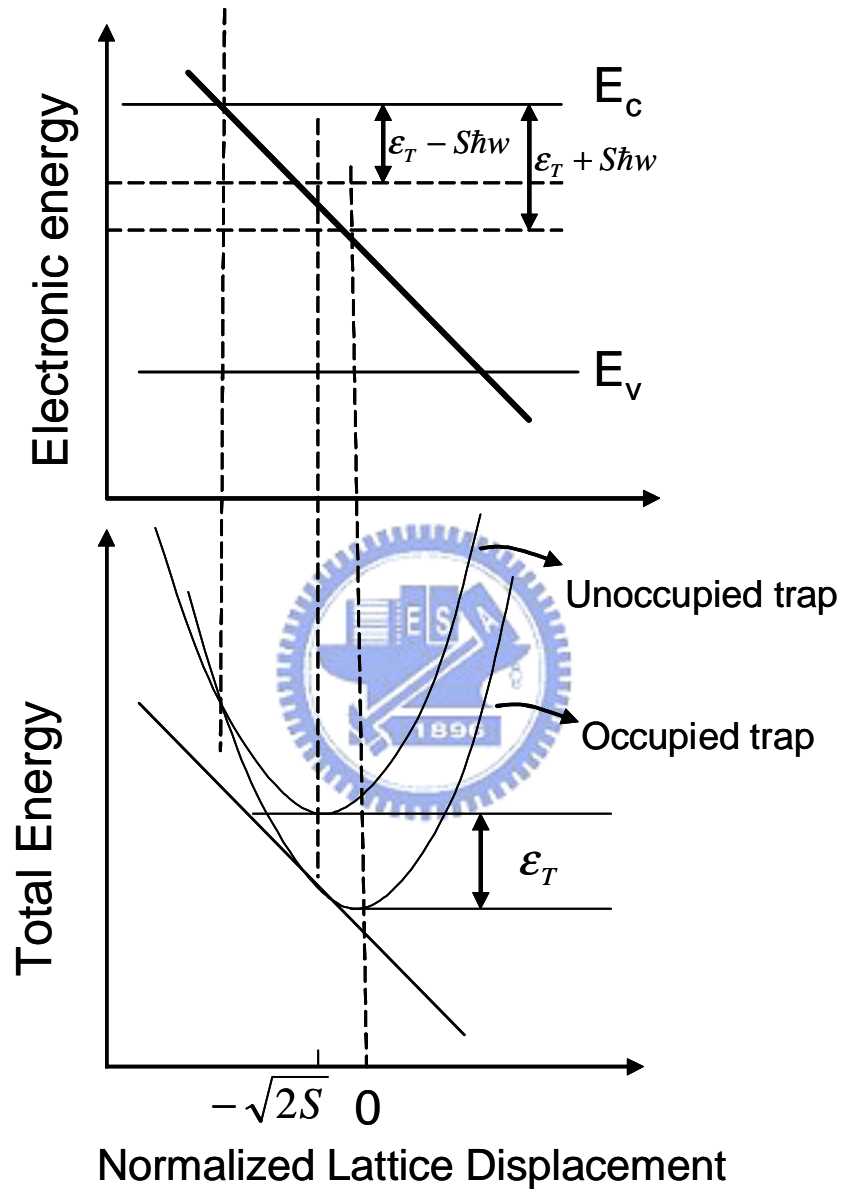
Figure 3.7: Configuration diagram showing the electron energy (above) and the sum of elastic and electron energy as a function of the generalized lattice coordinate.

F is applied along the z direction. In terms of the binding energy ε_T the escape rate can be written as[187]

$$W = \sum_{m=-\infty}^{\infty} W_m P(\varepsilon_T + \hbar w/2kT)$$

where

$$P(\varepsilon) = \frac{F}{2\hbar}(\frac{\hbar^2}{2m^*})^{1/2} \exp[\frac{-4}{3}(\frac{2m^*}{\hbar^2})^{1/2}\frac{\varepsilon^{3/2}}{F}]$$

$$W_m = \{\exp[\frac{-2\eta}{\sqrt{2S}}][(1 + \frac{\eta}{\sqrt{2S}})/(1 - \frac{\eta}{\sqrt{2S}})]\}^m \times W_m^0[S(1 - \frac{\eta^2}{\sqrt{2S}})]$$

and

$$W_m^0(S) = \exp[m\hbar w/2kT - S\coth(\hbar w/2kT)] \times \text{Im}[S/\sinh(\hbar w/2kT)]$$

Im is the Bessel function. m is the difference between the phonon numbers of the final and initial states. η is $-2(2S)^{1/2}\hbar w/\varepsilon_T$, k is the Boltzman constant, and T is temperature. $\hbar w$=0.17 eV is the optical phonon energy. The effective mass m^* is obtained from the band structures. The resonance integral of the distorted bond is expressed as $t(x) = t\mid_x^0 (1 + \alpha x)$. t is the resonance for the empty distorted bond which determines ε_T. x is the bond length change. α =4.1 eV/Å(Ref. [188]) is the effective electron-phonon coupling constant. The dimensionless lattice coordinate Q is defined by $x = \sqrt{\hbar/MvQ}$, where M is the carbon atom mass.[189] Using Fig. 3.2 and $t(x)$ the defect electronic energy can be expressed as a function of Q. When the defect is occupied the total energy is the sum of the electronic energy and the lattice energy $\hbar wQ^2/2$. The equilibrium lattice coordinate Q^* is located at the minimum of the total energy. The Huang-Rys factor S is $Q^{*2}/2$. The point defect escape rate W is plotted in Fig. 3.8. The rate drops several orders of magnitude as the binding energy ε_T increases. So the existence of a few deeper levels can have a dramatically large effect on the overall transport. The ionized acceptor/donor may also cause shallow traps for the carriers which are self-localized as polarons. For the polarons the escape rate out of the shallow ionic potential is given by[190]

$$W_{ion} = \frac{w_p}{2\pi} \exp(-\varepsilon_T + e_f/kT)$$

where $e_f = 2\sqrt{e^3F/\kappa}$. $\kappa = 8$ is the dielectric constant. ε_T is the barrier of the averaged ionic Coulomb potential experienced by a polaron. w_p is the oscillation frequency of the polaron around the bottom of the averaged potential well. The rates are shown in Fig. 3.8. The vertical distance between the ion and the backbone is taken as 2 Å about half the interchain distance.[191] The barrier disappears for a typical field around 10^8 V/m in a light-emitting diode. So the
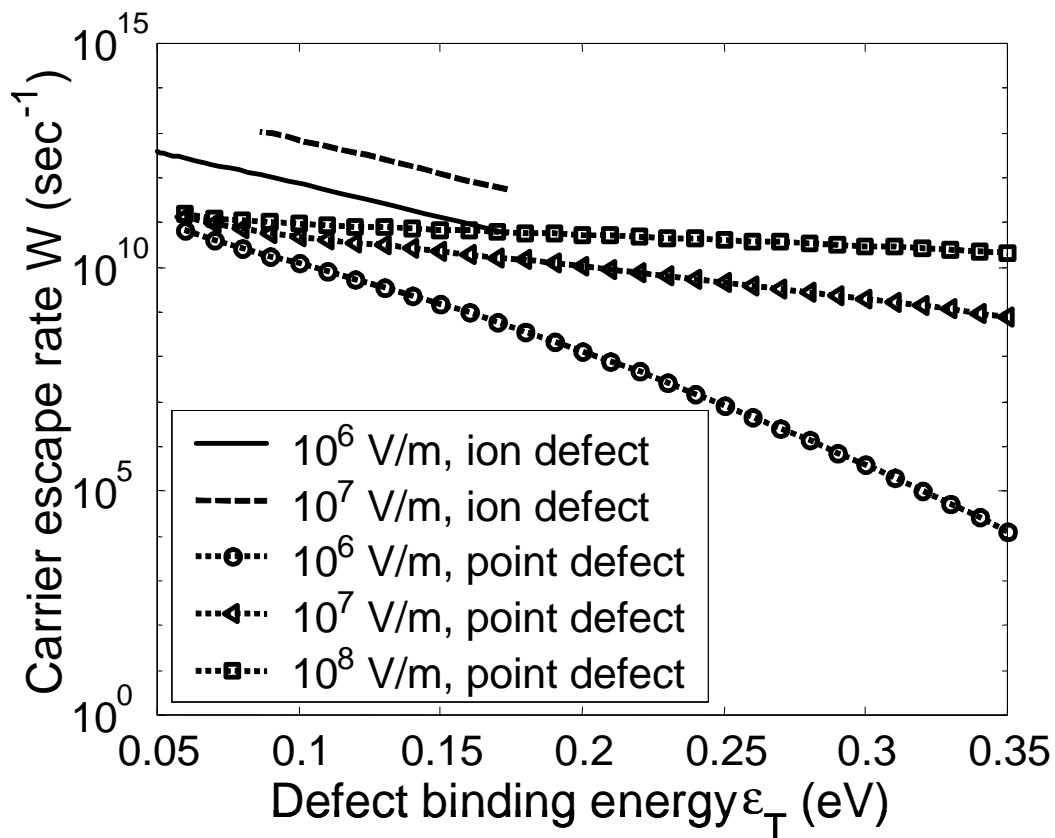
Figure 3.8: The escape rate W out of the trap is plotted as a function of the trap binding energy ε_T. The rate for shallow ionic defect due to doping is also shown. The electric field F is indicated.
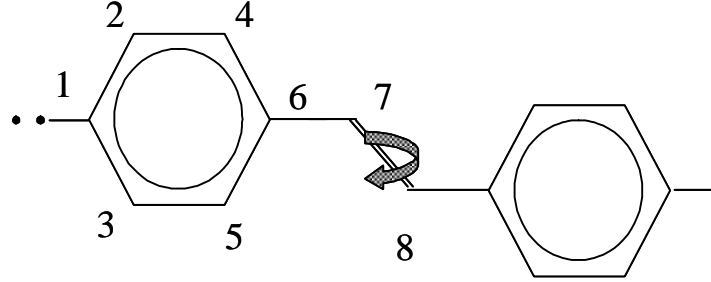
Figure 3.9: We trate the twins bond of PPV and get the structure defect.

ionic defects can hardly trap the carriers and are neglected in the calculation of mobilities.

3.3 Escape Rate

We consider that a p-type conjugated polymer, PPV, has intrinsic defect. The defect is induced from double bond twist, Fig. 3.9, i.e. such defect is structure defect. This kind of defects, which are induced from twist double band, are symmetric. It means that the defect is the same for electron and hole and the mobility of electron and hole are the same if there is no extrinsic carrier. But there are some inescapable impurities in the PPV from synthetic process and cause from PPV is p-type polymer. We assume this kind of impurity will apply the extrinsic hole to PPV and compensate the deep level of defect of hole. We calculate the hole and electron velocity at this picture, and apply another impurity into the PPV, which the impurity induce a shallow defect of electron and apply extrinsic electron into the polymer.

We consider the structure defect as point defect and the tunneling probability is

$$P(\varepsilon) = \frac{2\varepsilon}{3\hbar}\frac{e^A}{A} = \frac{F}{2\hbar}(\frac{\hbar^2}{2m^*})^{1/2}\exp[\frac{-4}{3}(\frac{2m^*}{\hbar^2})^{1/2}\frac{\varepsilon^{3/2}}{F}], \qquad (3.2)$$

where $A = 4/3 * (2m^*/\hbar^2)^{3/2}(\triangle_f)^{3/2}/F$, F is electric field and m^* is carrier effective mass. The defect carrier level is taken to be at an energy $\triangle_f$ under the band, under applied electric field F, varying linearly with the z position. Then the carrier escape time of point defect is τ_{point} .

The defect distribution is treated as $n_t(\varepsilon) = (N_t/k_B T_t)exp((\varepsilon - E_c)/k_B T_t)$ with $n_t(\varepsilon)$ the trap density of states at energy ε, E_c the energy of the conduction band, N_t the total density of traps, and $k_B T_t$ an energy characterizing the trap
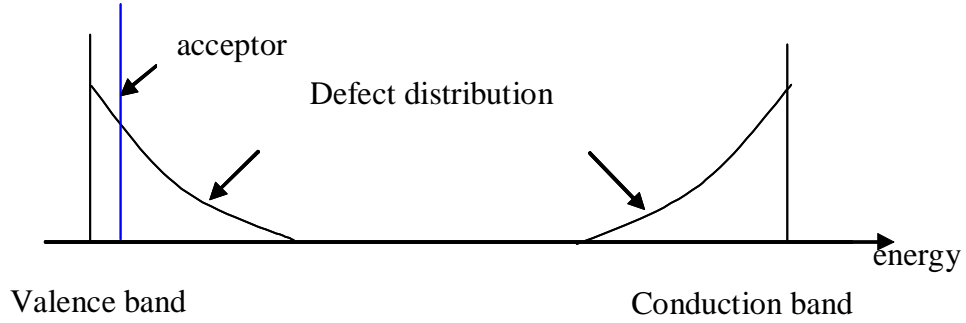
Figure 3.10: The diagram of structure of structure defect and ion defect.

distribution. The distribution of this kind defect of PPV is symmetric, Fig. 3.10.

We assume that some ions in PPV are as extrinsic carriers, and those ions will induce shallow level by Coulomb potential. The extrinsic carrier is treated as acceptors in PPV and the energy is at shallow level which closes to valence band. This potential shape is shallow and broad wide, not like point defect and carrier in the polymer is treated as polaron. Polaron is a complete system, and its behaviors in PPV are like classical particle. When a carrier is captured by acceptor level, it will absorb heat and oscillate until the carrier escapes the trap. The carrier escape rate[nonradiative recombination in semiconductors, V. N. Abakumov etc, is

$$e = \frac{\omega}{2\pi} \exp(-(\varepsilon_T - zeF)/k_B T)$$

where ω is oscillator frequency, ε_T is thermal ionization energy, z is the nearest distance to the ion defect, and F is applied electric field. Assume the distribution of ion defect is delta function, and the carrier escape time is τ_{ion} . Then the average escape time of p-type polymer is

$$\tau_{average} = \int [\tau_{point} \exp((\varepsilon - \varepsilon_c)/k_B T_t) d\varepsilon + \tau_{ion} N_a \delta(\varepsilon - \varepsilon_a) d\varepsilon]/(N_t + N_a)$$

for defect close to conduction band, and

$$\tau_{average} = \int [\tau_{point} \exp(-(\varepsilon_v - \varepsilon)/k_B T_t) d\varepsilon + \tau_{ion} N_a \delta(\varepsilon - \varepsilon_a) d\varepsilon]/(N_t + N_a)$$

for defect close to valence band where N_t is trap density, N_a is acceptor density, and ε_a is acceptor level energy.

Extrinsic carriers compensate the deep level of hole, so the velocity and mobility of hole will be higher than no extrinsic carrier. Therefore the hole
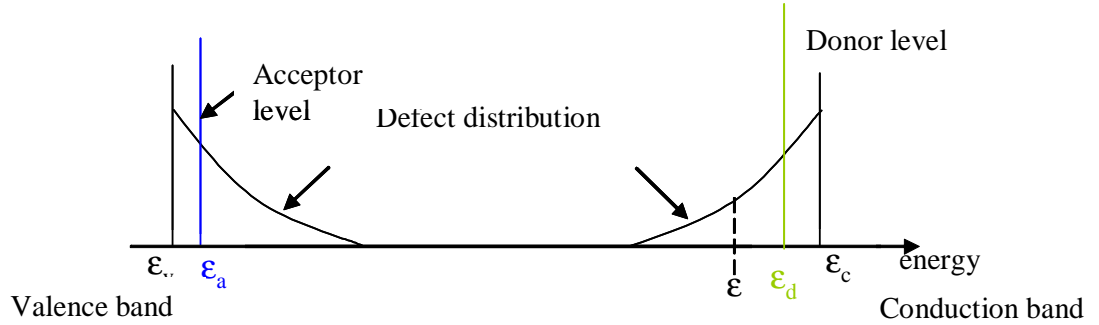
Figure 3.11: The diagram of structure defect, acceptor level and doror level.

mobility is higher than electron mobility and the recombination region will close cathode at low electric field.

In order to increase the electron mobility, we introduce another ions as donor. This impurity will provide extrinsic electrons and those carriers will compensate the deep level of electron. Therefore the electron mobility will be higher than no donor. At the same time, the hole mobility will decrease. When the donor is very large, the escape time of electron is very small and the electron velocity and mobility will approach free-trap mobility.

The compensate barrier ε is

$$\int [Nt \exp((\varepsilon - \varepsilon_c)/k_B T_t) + Nt \exp(-(\varepsilon - \varepsilon v)/k_B T_t)d\varepsilon] = N_d$$

$$\varepsilon = \frac{1}{2}E_g + k_B T_t \operatorname{arcsinh}[\exp(E_g/2k_B T_t)((Nd - Na)/2Nt)]$$

where N_d is donor density.

Because the distribution of structure defects is exponential function, the compensate barrier vary lot at low donor density. That implies that carrier transition time will change a lot even at low doping density.

3.4 Velocity

We change the one hopping between two carbon phenyl and one hopping value between thiophene tight binding method. If one hopping integral between two p_z orbital become larger, i.e. $t3$ of PF and tb of PT, the couple of orbital of two rings are stronger than others and the energy levels are splitting larger. The one of splitting energy will be low than others and the carrier will be trap at this low energy. For polyfluorene (PF), if one hopping integral between two carbon phenyls is larger than the hopping integrals of carbon phenyl, there are two symmetric defects induced in the band gap. It is the same for polythiophene,

58

if one hopping integral between two thiophenes is larger than hopping integrals on the thiophene, there are defects induced in the band gap. See the Fig. 3.12.

For polyfluorene, one of the t_3 is change from –1.5 to -12, and the twist mean bond value is $\frac{-1}{2}\cos(\theta)$. It is the same for polythiophene, but change tb form –1.3 to –8.0 and the twist mean hopping is $-8\cos(\theta)$. It is clear in the figure 6 that the larger hopping induce deeper defect. For PF, the defect is generated double, but it is different for PT.

When carrier passes the defect, the carrier will be trap by the defect because the energy of defect is lower than band. But how the hopping integral will be larger than other bond? One possible answer is some region of the material is more crowded and the bond between is weak and then is pressured easier than other bonds. This is possible but uncommon in the process. That is maybe the reason why polyfluorene is more stable than PPV. Polyfluorene and polythiophene are hardly oxidation and space pressure is not large, so the properties of such polymer are more air-stable than PPV.

For structure defect, we consider carrier effective mass, dielectric constant, temperature and electric field as parameters. We assume that the lattice is approach thermo equilibrium and normalized lattice coordinate is zero. As $P(\triangle)$ is given by equation 3.2, its behavior is dominated by exponential term. At this research, we only consider $\triangle_f - m\hbar\omega > 0$. If $\triangle_f - m\hbar\omega < 0$, there is no barrier and the carrier is free. The escape rates of structure defect are different at different temperatures and different barriers. We show four different temperatures in Fig 3.13. The Fig. 3.13 points that the influence of temperature is more significant when the barrier is deeper. At shallow barrier, the escape rates are high and temperature dependence is low. But the temperature dependence is stronger for deeper level. Although the escape time of structure defect is weak dependence of temperatures, it is stronger dependence of electric field. This result is corresponding to the measurement at experiment.

The escape rate of ion defect is shown in Fig. 3.14. The barrier is induced from Coulomb potential. The value of Coulomb potential is decided from the distance between ion and polymer backbone. The longer the distance is, the shallower the barrier is and escape time becomes shorter as well. At this research, we assume the distance between ion and polymer backbone is 9 Å. At result of our calculation, the temperature dependence of such defect is stronger than structure defect. This is because the dependence of temperature of escape rate of such defect is exponential term and the barrier dependence is not as strong as structure defect. When the barrier is too small or the applied electric field is too large ($k_BT > \varepsilon_T - eF$), the carrier is free, i.e. barrier is zero and no ion defect could trap the carrier. So the ion defect is a strong dependence of both temperature and electric field for one fixed barrier.

If we fix acceptor density to 1.5×10^{11} cm^{-3}, different donor densities will change the velocities of electron and hole at the same time. When donor density increases but far lower than acceptor density, electron velocity will increase slowly. As donor density approaches acceptor density, the electron velocity increases fast. When donor density is high enough, trap escape time is so little that electron is almost free. Unexpectedly, the minima donor density resulting
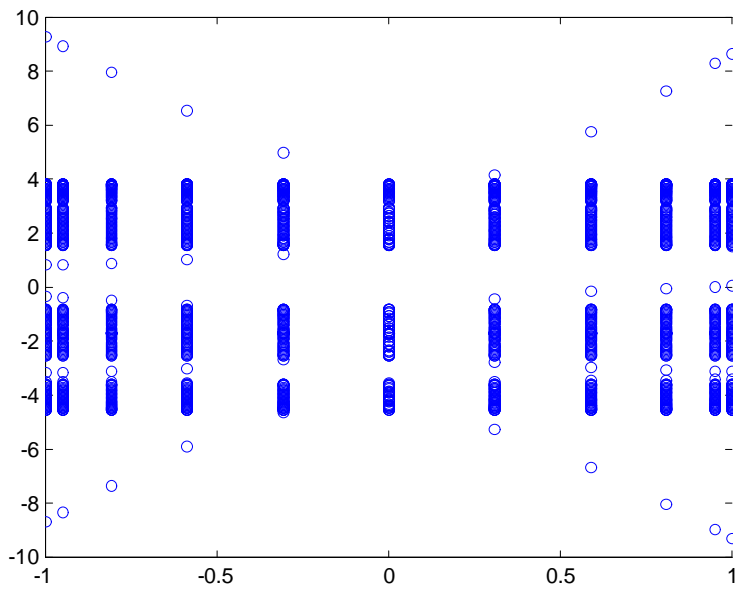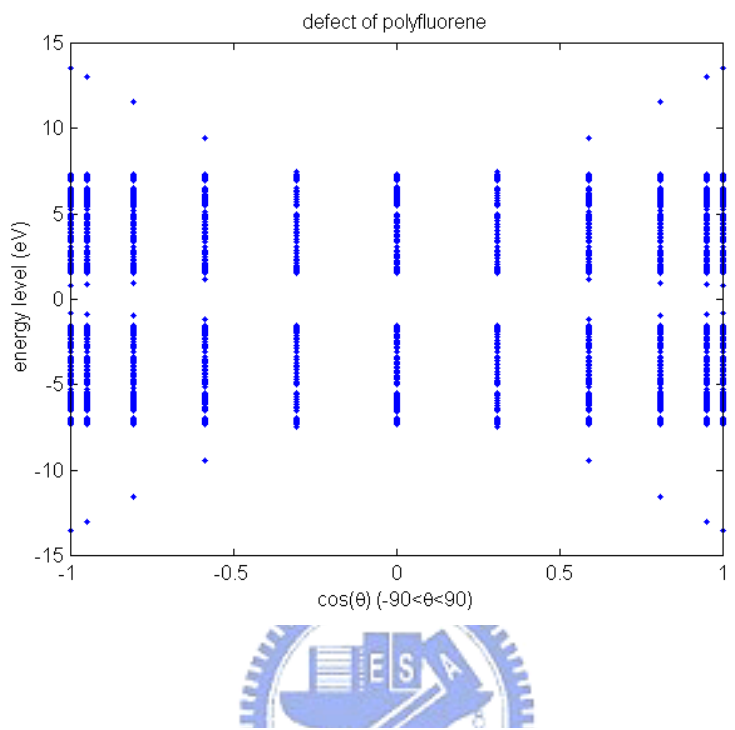
Figure 3.12: The diagram show the change of energy when we change the rotation angle.
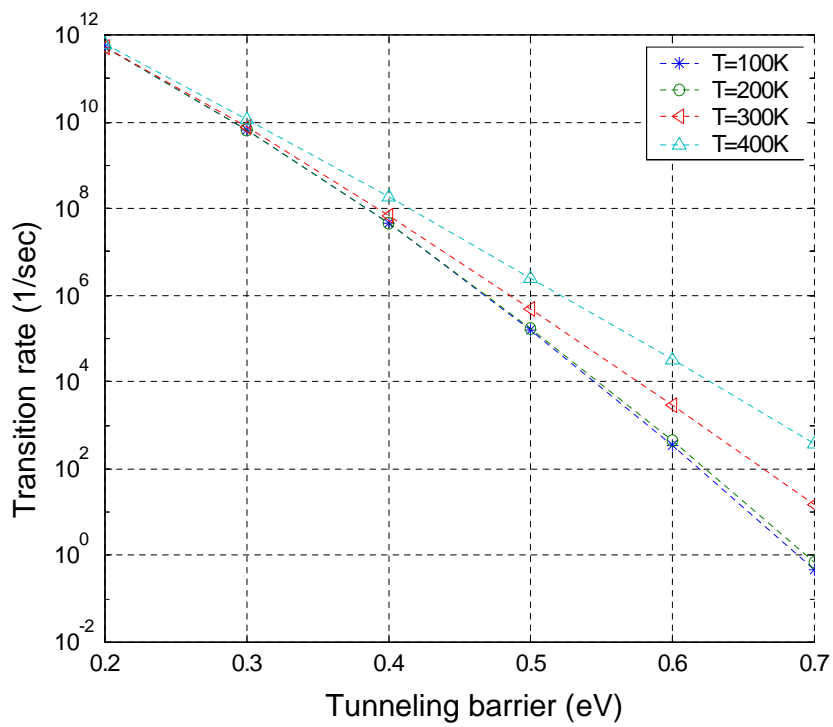
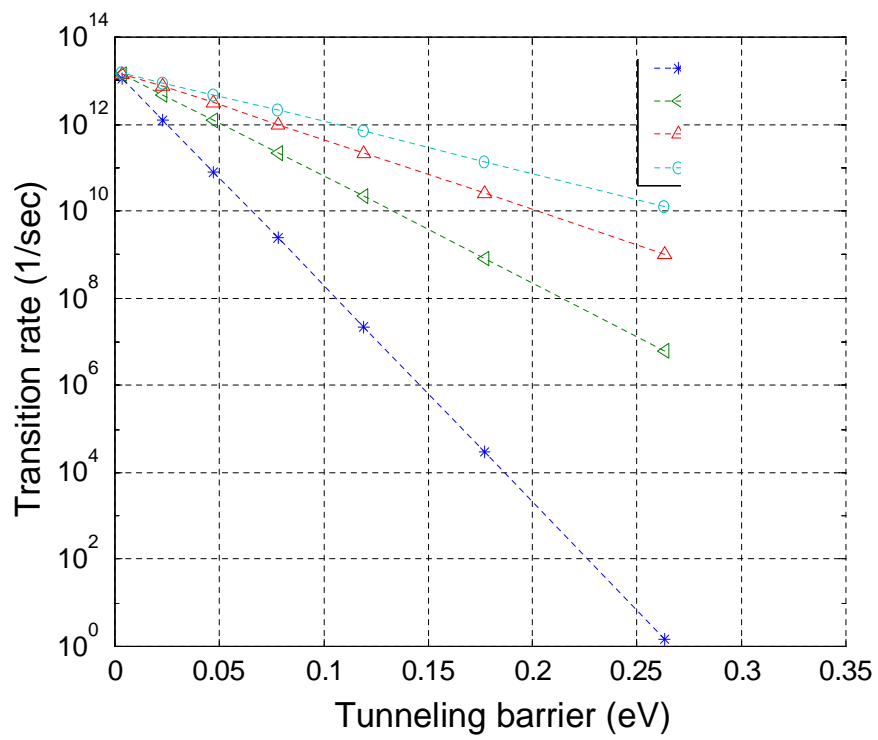Figure 3.13: The transition rate of structure defect in different temperature.

Figure 3.14: The transition rate of ion defect in different temperature.

from free electron is much lower than trap density even at low electric field. This is because extrinsic carriers compensate the very deep trap level of electron, and the escape time decreases quickly. The escape time is dominated by exponential term. For example, the donor density, which electron is almost free, approaches 10^{15} cm^{-3} at 5×10^7 V/m at room temperature. However the structure defect density is 10^{18} cm^{-3}, and the compensate rate is about 0.001. But it is a little different for hole. When donor increases, the velocity of hole is almost the same until donor density approaches acceptor density. Then the velocity decreases quickly and approaches constant value at very high dopant. That is because the deepest barrier for hole is similar ($\sim E_g$) at very high dopant, and the escape time is almost the same. For different temperature, the minima velocity of hole is different. Hole has faster velocity at higher temperature. See Fig. 3.15.

Although many research point that PPV is p-type material and the hole mobility is higher than electron mobility in experiment, but they did not explain why the mobility of hole is larger than electron. We use carrier compensation to explain this phenomenon and suggest to dop ion defect dopant to balance the mobility of hole and electron. PPV has intrinsic defect, which is reduced from the twist of double bond of PPV. The extrinsic carriers, from the synthetic process, will compensate the deep level of structure defect of hole and the velocity of hole is larger than electron. This result is corresponds the experiment. At the same time we use tight-binding method to explain the reason of the different stable properties between PF, PT and PPV. The double structure of PPV is more easily twist and oxidation than PF and PT, and then PF and PT are more air-stable than PPV. The structure of PF and PT are strong and have no structure defect unless receive big pressure.

If we dop ion into the PPV, the carrier transition time will change. The carrier transition time of structure defect and ion defect are different at the same temperature and electric field. The transition time of ion defect is strong dependence of temperature and electric field, but the point defect is weak dependence of temperature. Therefore the extrinsic carrier will compensate the deep level of structure defect and the carrier velocity and mobility will change as expectation. The only unexpected thing is the dopant density is smaller than structure defect density. If the ion density is very smaller than acceptor density, the velocities of hole and electron are almost unchanged until ion defect density is approach accepter density. That is because the extrinsic carriers compensate the deepest level defect and the velocities of hole and electron both change a lot.

3.5   Mobility

For structure defects the trap distribution is taken as exponential:

$$\rho_t(\varepsilon) = \frac{x_t}{\rho_t} \exp[(\varepsilon - E_c)/\rho_t]$$
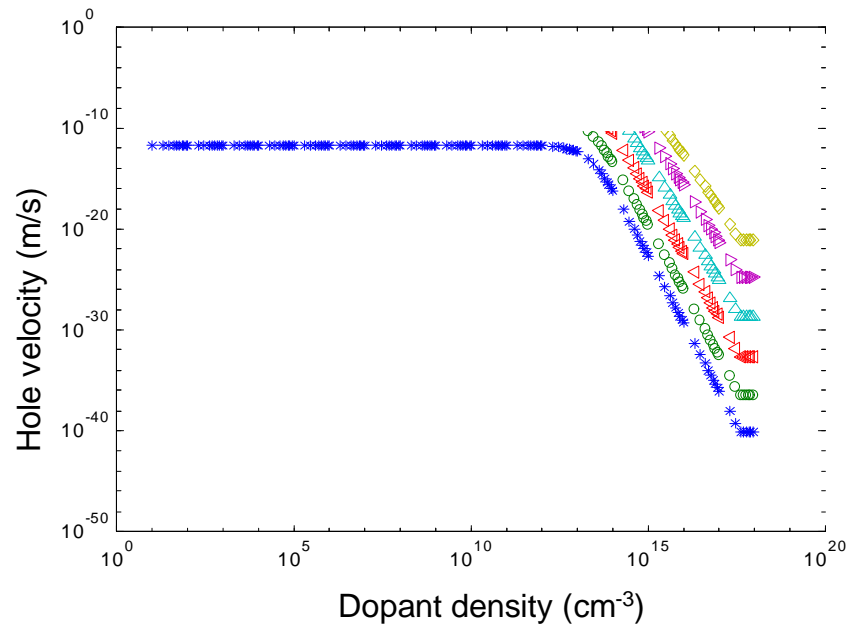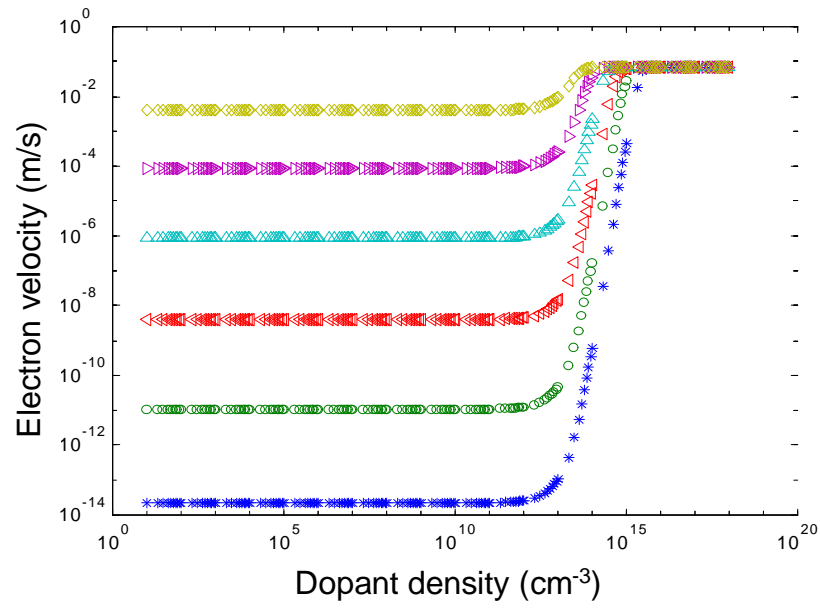
Figure 3.15: Electron and hole velocity with different dopant density

for point defect and

$$\rho_t(\varepsilon) = \frac{x_t}{\rho_t} \exp[(E_v - \varepsilon)/\rho_t]$$

for ion defect. For oxidation the electron traps have a d distribution:

$$\rho_t(x) = x_t \delta[\varepsilon - (E_c - \rho_t)]$$

. ε is the trap energy. The dimensionless trap density x_t is the averaged number of traps per repeat unit. For both electron and hole the trap density of states is cut off at the midgap. In conjugated polymers the electric transport is due to the carrier hopping among conjugation segments with variable energy. Without the traps the carriers are in the form of polarons in the segments, and the polaron hopping mobility follows the Poole-Frenkel law2

$$\mu_{PF} = \mu_0 \exp(\gamma\sqrt{F})$$

. In the presence of the point defects in the segments the carriers have to tunnel out of the traps into the free carrier continuum in order to form a mobile polaron and contribute to the hopping transport. The fraction of the carriers in the traps must be taken into account in the calculation of the overall mobility μ, which can be determined as follows. Assume n_T and n_F are the density of trapped and free carriers (mobile polarons), respectively. The total carrier density n_{tot} is $n_T + n_F$. The particle current j can be expressed as $j = n_{tot}\mu_F = n_F\mu_{PF}F$, which implies

$$\mu = \frac{1}{1 + \frac{n_T}{n_F}}\mu_{PF} \tag{3.3}$$

The ratio n_t/n_F between trapped and free carriers can be obtained from the transition rates. Let $W_{1(2)}$ be the transition rate from a free band state (trap) to a trap (free) state. W_2 can be decomposed as $W_2 = W_2^{th} + W_2^f$, where W_2^{th} is the thermal activation rate and W_2^f is the field tunneling rate defined in Eq. (3.1). For electrons without field we have $W_2^{th}/W_1 = \exp[-\beta/(E_c - \varepsilon)]$ in equilibrium. β is kT. The ratio between the trapping and escaping rates is therefore

$$W_2/W_1 = \exp[-\beta/(E_c - \varepsilon)][1 + (W_2^{th} + W_2^f)] = \exp[-\beta(E_c - \varepsilon)]\xi$$

, where $\xi = 1 + (W_2^{th} + W_2^f)$. W_2^{th} can be approximated as $w/2\pi \exp[-\beta/(E_c - \varepsilon)]$, where w is the optical phonon energy.19 Including the Pauli exclusion principle in detailed balance, the occupation probability g_T and $g_F = g(E_c)$ for trap and free states are related by

$$g(\varepsilon)W_2[1 - g(E_c)] = g(E_c)W_1[1 - g(\varepsilon)]$$

. The relation can be reorganized as

$$g(\varepsilon) = \frac{1}{[1 - g(E_c)]W_2/[g(E_c)W_1] + 1}$$

. Assuming $E_c - E_F >> 1/\beta$, the occupation probability $g(E_c)$ for the free state is approximated by the Boltzmann factor $\exp[-\beta/(E_c - \varepsilon)]$. The defect occupation probability becomes

$$g_T(\varepsilon) = \frac{1}{1 + \xi \exp[\beta/(E_c - \varepsilon)]}$$

. The Fermi distribution is recovered if there is no field ($\xi = 1$). The density of trapped electron

$$n_T = \int_{-\infty}^{E_c} g_T(\varepsilon)\rho_t(\varepsilon)d\varepsilon$$

The total density of free carrier nF is $X_c g_F$. $X_c = Ncv$, where N_c is the effective band density of state and v is the unit cell volume. The trapping ratio in Eq. (3.3) is finally expressed as

$$\frac{n_T}{n_F} = \frac{1}{X_c} \int_{-\infty}^{E_c} \frac{g_T(\varepsilon)}{g_F} \rho_t(\varepsilon)d\varepsilon \tag{3.4}$$

Equation (3.4) is substituted into Eq. (3.3) to obtain the mobility μ as a function of F and E_F. For holes the integral is from E_v to ∞.

In Fig. 3.16 we plot the hole mobility μ_h against electric field F for some trap density x_t. $\gamma = 5.2\times10^{-4}$ (m/V)$^{1/2}$, $N_c = 2.5 \times10^{19}$ cm^{-3}, and $v = 2.7\times10^{-22}$ cm^3. As $x_t = 0$, μ_h follows the usual Poole-Frenkel form. For finite x_t the mobility is significantly suppressed in the lower field region without background p doping ($E_F = 0$). As F increases the field tunneling rate out of the trap becomes larger than the thermal activation rate. The thermal equilibrium is broken and the carrier population in the traps start to be depleted. μ_h becomes identical to the trap-free value as F further increases. The transition from the trap-dominated to free mobility is more abrupt for the δ distribution than the exponential distribution as expected. In fact this difference can be used to tell whether the predominant traps are due to structure disorder or oxidation. As the polymer is p doped the deep hole traps are compensated and the mobility increases. There is a two orders of magnitude increase of μ_h for doping as slight as $x_a = 8\times10^{-5}$. In Fig. 3.17 we plot the electron and hole mobilities μ_e and μ_h as functions of intentional n doping x_d for a fixed unintentional p doping x_a. As x_d increases the deep hole traps are reactivated and μ_h drops. Eventually the electron traps start to be filled (inactivated) by the doping and μ_e starts to rise. There is a near mirror symmetry of the two curves around $x_d = x_a$. For a given material with fixed structure disorder, the ratio between μ_e and μ_h is therefore not a constant but can be continuously tuned by doping. EL efficiency can be improved by balancing the carrier injection if either chemical or electrochemical n doping can be made practical for the polymers like PPV and PF.

It is shown that the electron-hole symmetry exists in the trap levels for conjugated polymers with structure defects. The oxygen defects and the background p doping which compensates the hole traps are the origins for the imbalanced electron-hole transport. Equal electron and hole mobilities can be achieved by intentional n doping.
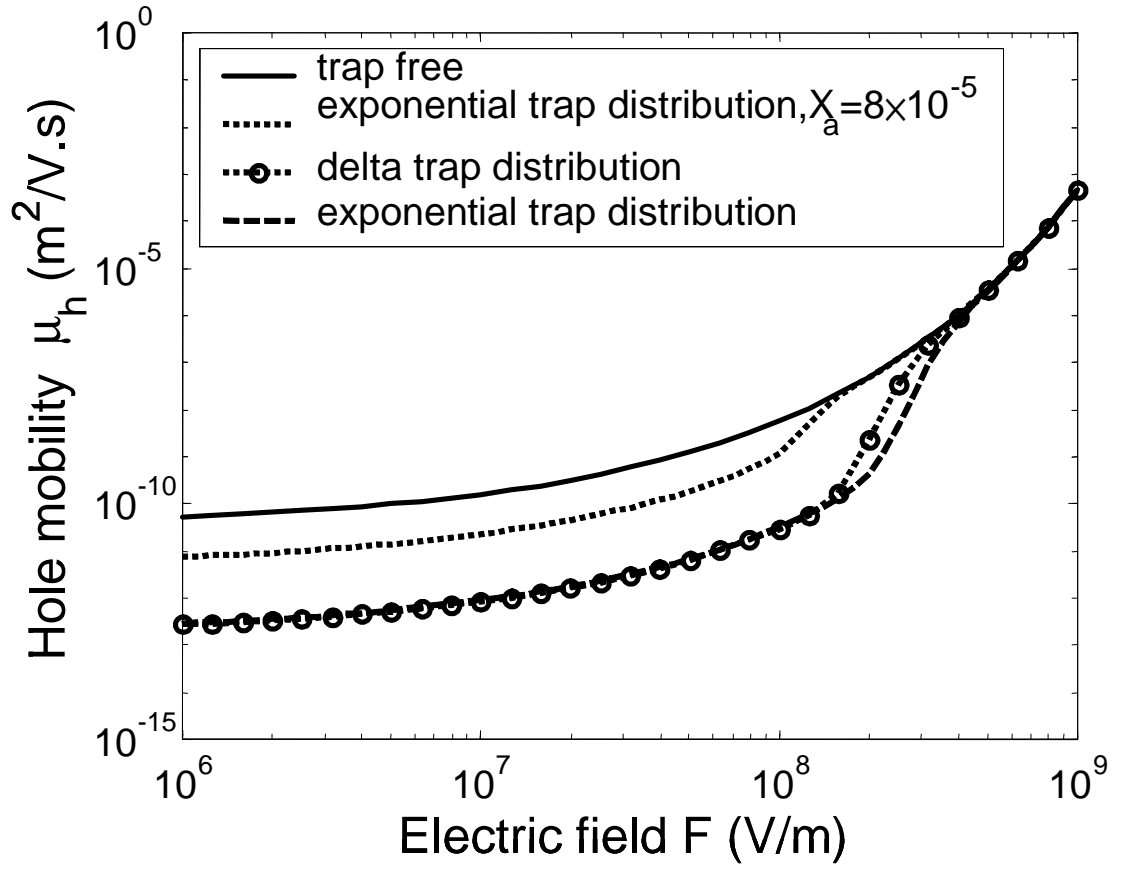
Figure 3.16: The effect of traps and their compensations on the hole mobility μ_h are shown. Solid line: no trap; dashed line: exponential traps without doping; dotted line: exponential traps with p doping; and dot-circle line: d traps without doping. σ_t=0.13 eV for exponential and σ_t=0.5 eV for δ distribution.
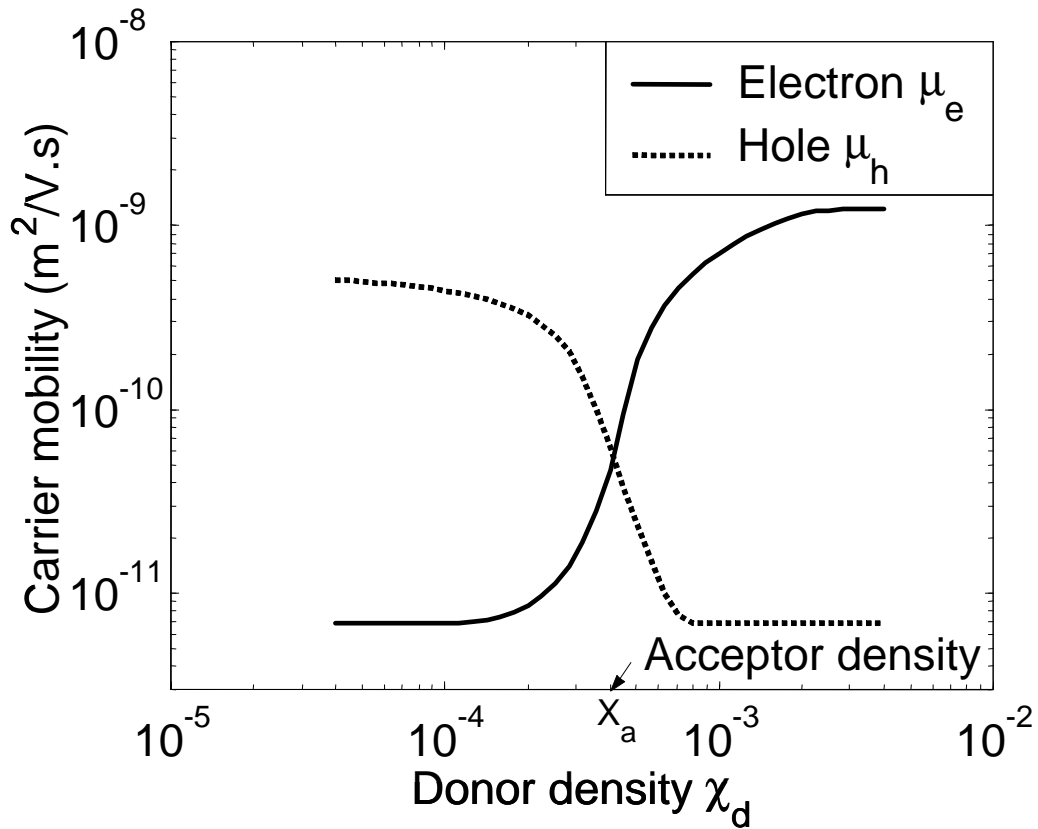
Figure 3.17: The carrier mobilities μ_e and μ_h, plotted as functions of the n-doping density x_d, are shown to have a near mirror symmetry with respect to the background p-doping density x_a. The compensated hole traps are reactivated while the electron traps are compensated as x_d crosses x_a. The Fermi level E_F is also shown.
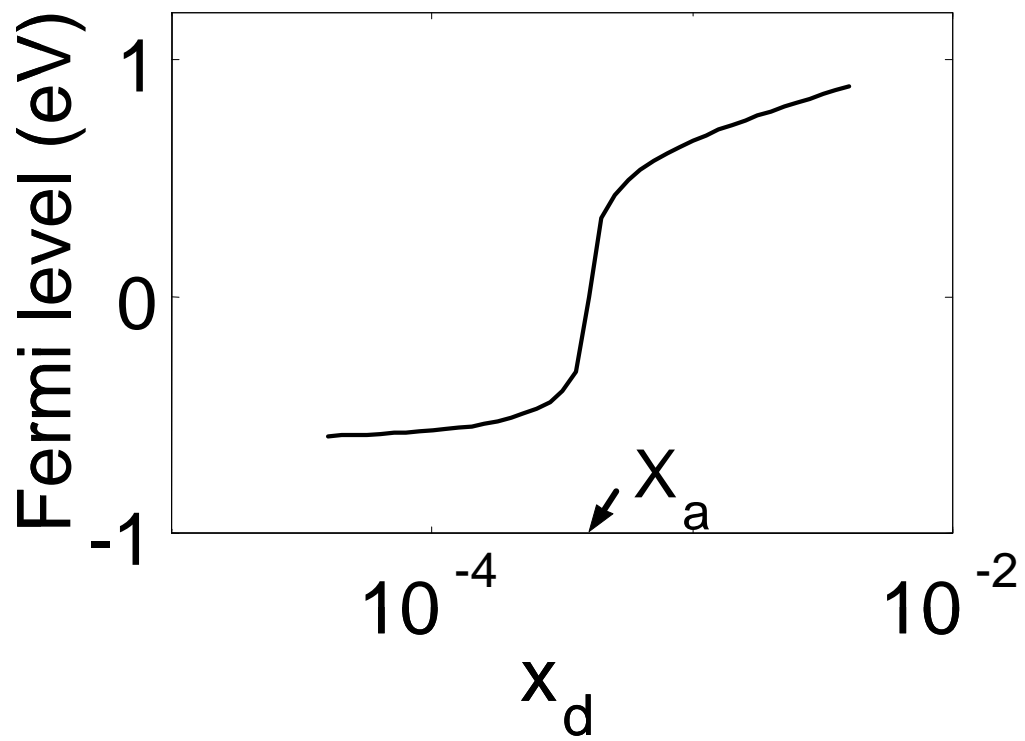
Figure 3.18: The Fermi level of polymer with different donor density.

Chapter 4

Device Model of Organic Materials

The majority of device models proposed thus far in the literature are based on traditional inorganic charge transport models. Electron and hole transport in the device is described using the continuity equations and a drift–diffusion or drift current, coupled to Poisson's equation. Along with the appropriate boundary conditions,which for OLEDs require appropriate formalisms for current injection at each of the contacts, these equations are solved to obtain solutions for the electron and hole current densities, carrier densities, electric field, and electrostatic potential. Owing to the simple device geometry in OLEDs, i.e. metal contact/organic layer(s)/metal contact, a one-dimensional device model is generally sufficient. A variety of models have been proposed, encompassing single-carrier (unipolar) models, double-carrier (bipolar) models, and time-dependent models. Many authors have simplified their models by neglecting the diffusion current contribution, since concentration gradients are generally small. Some models have also been extended to the investigation of multilayer (predominantly bilayer) devices. Multilayer device models use the same equations for current transport and injection, but impose special conditions at the organic–organic interface. These models are discussed below.

4.1   Equation defining the model

The time-dependent continuity equations have been used by [193][194]:.

$$\frac{\partial n}{\partial t} - \frac{1}{e}\frac{\partial J_n}{\partial x} = G - R, \quad \frac{\partial p}{\partial t} + \frac{1}{e}\frac{\partial J_p}{\partial x} = G - R \qquad (4.1)$$

where Jn (Jp) is the electron (hole) current density, e is the electronic charge, G is the carrier eneration rate, and R is the carrier recombination rate. Other

authors [195] [196, Kawabe][197][16] utilize the time-independent versions of these equations in which $\partial n/\partial t$ and $\partial p/\partial t$ are zero. The drift–diffusion current equations are given by the following expressions [195]]:

$$J_n = -e\mu_n n \frac{d\phi_n}{dx}, \quad J_p = -e\mu_p p \frac{d\phi_p}{dx} \tag{4.2}$$

where μ_n (μ_p) is the electron (hole) mobility, n (p) is the electron (hole) density, and ϕ_n (ϕ_p) is the electron (hole) quasi-Fermi potential. The carrier mobilities take the field-dependent Poole–Frenkel form described in section 3 below. J_n and J_p may also be expressed in the following form showing explicitly the drift and diffusion components, in which the diffusivities have been written in terms of the mobilities using the Einstein relation :

$$J_n = e\mu_n[nE + (\frac{k_B T}{e})\frac{\partial n}{\partial x}], \quad J_p = e\mu_p[pE + (\frac{k_B T}{e})\frac{\partial p}{\partial x}] \tag{4.3}$$

where k_B is Boltzmann's constant, E is the electric field, and T is the temperature.

Poisson's equation is

$$\frac{dE}{dx} = (\frac{e}{\epsilon})(p - n + N_D - N_A) \tag{4.4}$$

where ε is the static dielectric constant, N_D is the donor density, and N_A is the acceptor density. The electrostatic potential ϕ is related to E by

$$E = -\frac{d\psi}{dx} \tag{4.5}$$

Using Maxwell–Boltzmann statistics, i.e. assuming that the system is non-degenerate (so far, to our knowledge, OLEDs do not exist for which charge densities are so large that this assumption breaks down), n and p are given by

$$
\begin{aligned}
n &= N_c \exp[(e\psi - e\phi_n + \chi_c)/k_B T] \\
p &= N_v \exp[(-e\psi + e\phi_n - \chi_c - E_g)/k_B T]
\end{aligned}
\tag{4.6}
$$

N_c (N_v) is the density of states in the conduction (valence) band for an inorganic semiconductor, and here corresponds to the density of negatively (positively) chargeable sites in the film. N_c is often assumed equal to N_v, and determined from the molecular or polymeric density with single occupancy. Here, χ_c is the electron affinity of the semiconductor.

4.2   Recombination

For wide-band-gap materials, such as organic semiconductors, carrier generation by thermal excitation across the gap is very small and is usually neglected in calculations. Electron–hole pair recombination in organic semiconductors is bimolecular, taking the Langevin form [67]

$$R = \gamma np, \qquad \gamma = 4\pi q\mu/\varepsilon \tag{4.7}$$

where μ_r is an effective mobility which is taken to be the larger of the electron and hole mobilities. Recently, an alternative electron–hole capture mechanism that is more accurate at high fields has been proposed [29].

4.3   Contact

An important aspect of any device simulation is that of the boundary conditions, i.e. the contacts, which are responsible for current injection. The choice of contacts in OLEDs is an area of critical importance,as they can affect minority and majority current flow,and hence recombination rates and efficiency. In inorganic semiconductors, such as Si and GaAs, the Schottky energy barrier formed at a metal contact depends weakly on the choice of metal. At the metal–semiconductor interface of an organic semiconductor, there is a much wider variation in the values of the observed barrier height. In fact, the operation of organic LEDs depends on the asymmetry of the barrier heights at the two contacts. ITO is the preferred anode material due to its transparency and relatively high work function. On the other hand, metals such as Al, Ca, and Mg with lower work functions are employed as cathode materials. Although metal–semiconductor contacts are often referred to as Schottky contacts in the literature, this is not the case, and they can be of one of two types: low-resistance ohmic contacts; or rectifying Schottky contacts.

Fig. 4.1 illustrates the formation of a metal–semiconductor Schottky contact (the formation of an ohmic contact is discussed below). Although this discussion is based upon inorganic semiconductor theory, it is applicable since we are discussing band models. As the metal is brought into contact with the n-type semiconductor, thermal equilibrium is established and the Fermi levels in the metal and the semiconductor become continuous and equal through both materials. In order for the Fermi levels to align, electrons from the semiconductor flow into the metal, leaving behind positive ionized donors in the semiconductor. Therefore, the bands bend as shown in Fig. 4.1 and a Schottky diode is formed, provided that ϕ_m exceeds the semiconductor work function ϕ_s. If the semiconductor is p-type, electrons are injected from the metal into the semiconductor, causing a build-up of negative charge in the semiconductor, and consequently the bands bend the other way if $\phi_m < \phi_s$. Organic semiconductors have negligible doping and no intrinsic carriers due to the wide band gap, so no band
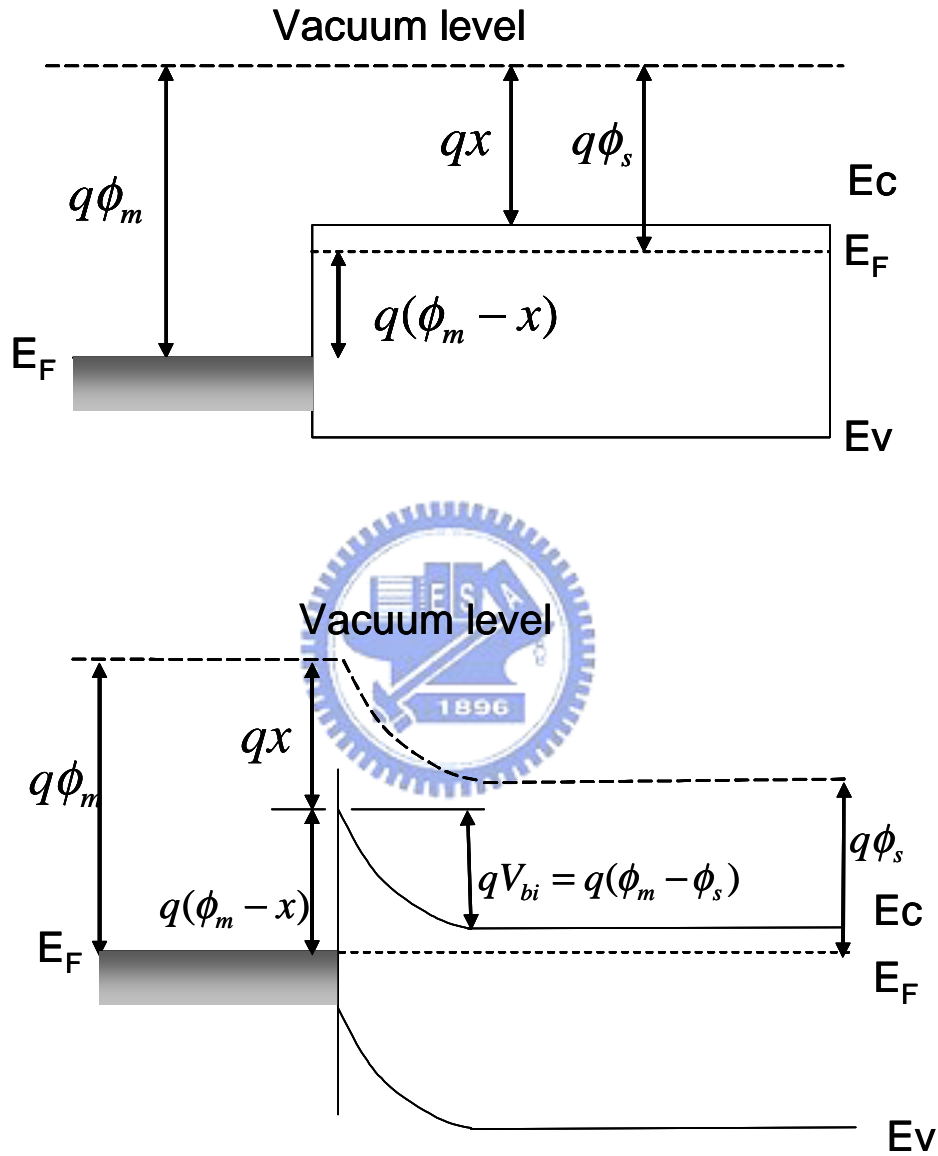
Figure 4.1: Top plan: the energy band diagram of an isolated adjacent to an isolated semiconductor under non-equilibrium conditions. Bottom plan: the energy band diagram of a metal-semiconductor contact in thermal equilibrium.

bending occurs. The barrier heights to electron and hole injection, ϕ_{bn} and ϕ_{bp} respectively, can be calculated as follows:

$$e\phi_{bn} = e(\phi_m - \chi_c), \qquad e\phi_{bp} = E_g - e\phi_{bm}$$

In an OLED, the built-in voltage is taken to be the difference between the two metal work functions.

An ohmic contact can also be formed at a metal–semiconductor junction by one of two methods. Firstly, a metal with a work function which is smaller than that of the semiconductor for n-type semiconductors, or greater than that of the semiconductor for p-type semiconductors, can be chosen and no barrier to carrier injection from the metal will be formed. However, this approach is not usually followed because the barrier height may be pinned by the high interface state density at the contact. A more practical method of creating an ohmic contact is to form a Schottky barrier contact, with heavily doped semiconductor at the interface, causing a narrow depletion width, significant band bending, and a barrier which is thin enough to tunnel through.

For most organic semiconductors, increasing the free charge-carrier density through the addition of dopants is difficult to achieve, and so an ohmic contact cannot be formed in this way. It is also difficult to make an ohmic contact via the choice of work function, particularly finding values above typical HOMO levels or below typical LUMO levels. In practice the barrier height is minimized by choosing appropriate contact materials. However, at high biases tunneling injection does fit experimental data (e.g. [193]), and for low barrier height values (<0.3 eV) SCLC has been observed, which means that contacts which tend towards ohmic behavior can be fabricated.

Fig. 4.2 shows the conduction band profiles for a metal contact on an n-type semiconductor material in forward and reverse bias. Considering electron flow from the semiconductor to the metal, the potential barrier is reduced and the current Ims (note that the current flows in the opposite direction to the electrons) is increased. However, for electron flow from the metal to the semiconductor, the potential barrier to electrons is independent of the field if image forces are neglected. Therefore, the current for electron flow in this direction Ism is a fixed contribution to the current flowing forward bias, which is matched by Ims at thermal equilibrium.

Under reverse bias conditions, the potential barrier to electrons flowing from the semiconductor to the metal increases, as does the depletion width, and so the current flowing from the metal to the semiconductor Ims is the dominant component. This situation causes a highly asymmetric current–voltage characteristic similar to that of a pn junction diode. However, current flow in Schottky
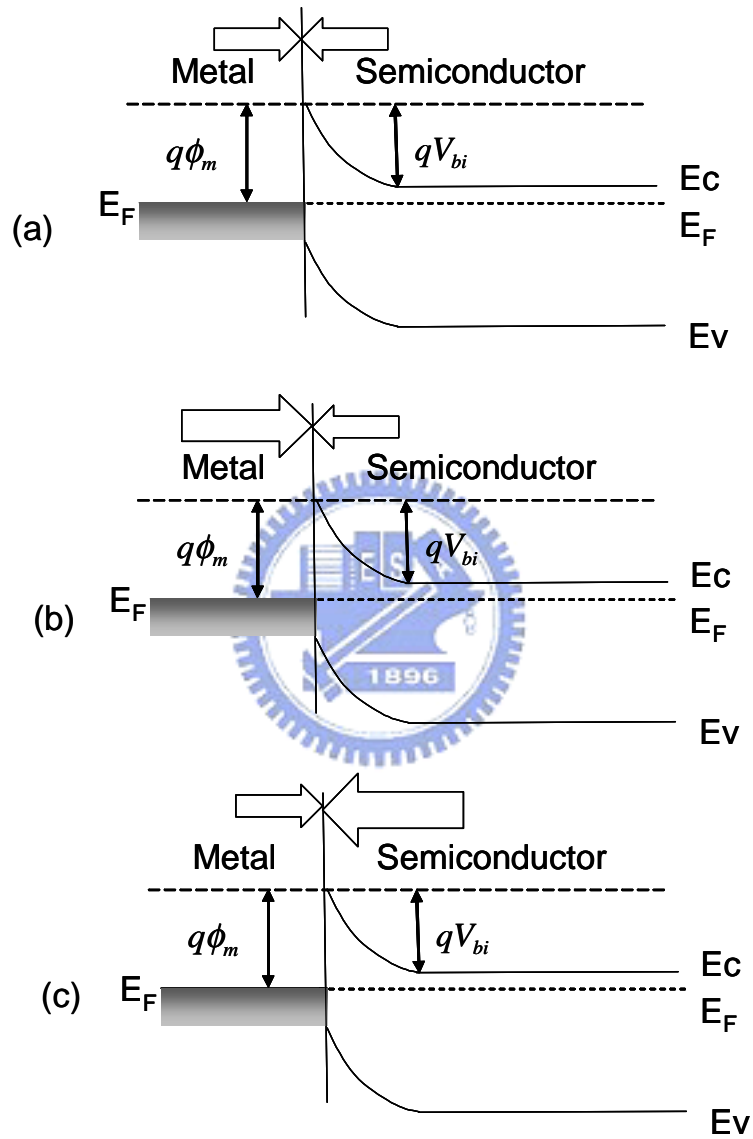
Figure 4.2: Energy band diagrams of rectifying metal-semiconductor contact at (a) the equilibrium, (b) forward bias, and (c) reverse bias.
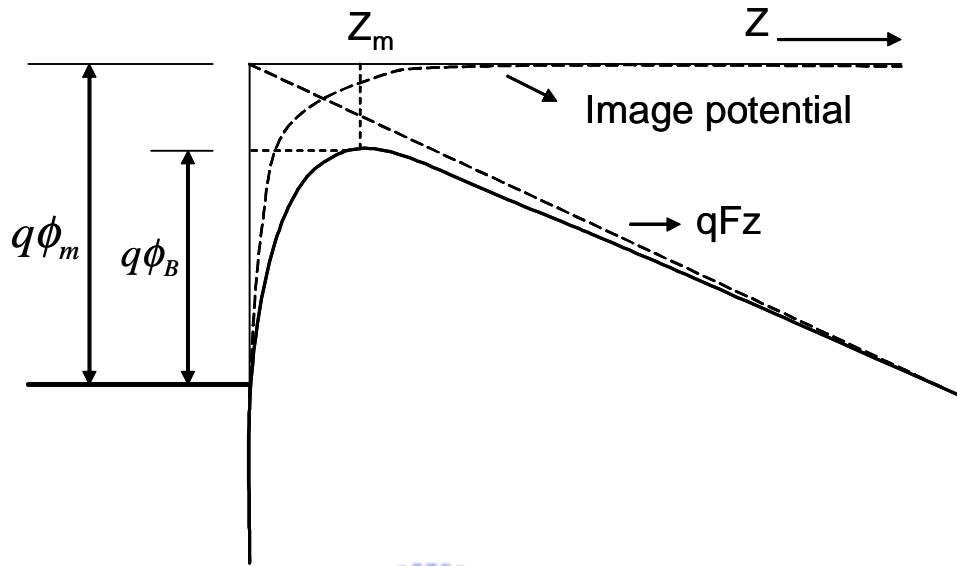
Figure 4.3: The energure diagram for theinterface between a metal surface and a vacuum. The metal work function is $e\phi_m$. The effective work function (or barrier) iw lowered when an electric field os applied to the surface. The lowering is due to the combined effects of the field and image force.

diodes is dominated by majority carriers, whilst in pn junction diodes it is dominated by minority carriers.

Charge transport across the metal–semiconductor interface can be summarized as arising from the following three processes.

• Transport of carriers from the semiconductor over the potential barrier into themetal. This is the dominant process for moderately doped semiconductors.

• Field emission of carriers through the barrier.

• Recombination in the semiconductor; this corresponds to minority carrier injection.

Subsubsubsection

This is just some harmless text under a subsubsubsection.

The heights of the barriers to carrier injection at the contacts for use in simulations are calculated from ϕ_m and the molecular energy levels. However, this assumes that these barrier heights are field independent. In reality, this is not the case. The barrier to injection is reduced under applied bias due to the image force of the carrier, as is illustrated in Fig. 4.3. The image force results from the electrostatic attraction of the carrier at a distance x from the electrode–

semiconductor interface leading to a charge build-up at the electrode interface that gives the same potential as an equal and opposite charge a distance -x from the electrode, the image charge. The attractive image force is then given by the following expression:

$$E = -\frac{e^2}{16\pi\varepsilon x^2}$$

The resulting potential energy is

$$U = \frac{e^2}{16\pi\varepsilon x^2} + eEx$$

The magnitude of the Schottky barrier lowering, ϕ_{bn}, is given by the condition that $dU/dx = 0$:

$$\Delta\phi_{bn} = \sqrt{\frac{eE}{4\pi\varepsilon}}$$

In organic semiconductors, the value of ε is much lower than for inorganic semiconductors, being typically $\approx 3\varepsilon_0$ in organic materials, compared with $12\varepsilon_0$ in Si and $13\varepsilon_0$ in GaAs, increasing the importance of the barrier-lowering term. This contribution must be included for any device model to be successful.

For a heavily doped inorganic semiconductor, or for operation at low temperature, the tunneling current may be the dominant contact current component. The expressions for Jms and Jsm are modified such that they consist of two terms, a thermionic emission term and a field emission or tunneling term. The thermionic emission current density

$$J_{th} = AT^2 \exp(\frac{-e\phi_b}{k_B T})\exp(\frac{-eV}{k_B T} - 1)$$

where A is Richardson's constant. Full expressions for the tunneling currents in inorganic metal–semiconductor contacts can also be found.

The tunneling current is

$$J_{tu} = BE^2 \frac{-4\sqrt{2m^*}\phi_b^{3/2}}{3\hbar eE} \tag{4.8}$$

which has been shown to hold in OLED at high electric fields. In the above equation m^* is the effective electron mass, ψ is the energy barrier, $\hbar$ is Plank's constant and B is the coefficient that contains the tunneling prefactor and the rate for current backflow. The value of B in Eq. 4.8 is taken from the fitting data of Parker[211] for carrier tunneling from electrodes We combine all the equations, then we could obtain the current density with different initial conditions and the results are shown below.

The contacts in a device model are included by describing the carrier currents at the boundaries of the device, x = 0 and l, where l is the length of

the device. Several types of injecting contact have been used in devicemodels: ohmic, thermionic emission, and tunnelling. Perhaps the most widely used contact injection model was introduced by Davids et al [23] and this has been used by numerous other groups (e.g. [35]). In this case, at each contact there are three components to each carrier current. In addition to the tunnelling current and to a thermionic emission component described above, there is a backflowing interface recombination current (the time-reversed version of the thermionic emission process).

4.4   experiment data and simultion results

We choose six kinds of polymers to study the properties of transport and efficiency. These polymers are poly[2-methoxy-5- (2-ethylhexyloxy) -1, 4-phenylenevinylene] (MEH-PPV, from ADS), poly (9, 9-dioctylfluorene) (PFO, from ADS), poly[(2-(4-(3, 7-dimethyloctoxy) phenyl) -3-phenyl-1,4-phenylenevinylene) (PDOC10), PDY [215], BP05[216] and poly [9,9-dioctyl-fluorene-co-N-(4-butylphenyl)- diphenylamine] (TFB,from ADS). MEH-PPV and PFO are two kinds of classical polymers due to they have developed and been studied for a long time. The PDY and BP105 have very high emitting efficiency, but reason is still unknow. The last one has good hole transporting property and is used as hole transport layer. The EA and IP of six polymers are shown in Fig. 4.4. The LEDs were fabricated on indium tin oxide (ITO) coated glass structures which is treated by oxygen-plasma and covered by poly (styrene sulfonic acid) (PEDOT:PSS) hole injection layer. The latter was spin coated emitting layer whose thickness approaches 100 nm. The LiF/Ca/Al layers were evaporated at pressure of 10^{-6} mbar to be the cathode. The LiF is used to increase the electron injection efficiency. In addition, because we want to understand the carrier transport process in the LED device, we also fabricated LED structure ITO/PEDOT/polymer/Al as the hole-only transport device, Al/polymer/LiF/Ca/Al as the electron-only device. These device structures are shown in Fig. 4.5. We evaporate LiF into the electron-only device in order to get higher electron current density. In our simulation, we ignore this fector. This is because Ca is active and easy to react to other elements at interface in the evaporating process. However, the interface between polymer and Ca is clear in the simulation and we don't consider the effect from LiF.

In Fig. 4.6, Fig. 4.7 and Fig. 4.8 we show the experiment and the simulation results. The hollow curves are experiment data and the thick lines are simulation results. We could use the simulation results of current in electron only and hole only devices to get the electron and hole mobilities of polymers. Then, we use both electron and hole mobilities to get the bipolar current. The results of bipolar current density are similar to the experiment data. The meaning of characters of six figures of Fig. 4.6, Fig. 4.7 and Fig. 4.8 are the same. The ∘ curves, △ curve and ◁ curves are bipolar current density, hole-only current density and electron-only current density. When we simulate PFO device behaviors without considering tunneling effect, the hole mobility of PFO is very
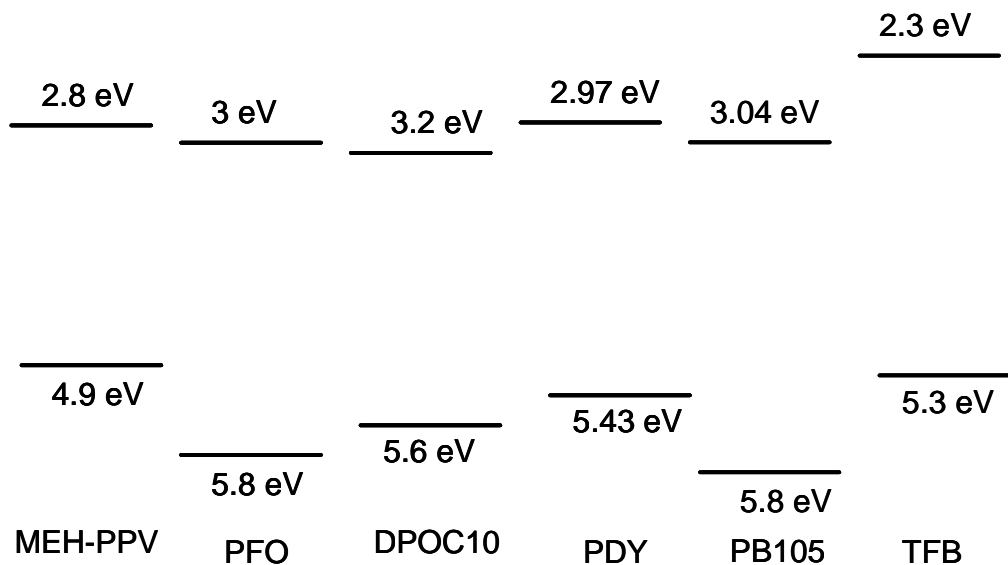
Figure 4.4: Electronic energy-level diagram relative to vacuum for six polymers.

large, 10^{-4} cm^2/Vs at 1 MV/cm. Comparing with the reported data[207], we know it is too large to believe. Because the junction barrier of hole is 0.6 eV, therefore the hole mobility must be large to get current density as large as experiment data. After we consider the tunneling injection, the simulation result of hole mobility of PFO is ~10^{-5} cm^2/Vs. We also use time resolved electroluminescence to get the hole mobility of PFO and the result is consistent with the simulation.

The mobilities of six polymers are shown in Fig. 4.9. The mobilities of hole are shown as hollow curves and electron mobilities are shown as solid curves. The hole mobility of MEH-PPV of our simulation is closed to the prior data and it means that our devices are as good as others[212]. However, electron mobility is hard to measure by time-of-fight technique and it is also difficult to find previous research data to compare with our results. But we believe the results of electron mobility are reasonable. In Fig. 4.9 (a) the hole mobility of MEH-PPV, PFO and DPOC10 are larger than their electron mobility, especially for DPOC10. The light emitting efficiency of three devices are PFO > MEH-PPV > DPOC10 in the real devices. From these results, we can observe that the mobility imbalance is one of reasons for low emitting efficiency.

In Fig. 4.9 (b), the electron and hole mobilities of PDY and BP105 are more balanced than MEH-PPV, PFO and DPOC10. The mobility of hole and electron of PDY and BP105 are in the same order at the operation bias. This
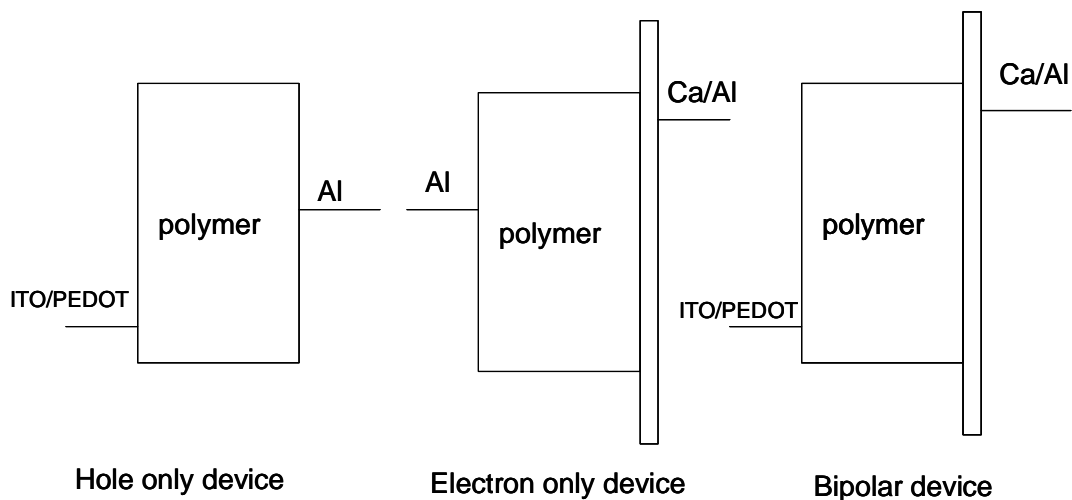
Figure 4.5: The device structures of hole-only, electron-only and bipolar carriers inject into the polymer device.

is an important factor for EL efficiency of PDY and BP105 are higher than the other polymers. From the results of Fig. 4.9, we think mobility balance is the main reason why PDY and BP105 have such high emission efficiency. However, there is a special polymer data in the Fig. 4.9. From our result, although the mobility of hole and electron of TFB are more balance than MEH-PPV, PFO and DPOC10 the EL efficiency of TFB can not catch up to these polymers. From the TFB simulation, we know the mobility balance is not the only factor to decide the high emitting efficiency. In addition to mobility, injection barrier is also important effect. The carrier density is decreased by high injection barrier seriously so the emitting efficiency is decreased.

There are another unusual results of TFB and DPOC10 current density in Fig. 4.7. The bipolar current density of BP105 and DPOC10 are lower than the current density in the single carrier device. These results are strange because the bipolar current density will be closed to the sum of the electron and hole only current density. Even we consider larger recombination rate and recombination current density in the bipolar device in our simulation, the current density in the bipolar device is still larger than that in the single carrier device. We consider that there are some hole traps in the BP105 from the synthetic process. When we inject the electrons to the electron only device, electron can't feel the hole traps, but when we inject bipolar carriers, hole carrier will be trapped into hole traps and influence the potential of electrons. Therefore, the current density and mobility of electron are lower than that in the electron-only device. This point has reported at Ref. 15 and 16, and our fitting parameters are in the reasonable rang. The diagram is shown in Fig.4.10.

Figure 4.6: The experiment datas and simulation results of MEH-PPV and PFO. The ∘ curves are experiment dada of bipolar injection, the △ curves are experiment data of hole-only injection and the ◁ curves are experiment data of electron-only injection. The dash-dot line is simulation curve of bipolar injection, the solid line is simulation curve of hole-only injection and the dot line is simulation curve of electron-only injection.

81
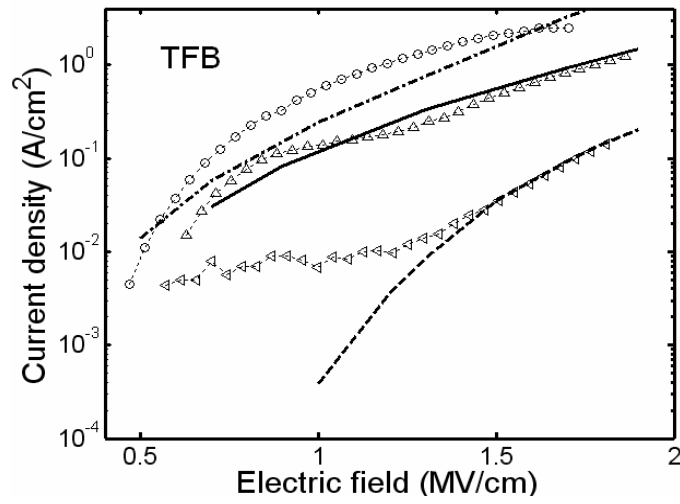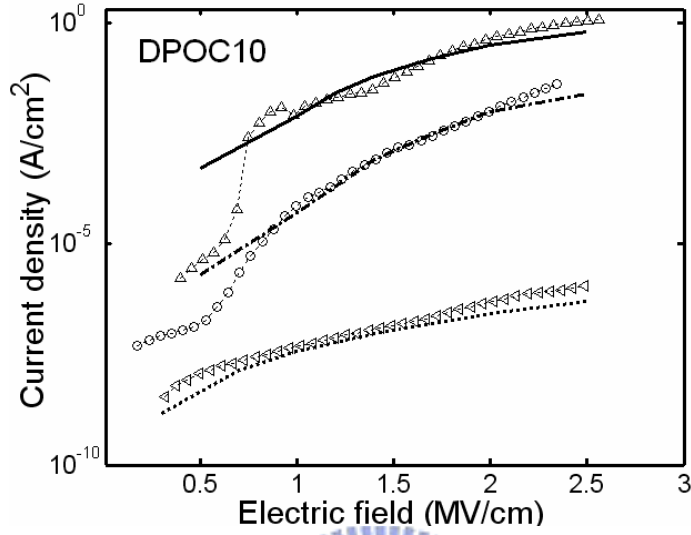
Figure 4.7: The experiment datas and simulation results of DPOC10 and TFB. The ○ curves are experiment dada of bipolar injection, the △ curves are experiment data of hole-only injection and the ◁ curves are experiment data of electron-only injection. The dash-dot line is simulation curve of bipolar injection, the solid line is simulation curve of hole-only injection and the dot line is simulation curve of electron-only injection.
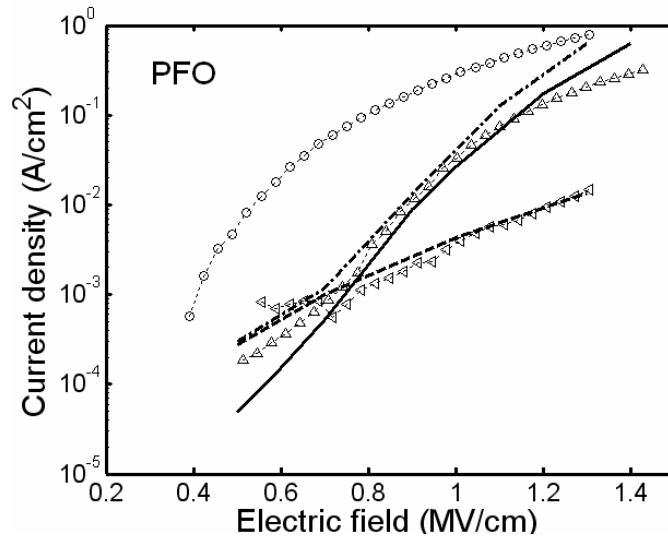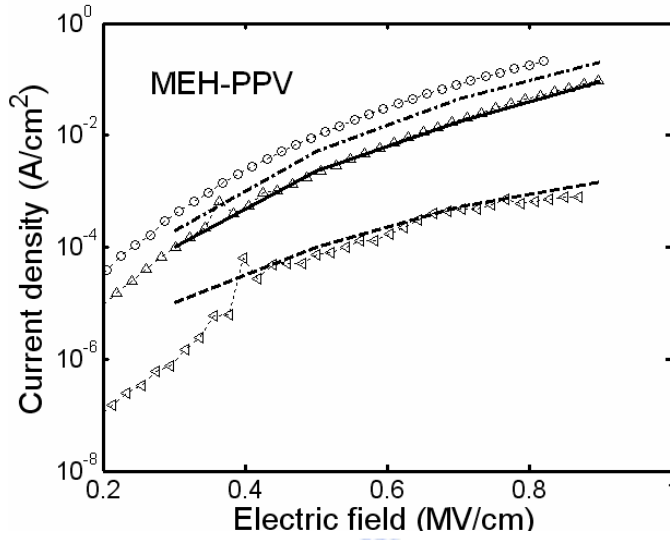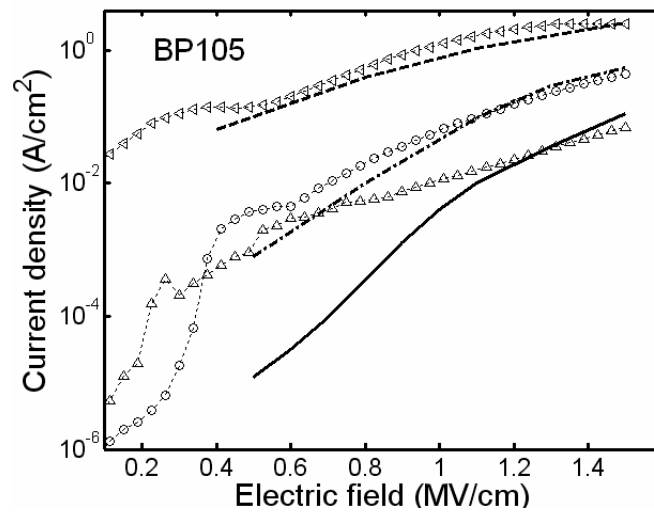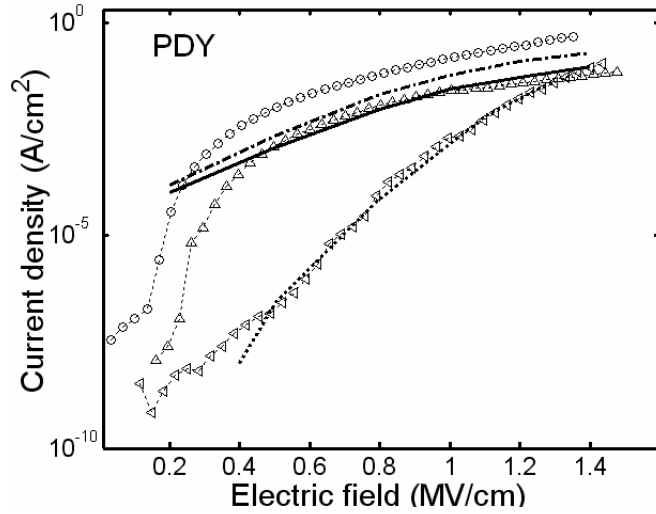
Figure 4.8: The experiment datas and simulation results of PDY and BP105. The ∘ curves are experiment dada of bipolar injection, the △ curves are experiment data of hole-only injection and the ◁ curves are experiment data of electron-only injection. The dash-dot line is simulation curve of bipolar injection, the solid line is simulation curve of hole-only injection and the dot line is simulation curve of electron-only injection.
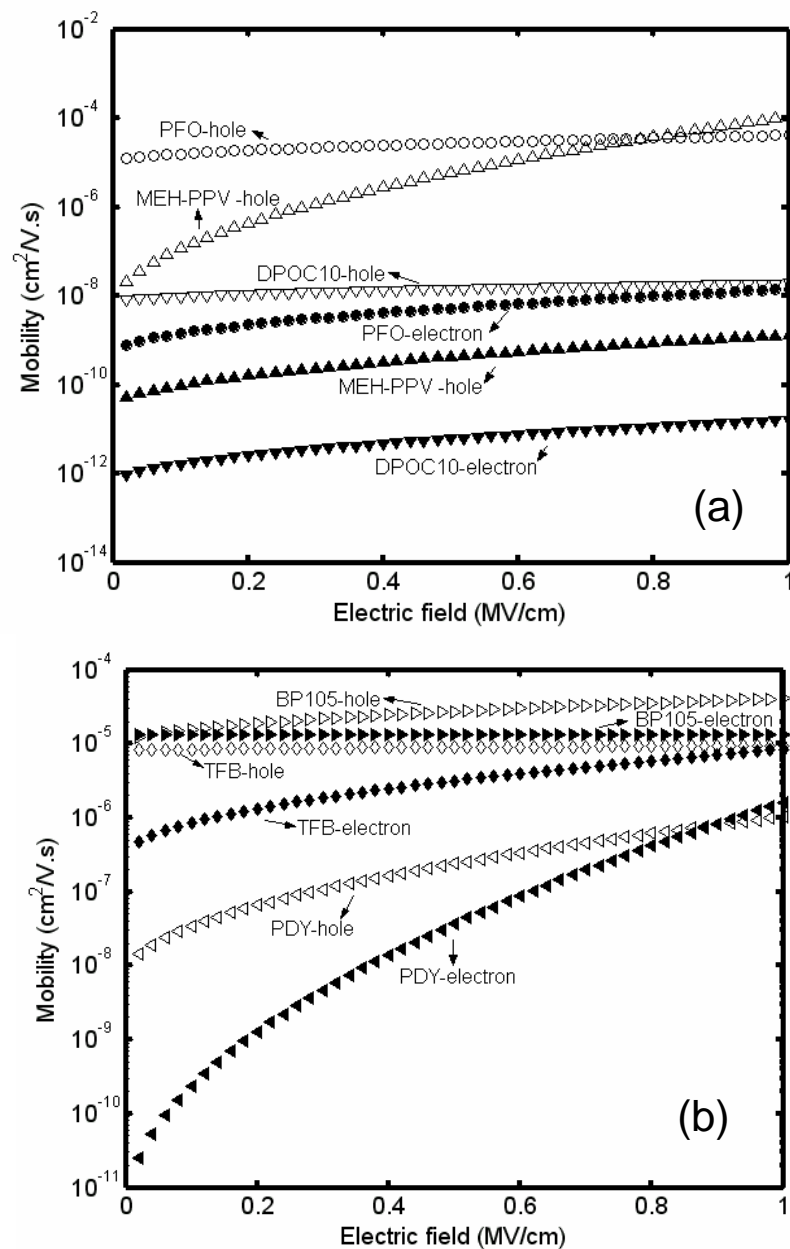
Figure 4.9: hese fugures is shown the simulation results of mobilities of electron and hole. The hollow curves are hole mobilities and solid curves are electron mobilities. The circle curves are mobilities for PFO, the $\triangle$ curves are mobilities for MEH-PPV, the $\triangledown$ curves are mobilities for DPOC10, the $\triangleright$ curves are mobilities for BP105, the $\diamond$ curves are mobilities for TFB and the $\triangleleft$ curves are mobilities for PDY.

From Fig.4.9, the hole mobility and the electron mobility of TFB are in the same order at the same working bias, but the EL efficiency is smaller than PFO. The mobility balance of electron and hole is an important factor of transition and EL efficiency but not the only one. Therefor, if we want to understand someone material properties and try to improve the EL efficiency we have a checking steps in sequence. We could use this method to analyze which factor is most important to EL efficiency. First, we get the electron-only, hole-only and biploar currents and observe the bipolar current is larger single carrier current or not. This step give us an idea of the influence of impurity. If bipolar current smaller than one of the electron and the hole currents, the influence of impurity is large and we will try to dop another impurity to change the potential. If the bipolar current larger than the electron and the hole currents, the influence of impurity is small. Then we can use the experiment current data to simulate the electron mobility and the hole mobility of material. From this results, we can comprehend if the electron mobility and the hole mobility are balance.

It will never stop that the scientists try to synthesis a new polymer or design new device structure which has better light efficiency. From the results of our research, the electron and hole balance and applicable injection barriers are two important factors to achieve the high efficiency. Electron and hole mobilities also have to be closed in the same order. Besides, if the differences of the injection barriers of electron and hole are closer, the carrier densities of both will be closed and due to the electron and hole current balance. This is one important factor of high efficiency. However, it is another matter to be concerned to some special organic materials. Some traps in the material which come from by synthetic process will cause potential changing and influence the transport property of material. This character can be found until we measure single carrier currents and bipolar current, respectively.

hole traps
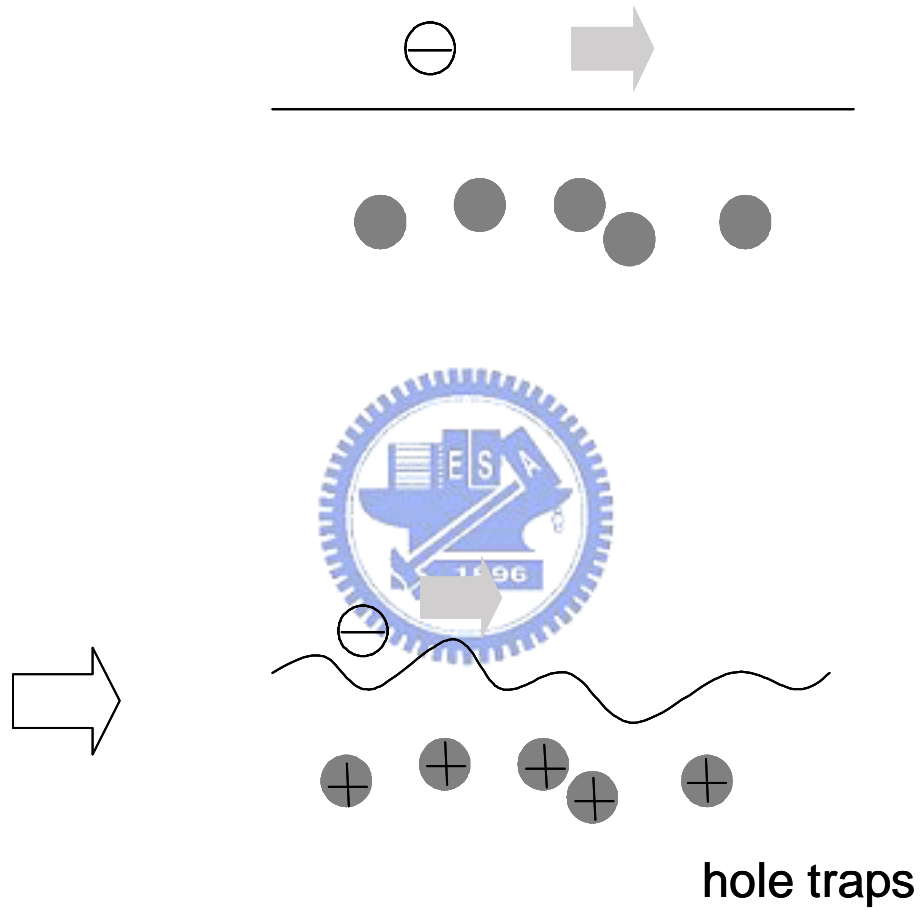
Figure 4.10: The diagram of carrier potatential at (a) single carrier injection, (b) bipolar carrier injection.

Bibliography

[1] R.L. Greene, G.B. Street, L.J. Sutude, Phys. Rev. Lett. **34** 577 (1975).

[2] H. Shirakawa, E.J. Louis, A.G. MacDiarmid, C.K. Chiang, A.J. Heeger, J. Chem. Soc. Chem. Commun. 578 (1977).

[3] T.A. Skotheim, *Handbook of Conducting Polymers*, vol. 1&2, Marcel Dekker, New York, 1986.

[4] K.S.V. Srinivasan, *Macromolecules: New Frontiers*, vol. 1&2, Allied Publishers, India, 1998.

[5] Ed.M. Aldissi, *Intrinsically Conducting Polymers: An Emerging Technology*, Kluwer, Dordrecht, Netherlands, 1993.

[6] T.S. Moss, *Handbook of Semiconductors, vol. 1, Elsevier*, Amsterdam, 1992.

[7] W.P. Su, J.R. Schrieffer, A.J. Heeger, Phys. Rev. B **22** 2099 (1980).

[8] D. Emin, T. Holstein, Phys. Rev. Lett. **36** 323 (1976).

[9] F. Genoud, M. Gugliemi, M. Nechtschtin, E. Genies, M. Salmon, Phys. Rev. Lett. **55** 118 (1985).

[10] M.G. Cross, U. Walton, D.J. Simmons, J. Electroanal. Chem. **189** 389 (1985).

[11] H.S. Nalwa, J. Mater. Sci. **26** 1683 (1991).

[12] X. Zhang, E.T. Kang, K.G. Neoh, K.L. Tan, D.Y. Kim, C.Y. Kim, J. Appl. Polym. Sci. **60** 625 (1996).

[13] S.Z. Lewin, Chem. Instrum. **43** A567 (1987).

[14] P.C. Pandey, R. Prakash, J. Electrochem. Soc. **145** 999 (1998).

[15] D.G. Lidzey, D.D.C. Bradley, S.F. Alvarado, D.F. Sedler, Nature **386** 135 (1997).

[16] Z. Shen, P.E. Burrows, V. Bulovic, S.R. Forest, M.E. Thompson, Science **276** 2009 (1997).

[17] M. Granstrom, K. Petrisch, A.C. Areas, A. Lux, M.R. Anderson, R.H. Friend, Nature **382** 695 (1996).

[18] A. Chaubey, K.K. Pandey, V.S. Singh, B.D. Malhotra, Anal. Chim. Acta **407** 97 (2000).

[19] M. Gerard, K. Ramanathan, A. Chaubey, B.D. Malhotra, Electroanalysis **11** 450 (1999).

[20] M.M. Verghese, K. Ramanathan, S.M. Ashraf, B.D. Malhotra, J. Appl. Polym. Sci. **70** 1447 (1998).

[21] A.L. Sharma, M. Gerard, R. Singhal, S. Annapoorni, B.D. Malhotra, Appl. Biochem. Biotechnol. **96** 155 (2001).

[22] A.L. Sharma, V. Saxena, S. Annapoorni, B.D. Malhotra, J. Appl. Polym. Sci. **81** 1460 (2001).

[23] K. Kaneto, M. Kaneko, in: B.D. Malhotra (Ed.), Handbook of Polymers in Electronics, Rapra Technology Ltd., Shawbury, U.K, 2002.

[24] Pei, Q.; Yu, G.; Zhang, C.; Yang, Y.; Heeger, A. J. ;, Science ,**269** 1086 (1995).

[25] Dick, D. J.; Heeger, A. J. Yang, Y.; Pei, Q., AdV. Mater. **8** 985 (1996).

[26] Richter, M. M.; Fan, F. R. F. Klavetter, F. Heeger, A. J. Bard, A. , J. Chem. Phys. Lett. **226** 115 (1994).

[27] Dini, D. Martin, R. E. Holmes, A. B., AdV. Funct. Mater. **12** 299 (2002).

[28] Nambu, H. Hamaguchi, M. Yoshino, K. , J. Appl. Phys. **82** 1847 (1997).

[29] Dini, D.; Janakiraman, U.; Doblhofer, K. ACS Symp. Ser. (Conducting Polymers and Polymer Electrolytes) **832** 103 (2003)..

[30] Bard, A. J. Science **270** 718 (1996).

[31] Pei, Q.; Yu, G.; Zhang, C.;Yang, Y.; Heeger, A. J. Science **270** 719 (1996).

[32] Manzanares, J. A.;Reiss, H.; Heeger, A. J. J. Phys. Chem. B **102** 4327 (1998).

[33] Braun, D. Mater. Today **5** 32 (2002).

[34] Shim, H. K.; Kang, I. N.;Zyung, T. Plast. Eng. **45** 935 (1998).

[35] Prieto, I.; Teetsov, J.; Fox, M. A.; Vanden Bout, D. A.; Bard, A. J. J. Phys. Chem. A **105** 520 (2001).

[36] Tsionsky, M.; Bard, A. J. Dini, D.; Decker, F. Chem. Mater. **10** 2120 (1998).

[37] Sandman, D. J. Trends Polym. Sci. **2** 44.(1994)

[38] Seo, D. K.; Hoffmann, R. Theor. Chem. Acc. **102** 23 (1999).

[39] Walker, A. B.; Kambili, A.; Martin, S. J. J. Phys. Condens. Matter **14** 9825 (2002).

[40] Baughman, R. H.; Shacklette, L. W. J. Chem. Phys. **90** 7492 (1989).

[41] Duke, C. B. Can. J. Chem. **63** 236 (1985).

[42] Kowalsky, W.; Becker, E.; Benstem, T.;Johannes, H. H.; Metzdorf, D.; Neuner, H.; Schobel, J. AdV. Solid StatePhys. **40** 795 (2000).

[43] Dyakonov, V.; Frankevich, E. Chem. Phys. **227** 203 (1998).

[44] Mott, N. F.; Davis, E. A. Electronic Processes in Non-CrystallineMaterials; Clarendon Press: Oxford, 1979.

[45] Gutmann, F.; Lyons, L. E. Organic Semiconductors; Wiley: New York,1967.

[46] Eley, D. D. J. Polym. Sci. Polym. Symp. 1967, 73.

[47] Jiang, X.; Osterbacka, R.; Korovyanko, O.; An, C. P.; Horovitz, B.;Janssen, R. A. J.; Vardeny, Z. V. AdV. Funct. Mater. **12** 587 (2002).

[48] Wu, M. W.; Conwell, E. M. Phys. ReV. B **56** R10060 (1997).

[49] Tang, C. W.; Van Slyke, S. A.; Chen, C. H. J. Appl. Phys. ,**63** 610 (1987).

[50] Wilkinson, F. Quart. ReV. Chem. Soc. **20** 403 (1966).

[51] Neher, D.; Grüer, J.; Cimrova, V.; Schmidt, W.; Rulkens, R.; Lauter, U.Polym. AdV. Technol. 1998, 9, 461.

[52] Nguyen, T. Q.; Martini, I. B.; Liu, J.; Schwartz, B. J. J. Phys. Chem. B2000, 104, 237.

[53] de Leeuw D, Phys. World **12** 31 (1999)

[54] Sirringhaus H, Wilson R J, Friend R H, Inbasekaran M, Wu W, Woo E P, Grell M and Bradley D D C , Appl. Phys. Lett. **77** 406 (2000)

[55] Redecker M, Bradley D D C, Inbasekaran M and Woo E P , Appl. Phys. Lett. **74** 1400 (1999)

[56] Pope M and Swenburg C E 1982 *Electronic Processes in Organic Crystals* (Oxford: Clarendon)

[57] Tang C W and VanSlyke S A, Appl. Phys. Lett. **51** 913 (1987)

[58] Burrows P E, Shen Z, Bulovic V, McCarty D M, Forrest S R, Cronin J A and Thompson M E , J. Appl. Phys. **79** 7991 (1996)

[59] Burroughes J H, Bradley D D C, Brown A R, Marks R N, Mackay K, Friend R H, Burns P L and Holmes A B , Nature **347** 539 (1996)

[60] Phillips P J 1990 Rep. Prog. Phys. 53 549

[61] Campbell I H and Smith D L 2000 *Semiconducting Polymers: Chemistry, Physics and Engineering* ed G Hadziioannou and P F van Hutten (Weinheim: Wiley–VCH)

[62] Wilson J S, Dhoot A S, Seeley A J A B, Khan M S, Kohler A and Friend R H , Nature **413** 828 (2001)

[63] Marshall J M , Rep. Prog. Phys. **46** 1235 (1983)

[64] Brütting W, Berleb S and Mückel A G , Org. Electron. **2** 1 (2001)

[65] Lampert M A and Mark P 1993 *Current Injection in Solids* (New York: Academic)

[66] Baldo M A and Forrest S R , Phys. Rev. B **64** 085201 (2001)

[67] Crone B K, Davids P S, Campbell I H and Smith D L , J. Appl. Phys. **87** 1974 (2000)

[68] Blades C D J and Walker A B , Synth. Met. **111**–**12** 335 (2000)

[69] Martin S J, Walker A B, Lupton J M and Samuel I D W 2002 J. Phys.: Condens. Matter at press

[70] Schmitz C, Pösch P, Thelakkat M and Schmidt H-W , Phys. Chem. Chem. Phys. **1** 1777 (1999)

[71] Cacialli F , Phil. Trans. R. Soc. A **358** 173 (2000)

[72] Friend R H et al Nature **397** 121 (1999)

[73] Bässler H 2000 *Semiconducting Polymers: Chemistry, Physics and Engineering* ed G van Hutten (Weinheim: Wiley–VCH)

[74] Doblhofer, K.; Rajeshwar K. *In Handbook of Conducting Polymers*,2nd ed., revised and expanded; Skotheim, T. A., Elsenbaumer, R. L., Reynolds, J. R., Eds.; Marcel Dekker: New York, 1998.

[75] Rajeshwar, K. *In Encyclopedia of Electrochemistry-Volume 6 (Semiconductor electrodes and photoelectrochemistry)*; Licht, S., Ed.; Wiley- VCH: Weinheim, 2002;

[76] Ohtake, T.; Sonoyama, N.; Sakata, T. Chem. Phys. Lett. **318** 517 (2000).

[77] Butler, M. A.; Ginley, D. S. Appl. Phys. Lett. **36** 845(1980).

[78] Ding, Z.; Quinn, B. M.; Haram, S. K.; Pell, L. E.; Korgel, B. A.; Bard, A. J. Science **296** 1293 (2002).

[79] Bobylev, B. A.; Kravchenko, A. F.; Loburets, Yu. V.; Salomon, S. N. J. Appl. Phys. **43** 2320 (1972).

[80] Gregg, B. A. ACS Symp. Ser. **844** 243 (2003).

[81] Monk, P. M. S. *In Handbook of Luminescence, Display Materials, and De-Vices*; Nalwa, H. S., Rohwer, L. S., Eds.; American Scientific Publishers: Stevenson Ranch, CA, 2003

[82] Faulkner, L. R. Methods Enzymol. **57** 494 (1978).

[83] Unwin, P. R., Ed. Encyclopedia of Electrochemistry-Volume 3 (Instrumentation and Electroanalytical Chemistry); Wiley-VCH: Weinheim, 2003.

[84] Joo, J.; Oblakowski, Z.; Du, G.; Pouget, J. P.; Oh, E. J.; Weisinger, J. M.; Min, Y.; MacDiarmid, A. G.; Epstein, A. J. Phys. ReV. B **69** 2977 (1994).

[85] Forrest, S. R. J. Phys. Condens. Matter **15** S2599 (2003).

[86] Kapturkiewicz, A. AdV. Electrochem. Sci. Eng. **5** 1 (1997).

[87] Sworakowski, J.; Ulanski, J. Ann. Rep. Prog. Chem. Sect. C: Phys. Chem. **99** 87 (2003).

[88] Kalyuzhny, G.; Buda, M.; McNeill, J.; Barbara, P.; Bard, A. J. J. Am. Chem. Soc. **125** 6272 (2003).

[89] Rubinstein, I.; Bard, A. J. J. Am. Chem. Soc. **103** 5007 (1981).

[90] Moderegger, E.; Wenzl, F. P.; Tasch, S.; Leising, G. MRS Symp. Proc. **598** BB3.47/1-BB3.47/6 (2000).

[91] Pei, Q.; Yang, Y.; Yu, G.; Zhang, C.; Heeger, A. J. J. Am. Chem. Soc. **118** 3922 (1996).

[92] Edman, L.; Pauchard, M.; Liu, B.; Bazan, G.; Moses, D.; Heeger, A. J. Appl. Phys. Lett. **82** 3961 (2003).

[93] Li, Y.; Gao, J.; Yu, G.; Cao, Y.; Heeger, A. J. Chem. Phys. Lett. **287** 83 (1998).

[94] Armstrong, N. R.; Wightman, R. M.; Gross, E. M. Annu. ReV. Phys. Chem. **52** 391 (2001).

[95] Horiuchi, T.; Niwa, O.; Hatakenaka, N. Nature **394** 659 (1998).

[96] Braun, D.; Heeger, A. J. Appl. Phys. Lett. **58** 1982 (1991).

[97] Kraft, A.; Grimsdale, A. C.; Holmes, A. B. Angew. Chem., Int. Ed. **37** 402 (1998).

[98] Kodak, http://www.kodak.com/US/ en/corp/display/index.jhtml.

[99] Borsenberger, P. M.; Weiss, D. S. *Organic Photoreceptors for Xerography*; Marcel Dekker: New York, 1998.

[100] Hercules, D. Science **143** 808 (1964).

[101] S. Panero, P. Prosperi, B. Klapste, B. Scrosati, Electrochim. Acta **31** 1597 (1986).

[102] Hung L.S., Tang C.W., Mason M.G., Appl. Phys. Lett. **70** 152 (1997).

[103] Jabbour G.E., Kawabe Y., Shaheen S.E., Morell M.M., Wang J.-F., Kippelen B., Peyghambarian N., Appl. Phys. Lett. **71** 1762 (1997).

[104] Kim J.S., Granström M., Friend R.H., Johansson N., SalaneckW.R., Daik R., FeastW.J., Cacialli F., J. Appl. Phys. **84** 6859 (1998).

[105] Van Slyke S.A., Chen C.H., Tang C.W., Appl. Phys. Lett. **69** 2160 (1996).

[106] Carter J.C., Grizzi I., Heeks S.K., Lacey D.J., Latham S.G., May P.G., Delospanos O.R., Pichler K., Townsand

[107] C.R.,Wittmann H.F., Appl. Phys. Lett. **71** 34 (1997).

[108] Lee S.T., Gao Z.Q., Hung L.S., Appl. Phys. Lett. 75 (10) (1999) 1404.

[109] Cumpston B.H., Parker I.D., Jensen K.F., J. Appl. Phys. **81** 3716 (1997).

[110] G. Horowitz, Adv. Mater. Weinheim, Ger. **10**, 365 (1998) .

[111] Y. Y. Lin, D. J. Gundlach, and T. N. Jackson, Appl. Phys. Lett. **72**, 1854 (1998) .

[112] C. D. Dimitrakopoulos and P. R. L. Malenfant, Adv. Mater. Weinheim, Ger. **14**, 99 (2002) .

[113] R. W. I. de Boer, M. E. Gershenson, A. F. Morpurgo, and V. Podzorov, Phys. Status Solidi A **201**, 1302 (2004) .

[114] C. R. Newman, R. J. Chesterfield, J. A. Merlo, and C. D. Frisbie, Appl. Phys. Lett. 85, 422 2004 .

[115] J. Takeya, C. Goldmann, S. Haas, K. P. Pernstich, B. Ketterer, and B. Batlogg, J. Appl. Phys. **94**, 5800 (2003) .

[116] V. Podzorov, E. Menard, A. Borissov, V. Kiryukhin, J. A. Rogers, and M. S. Makram-Ebeid and M. E. Gershenson, Phys. Rev. Lett. **93**, 086602 (2004) .

[117] V. C. Sundar, J. Zaumseil, V. Podzorov, E. Menard, R. L. Willett, T. Someya, M. E. Gershenson, and J. A. Rogers, Science **303**, 1644 (2004) .

[118] P. M. Bouchoms, W. A. Schoonveld, J. Vrijmoeth, and T. M. Klapwijk, Synth. Met. **104**, 175 (1999) .

[119] K. Seshadri and C. D. Frisbie, Appl. Phys. Lett. **78**, 993 (2001) .

[120] W. A. Schoonveld, J. Vrijmoeth, and T. M. Klapwijk, Appl. Phys. Lett. **73**, 3884 (1998) .

[121] A. B. Chwang and C. D. Frisbie, J. Phys. Chem. B **104**, 12202 (2000) .

[122] W. A. Schoonveld, J. Wildeman, D. Fichou, P. A. Bobbert, B. J. van Wees, and T. M. Klapwijk, Nature London **404**, 977 (2000)

[123] J. Luo, M. Haller, H. Li, T.-D. Kim, and A. K.-Y. Jen, Adv. Mater. Weinheim, Ger. **15**, 1635 (2003) .

[124] L. Wang, D. Fine, T. Jung, D. Basu, H. von Seggern, and A. Dodabalapur, Appl. Phys. Lett. **85**, 1772 (2004) .

[125] Garnier F, Hajlaoui R, Yassar A, Srivastava P , Science **265** 1864 (1994)

[126] Choi HY, Kim SH, Jang J , Adv Mater **16** 732 (2004)

[127] Torsi L, Dodabalapur A, Sabbatini L, Zambonin P ,Sens Actuators B **67**:312 (2000)

[128] Crone B, Dodabalapur A, Gelperin A, Torsi L, Katz HE, Lovinger AJ, Appl Phys Lett **78** 2229 (2001)

[129] Katz HE, Bao Z, J Phys Chem B **104** 671 (2000)

[130] C.J. Brabec, N.S. Sariciftci, J.C. Hummelen, Adv. Func. Mater. **11** 15 (2001).

[131] H. Spanggaard, F.C. Krebs, Sol. Energy Mater. Sol. Cells **83** 125 (2004).

[132] C. Waldauf, P. Schilinsky, J. Hauch, C.J. Brabec, Thin Solid Films **451-452** 503 (2004).

[133] C.J. Brabec, Sol. Energy Mater. Sol. Cells **83** 273 (2004).

[134] S. Sun, et al. (Eds.), *Organic Photovoltaics: Mechanisms, Materials and Devices*, Marcel Dekker, New York, 2004.

[135] Z. Kafafi, P. Lane (Eds.), *Organic Photovoltaics IV*, SPIE, Bellingham, WA, 2004.

[136] C. Tang, Appl. Phys. Lett. **48** 183 (1986).

[137] N.S. Sariciftci, L. Smilowitz, A.J. Heeger, F. Wudl, Science **258** 1474 (1992).

[138] B. Kraabel, J.C. Hummelen, D. Vacar, D. Moses, N.S. Sariciftci, A.J. Heeger, F. Wudl, J. Chem. Phys. **104** 4267 (1996).

[139] G. Yu, J. Gao, J.C. Hummelen, F. Wudl, A.J. Heeger, Science **270** 1789 (1995).

[140] M. Granstrom, K. Petritsch, A. Arias, A. Lux, M. Andersson, R. Friend, Nature **395** 257 (1998).

[141] S. Sun, Z. Fan, Y. Wang, C. Taft, J. Haliburton, S. Maaref, Organic Photovoltaics II, SPIE Proc. **4465** 121 (2002).

[142] S. Sun, Z. Fan, Y. Wang, J. Haliburton, C. Taft, K. Seo, C. Bonner, Synth. Met. **137** 883 (2003).

[143] S. Sun, Organic Photovoltaics IV, SPIE, **5215** 195 (2004)

[144] S. Sun, Sol. Energy Mater. Sol. Cells **79** 257 (2003)

[145] S. Sun, Sol. Energy Mater. Sol. Cells **85** 261 (2005).

[146] M. Knupfer, Appl. Phys. A **77** 623 (2003).

[147] S. Sensfuss, et al., in: Z. Kafafi, P. Lane, (Eds.), Organic Photovoltaics IV, SPIE-Proc. **5215** 129 (2004).

[148] D. Gosztola, B. Wang, M. Wasielewski, J. Photochem. Photobiol. A: Chem. **102** 71 (1996).

[149] E. Peeters, P. Hal, J. Knol, C. Brabec, N. Sariciftci, J. Hummelen, R. Janssen, J. Phys. Chem. B **104** 10174 (2000).

[150] J. Bredas, et al., J. Am. Chem. Soc. **125** 8625 (2003).

[151] V. Balzani (Ed.), Electron Transfer in Chemistry, Wiley-VCH, New York, 2000.

[152] R. Marcus, et al., J. Phys. Chem. B **107** 6668 (2003).

[153] C. Brabec, A. Cravino, D. Meissner, N. Sariciftci, T. Fromherz, M. Rispens, L. Sanchez, J. Hummelen, Adv. Func. Mater. 11 374 (2001)

[154] W. Salaneck, Nature **397**, 121 (1999).

[155] M.D. McGehee and A.J. Heeger, Adv. Mater. **12**, 1655 (2000).

[156] N. Tessler, Adv. Mater. **11**, 363 (1999).

[157] K. Wong, M. Skaf, C.-Y. Yang, P.J. Rossky, B. Bagchi, D. Hu, J. Yu, and P.F. Barbara, J. Phys. Chem. B **105**, 6103 (2001).

[158] H.S. Woo, O. Lhost, S.C. Graham, D. Bradley, and R. Friend, Synth. Met. **59**, 29 (1993).

[159] S. Kishino, Y. Ueno, K. Ochiai, M. Rikukawa, K. Sanui, T. Kobayashi, H. Kunugita, and K. Ema, Phys. Rev. B **58**, R13430 (1998).

[160] S. Kuroda, T. Noguchi, and T. Ohnishi, Phys. Rev. Lett. **72**, 286 (1994).

[161] E. Conwell, Phys. Rev. B **57**, R12670 (1998).

[162] P. Blom and M. de Jong, IEEE J. Sel. Top. Quantum Electron. **4**, 105 (1998).

[163] H.-F. Meng and T.-M. Hong, Physica B **304**, 119 (2001).

[164] C. A. Coulson, B. O'Leary, and R. B. Mallion, *Hükel Theory for Organic Chemists* (Academic, London, 1978).

[165] R. Morrison and R. Boyd, Organic Chemistry (Allyn and Bacon, Boston, 1987).

[166] M. Rohlfing and S. Louie, Phys. Rev. Lett. **82**, 1959 (1999).

[167] V. F. Traven, *Frontier Orbitals and Properties of Organic Molecules* (Ellis Horwood, New York, 1992)

[168] S. Rakhmanova and E.M. Conwell, Appl. Phys. Lett. **75**, 1518 (1999).

[169] A. Johansson and S. Stafstro, Phys. Rev. Lett. **86**, 3602 (2001).

[170] A.R. Bishop, D.K. Campbell, P.S. Lomdahl, B. Horovitz, and S.R. Phillpot, Phys. Rev. Lett. **52**, 671 (1984).

[171] K. Seeger, *Semiconductor Physics*, 2nd ed. (Springer-Verlag, Berlin, 1982).

[172] S. Jeyadev and E.M. Conwell, Phys. Rev. B **35**, 6253 (1987).

[173] E.M. Conwell, Phys. Rev. B **22**, 1761 (1980).

[174] Polycrystalline and Amorphous Thin Films and Devices, edited by L. Kazmerski (Academic, New York, 1980).

[175] P. W. M. Blom and M. C. J. M. Vissenberg, Mater. Sci. Eng. **27**, 53 (2000).

[176] L. Bozano, S. Carter, J. Scott, G. Malliraras, and P. Brock, Appl. Phys. Lett. **74**, 1132 (1999).

[177] P. Gomes da Costa, R. Dandrea, and E. M. Conwell, Phys. Rev. B **47**, 1800 (1993).

[178] A. Babel and S. Jenekhe, Adv. Mater. (Weinheim, Ger.) **14**, 371 (2002).

[179] R. J. O. M. Hoofman, M. P. de Haas, L. D.A. Siebbeles, and J. M. Warman, Nature **392**, 54 (1998).

[180] G. Greczynski, M. Fahlman, W. R. Salaneck, N. Johansson, D. A. dos Santos, A. Dkhissi, and J. L. Bröas, J. Chem. Phys. **116**, 1700 (2002).

[181] J. D. Weibel and D. Yaron, J. Chem. Phys. **116**, 6846 (2002).

[182] M. Redecker, D. D. C. Bradley, M. Inbasekaran, and E. P. Woo, Appl. Phys. Lett. **73**, 1565 (1998).

[183] P. Stallinga, H. Gomes, H. Rost, A. Holmes, M. Harrison, and R. Friend, Synth. Met. **111**, 535 (2000).

[184] M. Silberberg, *Chemistry*, 2nd ed. (McGraw-Hill, New York, 2000).

[185] M. Onoda, J. Appl. Phys. **78**, 1327 (1995).

[186] Y. S. Chen and H. F. Meng, Phys. Rev. B **66**, 035202 (2002).

[187] S. Makram-Ebeid and M. Lannoo, Phys. Rev. Lett. 48, 1281 (1982).

[188] W. P. Su, J. Schrieffer, and A. Heeger, Phys. Rev. B **22**, 2099 (1980).

[189] B. K. Ridley, *Quantum Processes in Semiconductors*, 2nd ed. (Oxford, New York, 1988).

[190] V. N. Abakumov, V. I. Perel, and I. N. Yassievich, *Nonradiative Recombination in Semiconductors* (Elsevier Science, Amsterdam, 1991).

[191] E. Conwell, J. Perlstein, and S. Shaik, Phys. Rev. B **54**, R2308 (1996).

[192] Lannoo, Phys. Rev. Lett. **48**, 1281, 1982.

[193] Davids P S, Campbell I H and Smith D L, J. Appl. Phys. **82,** 6319, 1997

[194] Malliaras G G and Scott J C , J. Appl. Phys. **83,** 5399, 1998

[195] Blades C D J and Walker A B , Synth. Met. **111**–**112,** 335, 2000

[196] Lupton J M and Samuel I D W , J. Phys. D: Appl. Phys. **32,** 2973, 1999

[197] Kawabe Y, Jabbour G E, Shaheen S E, Kippelen B and Peyghambarian N , Appl. Phys. Lett. **71,** 1290, 1997

[198] Shen J and Yang J , J. Appl. Phys. **83,** 7706, 1998

[199] Barker J A, Foden C L and Greenham N C 2002 European Conf. on Molecular........................

[200] Wolfgang Brüutting, Stafen Berleb and Anton G. Mückl, Organic Electron **2**, 1 (2001)

[201] Yu-Hua Niu, Hong Ma, Qingmin Xu, and Alex K.-Y. Jena, Appl. Phys. Lett. **86**, 083504 (2005)

[202] Yu-Hua Niu, Jian Huang,and Yong Cao, Adv. Mater. **15**, 807 (2003)

[203] B. K. Crone, I. H. Campbell, P. S. Davids, and D. L. Smith, Appl. Phys. Lett. **73**, 3162 (1998)

[204] D. J. Pinner, R. H. Friend, and N. Tessler, J. Appl. Phys. **86**, 5116 (1999)

[205] B. Ruhstaller, S. A. Carter, S. Barth, H. Riel, W. Riess, and J. C. Scott, J. Appl. Phys. **89**, 4575 (2001)

[206] G. Nunes, Jr., S. G. Zane, and J. S. Meth, J. Appl. Phys. L **98**, 104503 (2005)

[207] M. Redecker, D. D. C. Bradley, M. Inbasekaran and E. P. Woo, Appl. Phys. Lett. **73**, 1565 (1998)

[208] G. G. Malliaras and J. C. Scott, J. Appl. Phys. **83**, 5399 (1998)

[209] P. S. Davids, I. H. Campbell, and D. L. Smith, J. Appl. Phys. **82**, 6319 (1997)

[210] V. I. Arkhipov, E. V. Emelianova, Y. H. Tak, and H. Bä ssler, J. Appl. Phys. **84**, 848 (1998)

[211] I. D. Parker, J. Appl. Phys. **75**, 1656 (1994)

[212] J. C. Scott , P. J. Brock , J. R. Salem, S. Ramos, G. G. Malliaras, S. A. Carter and L. Bozano, Synth. Met. **111-112** 289-293 (2000)

[213] X. Jiang, Y. Harima, K. Yamashita, Y. Tada, J. Ohshita and A. Kunai, Chem. Phys. Lett. **364**, 616 (2002)

[214] V. I. Arkhipov, P. Heremans, E. V. Emelianova and H. Bässler, Phys. Rev. B **71** 045214 (2005)

[215] supplied by Merck OLED Materials

[216] supplied by Dow Chemical Company